Fatigue of Flexible Riser in Bend Stiffner Area

Stud.tech. Gunnhild Grytå

June 6, 2011

NTNU
Faculty of Engineering Science
and Technology
Department of Marine Technology

THESIS WORK SPRING 2011

for

Stud. tech. Gunnhild Grytå

Fatigue of flexible riser in bend stiffener area

Utmatning av fleksible rør i bøyestiverområdet

Background

Oil and gas field developments internationally face a range of challenges with regard to deeper water, extreme environmental conditions, more complex reservoirs including high pressure and temperatures. This trend also makes way for exploring a range of different floater concepts, which again result in challenges for the design of suitable riser systems. Among several different riser concepts, dynamic unbonded flexible pipes are commonly used for water depths up to 1000m. Dynamic flexible pipes are used for a wide range of applications; typically application areas are production of oil, condensate and gas and injection of gas, water, methanol and other chemicals. The often high consequences of a failed flexible pipe together with its complex characteristic require advanced and accurate methods of calculating both global and local response due to floater motions, environmental conditions and internal fluid/gas characteristics. The design life of a typical dynamic flexible pipe is 20-25 years, but the technology development regarding improved oil recovery and cost efficient tie-backs to existing fields, has resulted in a trend for extending the lifetime of mature fields beyond their original design life. Fatigue of the dynamic risers is hence a major challenge in order to operate the fields safe for a prolonged lifetime. Additionally, the riser system will be exposed to varying operational boundaries during a field's lifetime, i.e. pressure, temperature, flow velocity and bore composition may change significantly over years.

Scope of work

The following topics are proposed addressed in the master thesis:

1. Perform a literature study focusing on the following:
   (a) Summarize analysis procedure assessment of long term distribution of fatigue loads in a flexible unbounded pipe including references to relevant guidelines.
   (b) Summarize analysis procedure for fatigue assessment in tensile and pressure armour wires of a flexible unbonded pipe, including references to relevant guidelines.
   (c) Summarize design acceptance criteria for steel components in flexible pipes with reference to applicable design guidelines.
   (d) Give an introduction to the theory describing the tailor-made software Bflex (v.2010) for assessment of stress and strain in flexible pipe structures.
2. Perform global operation analysis to establish extreme interface loads during operation for a typical deep water riser application offshore Brazil. A free hanging configuration shall be adopted. Riser cross section data, environmental data and vessel date will be made available by SRT
3. Based on the extreme loads, propose a bend stiffener design to protect the risers from excessive bending at the hang-off interface. A design tool will be made available by SRT.
4. Based on the methodology described under item 1) perform global analysis of free hanging catenary riser configuration in order to establish long term distribution of fatigue loads.

Focus shall be on the bend stiffener area.

5. Based on bend stiffener design proposed under item 3) and the extreme loads derived under item 4) verify that the bend stiffener distributes the curvature satisfactory and that stress in armoring wires and the pressure spiral are acceptable according to relevant guidelines, ref. item 1). Discuss results with regard to the different stress components acting and their contribution. The analysis shall be performed with Bflex 2010.
6. Perform parametric study using Bflex, in order to outline the effect on stress level in the bend stiffener area due to the following:
   (a) Vary ambient temperature and temperature in the riser annulus
   (b) Compare effects using linear or non-linear material properties of the bend stiffener
7. Perform local stress analysis based on long term distribution of fatigue loads established in 4) and calculate fatigue damage of the tensile armour wires. The Bflex module Lifetime shall be used. A base case temperature level according to the conclusions in item 7) shall be proposed.
8. Based on results from 6) and 7), briefly outline possible effect of varying temperature on resulting fatigue damage.

General

The candidate shall by the work performed demonstrate understanding of general design requirements for a flexible pipe by proposing a bend stiffener design which protects the risers from excessive bending during extreme operation as well as provides sufficient fatigue life. The parametric study shall give more in-depth understanding of effects locally in the bend stiffener area.

The work scope may prove to be larger than initially anticipated. Subject to approval from the supervisors, topics may be deleted from the list above or reduced in extent. In the thesis the candidate shall present his personal contribution to the resolution of problems within the scope of the thesis work theories and conclusions should be based on mathematical derivations and/or logic reasoning identifying the various steps in the deduction. The candidate should utilize the existing possibilities for obtaining relevant literature.

Thesis format

The thesis should be organized in a rational manner to give a clear exposition of results, assessments, and conclusions. The text should be brief and to the point, with a clear language. Telegraphic language should be avoided.

The thesis shall contain the following elements: A text defining the scope, preface, list of contents, summary, main body of thesis, conclusions with recommendations for further work, list of symbols and acronyms, references and (optional) appendices. All figures, tables and equations shall be numerated.

The supervisors may require that the candidate, in an early stage of the work, presents a written plan for the completion of the work.

The original contribution of the candidate and material taken from other sources shall be clearly defined. Work from other sources shall be properly referenced using an acknowledged referencing system. The report shall be submitted in three copies:

- Signed by the candidate

– The text defining the scope included

– In bound volume(s)

– Drawings and/or computer prints which cannot be bound should be organized in a separate folder.

Ownership

NTNU has according to the present rules the ownership of the thesis. Any use of the thesis has to be approved by NTNU (or external partner when this applies). The department has the right to use the thesis as if the work was carried out by a NTNU employee, if nothing else has been agreed in advance.

Thesis supervisors:

Prof. Svein Sævik, *NTNU*
Boje Tveraaen, *Kongsberg Oil and Gas Technologies*

Deadline: June 14, 2011

Trondheim, June 6, 2011

Svein Sævik

Gunnhild Grytå

Preface

This thesis is written as the final work of my five years Master of Science program at the Department of Marine Technology, at NTNU. The work was carried out during the spring semester of 2011.

The topic of this thesis is a result of conversations and discussions during a summer internship at SeaFlex Riser Technologies, Kongsberg Oil and Gas Technologies AS. The work carried out during my summer internship and through my project thesis in the fall semester 2010, gave me a desire to gain more knowledge about risers and the challenges met in a design phase at deep-water offshore fields.

The thesis has been carried out under supervision of Professor Svein Sævik at the Department of Marine Technology, NTNU. I would like to thank him for his guidance and assistance during the work. The fact that he has developed Bflex *(v.2010)*, which is the main software applied in this thesis, has been helpful by his way of showing great enthusiasm in addition to his theoretical knowledge.

Further guidance has been given by Boje Tveraaen, Håkon Ward, Paul Gundersen, Sindre Hilden, Horst Vogel and Eirik Rø from SeaFlex Riser Technologies, Kongsberg Oil and Gas Technologies AS. I am very grateful for the help and advices given, concerning software use, theory and general motivation for my work.

Trondheim, Norway

June 6, 2011

Gunnhild Grytå

Summary

The development of offshore fields has reached large water depths, and hence more challenges are met in design of offshore systems. The large water depths challenge the designer in terms of high temperature and pressure in complex reservoirs in addition to extreme environmental conditions. Pipelines and risers are normally designed for a service life of 20–25 years. For some oil fields, the average service life of a riser is only 50% of its planned service life. Hence, it is important to perform extensive global and local analyses to provide a desirable service life of the riser system. One of the main topics that should be evaluated thoroughly is the fatigue damage of the riser. By performing local fatigue analyses, the fatigue life can be determined and so also a desirable service life.

Fatigue is mainly a condition of structural damage that occurs as a result of a cyclic loading. When looking at fatigue of flexible risers, the cyclic loading is initiated by environmental loads causing movement of the floater and hence induces dynamic loading on the riser. The intersection between the riser and the floater is then one of the most vulnerable area for fatigue, depending on floater type, riser system, etc. When evaluating fatigue life of a flexible unbonded riser, the expected life of the pipe structural layers is found. The main focus is on the tensile armor and pressure armor layers, as they are generally exposed to fatigue failure and known to limit the service life of the pipe. As of today, there are no recognized, well-defined mathematical methods to calculate aging of the plastic layers in the cross-section. Hence; this is not discussed further in the thesis.

Typically, the hang-off area must be protected from over-bending so additional devices are added. A common choice is to use a bend stiffener, which is a device that contributes to a moment transition between the riser and the end connection on the floater.
The most common approach for evaluation of the fatigue life of a riser, is by making use of S–N curves and Minor summation method. Each layer of the riser cross-section has its own material properties, and hence its own S–N curve. The Minor summation method provides a failure criterion for the fatigue damage, and this should be fulfilled to gain a suitable riser configuration.

A basic procedure of fatigue assessment is provided by DNV, *DNV-RP-F204*:

1. Define fatigue loading
2. Identify locations to be assessed
3. Global riser fatigue analysis
4. Local stress analysis
5. Identify fatigue strength data
6. Fatigue analysis
7. Further actions if too short fatigue life

Global analyses are performed to establish extreme interface loads during operation and long term distribution of fatigue loads for the deep-water riser application.
In the global extreme analysis carried out in this thesis, it is found that near position of the vessel contribute to the highest maximum tension in addition to compression of the riser at touch down point, TDP. The far position normally cause highest value of top tension since this is where the riser is stretched the most. The curvature obtained in the analysis show a high result at the TDP, which has been found unacceptable in comparison with the minimum-bending radius, MBR. Even though the curvature result is unacceptable, it may be a result of numerical errors in the computations. Thus, the extreme analysis should be evaluated more thoroughly and optimizations of the riser configuration should be carried out.

The highest and lowest results of tension in combination with bending angle found from the global extreme analysis are applied for the bend stiffener design. In the bend stiffener design, maximum shear force is applied. The maximum shear force is found for far position of the vessel.
When the initial design of the bend stiffener is found by applying the shear force with accompanying bending angle, the design should then be verified by local analysis. Two cases are evaluated, where maximum bending angle in combination with maximum and minimum tension for the specific load case are applied. The verification has been done in terms of curvature and stress distribution along the riser in the bend stiffener area. The curvature is distributed with small values at the root of the riser and at the intersection between the bend stiffener and the riser. All stresses found for the riser cross-section are acceptable with reference to design criterion given by *ISO 13628-2*.

The global analysis performed to establish long term distribution of fatigue loads, provides time series of maximum top tension and bending angles for the riser. The results obtained are applied in fatigue analysis of the structural layers of the riser, with focus on the bend stiffener area and the first tensile armor layer.
The fatigue analysis is based on longitudinal failure mode, with evaluation in reference to the failure criterion of fatigue damage found in *DNV-RP-F204*. Sixteen different cases, with different combinations of wave height, period and direction, are assessed. Maximum fatigue damage was found for the same node in each case, and evaluated based on a safety-factor of 10. By summation of the individual fatigue damage the total fatigue damage was found to exceed the damage criterion. Even though the criterion is not fulfilled, it is important to know that no optimization of the configuration has been carried out.

A parametric study has been performed to outline the effect on stress level in the bend stiffener area. Temperature variation in the annulus of the riser and change of material properties has been assessed.
The variation of temperature in the annulus of the riser resulted in a small increase of the stresses in the structural layers of the cross-section. However, the increased stresses obtained did not exceed the design criterion for the tensile armor wire.
Fatigue damage has been evaluated for change of temperature. An overall increase of the fatigue damage was found, and as for the base case, the failure criterion was exceeded.
The change from non-linear to linear material resulted in a decrease of the stress level in the bend stiffener area. Fatigue damage was not evaluated for this case.

Contents

List of Figures

List of Tables

Nomenclature

Abbreviations

ALS	Accidental Limit State
CoG	Center of Gravity
DNV	Det Norske Veritas
E	East Direction
FE	Finite Element
FPSO	Floating Production Storage and Offloading
HF	High Frequency
ID	Inner Diameter
ISO	International Organization for Standardization
LCB	Longitudinal Center of Buoyancy
LCG	Longitudinal Center of Gravity
LF	Low Frequency
MBR	Minimum-Bending Radius
MM	Moment Formulation
MWA	Mid-Water Arch
N	North Direction
NA	Neutral Axis
NE	Northeast Direction
NW	Northwest Direction
OD	Outer Diameter
RAO	Response Amplitude Operator
S	South Direction
SBM	Sandwich Beam Theory
SCF	Stress Concentration Factor
SE	Southeast Direction
SRT	Seaflex Riser Technologies
SW	Southwest Direction

TCB	Transverse Center of Buoyancy
TCG	Transverse Center of Gravity
TDP	Touch Down Point
ULS	Ultimate Limit State
UTS	Ultimate Tensile Strength
VCB	Vertical Center of Buoyancy
VCG	Vertical Center of Gravity
VIV	Vortex Induced Vibrations
W	West Direction
WF	Wave Frequency

Greek Symbols

γ_0	Partial safety factor related to the seriousness of the particular limit state
γ_f	Partial safety factor related to loads
${\sigma_f}^i$	Full stress for cross-section
α	Lay angle of tendon
α_{max}	Maximum, absolute value of relative force angle
$\alpha_o(t)$	Direction of centerline at the support
$\alpha_R(t)$	Relative force angle
β_{yc}	Critical curvature
β_{2c}^i	Critical curvature defining region II
β_{2f}^i	Curvature from friction defining region II
β_y	Global bending quantity, y-direction
β_z	Global bending quantity, z-direction
δ	Eccentricity
δ_0	Eccentricity inherent in S-N curve
γ	Shear deformation
γ_c	Partial safety factor for the structure
γ_M	Capacity-related safety factor
γ_m	Partial safety factor for material properties
κ_c	Critical curvature
κ_{max}	Maximum curvature along the bend stiffener
μ	Friction coefficient
μ_i	Friction coefficient for inner side of helix element
μ_i	Friction coefficient for outer side of helix element

ω_i	Curvature quantities
σ_e	Equivalent stress
σ_t	Tensile hoop stress
σ_{xx-fx}	Axial stress of armor
σ_{xx-my}	Normal curvature stress
σ_{xx-mz}	Transverse curvature stress
σ_{yz}	Torsion stress
φ_{o}	Transition angle

Roman Letters

A	Cross-sectional area
a	Constant characterizing the S-N curve
b	Width of beam
C_d	Design 'capacity'
C_k	Characteristic measure of capacity
D	Fatigue damage
D_d	Design 'demand'
D_{ki}	Characteristic measure of demand for load type
D_{max}	Maximum water depth including tidal and wave effects
D_{f}	Failure criterion
E	Young's modulus
e_{i}	Tangential unit vector
EA	Axial Stiffness
EI	Bending stiffness
EI_{o}(s)	Initial design of bending stiffness
f	Available friction force per unit length along helix element
F_k	Characteristic measures of load
F_x	Axial force from pressure and hoop effect
G	Shear Modulus
GI_t	Torsional stiffness
I_{xx}	Roll moment of inertia
I_{yy}	Pitch moment of inertia
I_{zz}	Yaw moment of inertia
k	Shear stiffness
m	Constant characterizing the S-N curve

M_c^i	Start slip bending moment for pipe-layer i
M_f^i	Friction moment for pipe layer i
M_r	Bending moment at end of bend stiffener
M_y	Bending moment due to riser bending
M_z	Bending moment induced by global riser bending
M_s	Support moment
N	Constant amplitude endurance
n	Permissible utilization factor
N_a	Axial force in helix element
n_j	Number of wires
n_t	Number of tendons in the layer
N_w	Total number of wires
N_i	Number of Cycles to failure
n_i	Number of cycles with contributing stress range
P	External loading
q_i	Contact force per unit length along inner side of helix element
q_o	Contact force per unit length along outer side of helix element
${q_r}^i$	Radial load per unit length along helix path
R	Layer radius
R_j	Radius to middle of wire
R_1	Radius of curvature bend stiffener nr.1
R_2	Radius of curvature bend stiffener nr.2
R_c	Critical radius of curvature
R_D	Design radius of curvature
S	Cyclic Stress
s	Length coordinate of bend stiffener
S_0	Nominal stress range
S_B	Length of bend stiffener
$S_{r,i}$	Stress ranges
T	Force effective tension
t	Thickness
T(t)	Force on bend stiffener
t_{corr}	Corrosion allowance
T_D	Design force

t_{fat}	Fatigue thickness
T_{max}	Maximum force
T_{min}	Minimum force
t_{nom}	Nominal pipe wall thickness
t_{ref}	Reference thickness
V	Shear Force
v_p	Tendon displacement if plane surfaces remain plane after bending
v_s	Actual longitudinal displacement along tendon

1 Introduction

1.1 Background

Exploration and development of oil and gas fields at large water depths face challenges in the design of offshore systems. Different floater concepts may be evaluated for a specific deep water field, which in turn leads to challenges in finding a suitable riser system.

The most common riser concept for deep water applications are dynamic unbounded flexible pipes. This type of risers has been applied in offshore oil and gas industry for over 20 years. They connect seabed flow-lines to floating production facilities such as floating production storage and offloading units, FPSO's. Other areas of application are to connect two floating production facilities, or as static seabed flow-lines.

In general, pipelines and risers are designed for a lifetime in the order of 20–25 years, but for some oil fields, the average flexible riser has been in service for only 50% of its planned service life. Due to this, prolonged service life of risers are desirable. For dynamic flexible unbounded risers, major challenges are the fatigue life, collapse and axial compression loading of tensile armor wires. In addition, challenges are met in terms of aging and damage of the plastic layers as they contribute to great problems for a riser. The riser's complex composition requires advanced methods for computation of response, both global and local, from the environment, floater motions and internal fluid characteristics.

Figure 1.1 presents some of the challenges met in deep-water riser design.

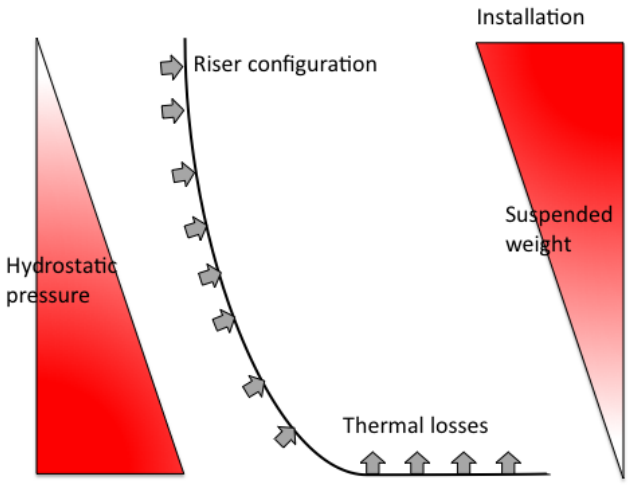

Figure 1.1: Illustration of challenges met in riser design at deep-water

1.2 Objectives

The aim of this thesis is to gain knowledge of the challenges encountered when applying a free hanging, unbounded flexible riser in deep-water environments. The main subject of the thesis is the fatigue life of the unbounded flexible riser, with focus on critical areas along the riser. The main focus in this thesis will be on the armor layers of the riser. The touch down point and hang-off of the riser are most prone to fatigue damage, and this thesis will concentrate on the hang-off area.

1.3 Structure of Report

Chapter 2 gives an introduction to the theory behind fatigue analysis of unbounded flexible risers. Critical areas of fatigue damage and failure modes are presented, and design criteria are stated.

Chapter 3 presents the theory behind the local analysis tool, Bflex *(v.2010)*.

Chapter 4 describes how a fatigue analysis is performed step-by-step, so-called analysis methodology.

Chapter 5 presents the steps of bend stiffener design, to obtain a suitable bend stiffener for the riser.

Chapter 6 presents the basis for the analysis, with all input and specifications for the riser configuration.

Chapter 7 presents the global analysis where the extreme loads affecting the riser configuration at a specific oil field are introduced. Critical areas of interest are evaluated to obtain a feasible configuration.

Chapter 8 presents a proposition of a bend stiffener design based on *chapter 7*. The bend stiffener is verified in terms of desirable curvature distribution.

Chapter 9 applies the loads found in *chapter 7* to verify that the bend stiffener is acceptable in terms of acceptance criteria of stress distribution.

Chapter 10 presents results from a group of global analyses with different specifications for waves and current. Long term distribution of the fatigue loads acting on the configuration are established. The loads found are applied to perform a fatigue analysis. In addition, the stress level of the riser cross-section in the bend stiffener area is evaluated.

Chapter 11 presents a parametric study performed for evaluation of stress level when temperature in the annulus is changed. In addition, linear material properties are evaluated in comparison with non-linear material properties of the bend stiffener.

2 Literature Study

2.1 Fatigue

Fatigue is a condition of structural damage that occurs as a result of cyclic loading. The damage will take place even though the nominal maximum stress values are below the yield stress limit of the material and less than the ultimate tensile stress, (Wikipedia, 2011a).
Fatigue is an important aspect in the design of marine structures, e.g. riser systems. Environmental conditions, such as wave loads, initiate movement of the floater connected to the riser system. The dynamic movement induces large dynamic loading on the riser, causing the riser to flex about its fixed location. The effect of the varying load may initiate fatigue cracks at locations of high stress in the riser. The cracks initiated by the cyclic loading tend to grow in an accelerating rate leading to reduction of structural integrity, (Berge, 2004b).

For a typical riser system, the most vulnerable area for fatigue is the intersection between the floater and the pipe. This area is prone to over-bending; so additional devices need to be included in the design of the system. Such devices can be bend stiffeners and bell mouths, as illustrated in figure 2.1. These are designed separately from the pipe cross-section analysis. Bell mouths are used in dynamic applications where flexible risers are pulled through guide tubes to floater deck level. A bend stiffener is fixed to the end of the riser tube and it provides a gradual stiffening of the riser. The function is to contribute to a moment transition between the riser and a rigid end connection. Which device to use, depends on the choice made by the manufacturer. The decision depends on the specific offshore field, outlay of the field and also type or riser system chosen by the operator. Even so, bend stiffeners are known to provide better performance when making use of high motion vessels, (Rahman, 2011).

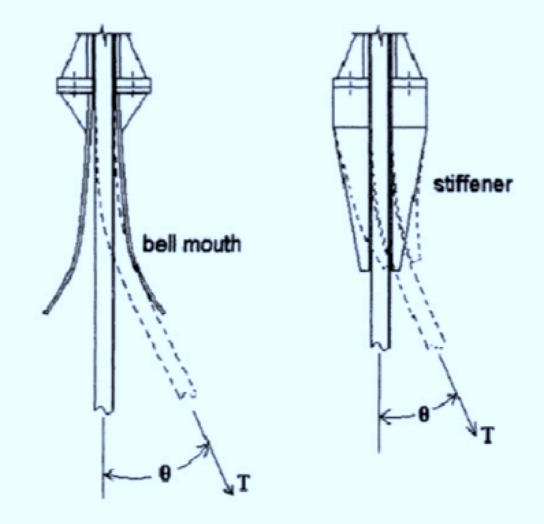

Figure 2.1: Illustration of a bend stiffener and a bell mouth,(Rahman, 2011)

Other areas of a riser system that are at risk of fatigue damage are at TDP and in the sag and hog bends of the riser. An illustration of free hanging catenary and lazy wave riser configurations is given in figure 2.2. Red circles illustrate typical areas prone to fatigue damage.

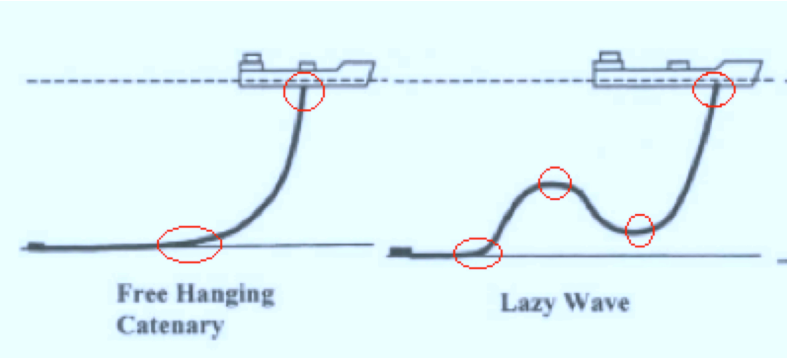

Figure 2.2: Exposed areas of fatigue for two riser configurations,(Bai & Bai, 2005)

The most common approach for fatigue analysis of standard flexible pipes is by making use of S-N curves and Miner Summation method. An other approach is fracture mechanics, where the life of a joint through crack growth is predicted when assuming a certain initial defect and residual stress, (Campbell, 1999). The focus in this thesis will be on the S-N curve approach.

2.1.1 S-N Curves

The following originate from (DNV, 2005b) and (DNV, 2005a):

In fatigue design, the material performance can be described by an S-N curve, or Wöler curve. The S-N data is obtained from fatigue testing of small specimens in test laboratories.
Figure 2.3 illustrates a typical S-N curve.

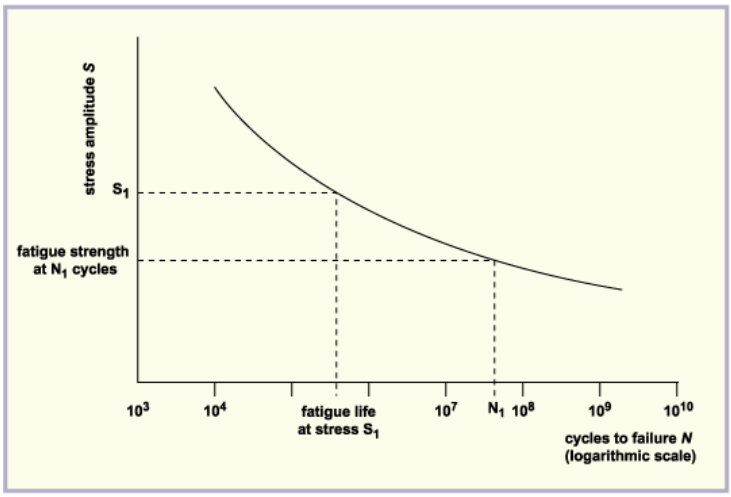

Figure 2.3: Typical S-N curve, (Martin Tarr, 2011)

The life expectancy for a given cyclic stress, S, against the scale of cycles to failure, N_i, is given by equation 2.1:

$$N_i = a \cdot S^{-m} \tag{2.1}$$

where a and m are constants that are established by experiments.

The stress range, S, is found by applying a stress concentration factor, SCF, in combination with a thickness correction factor to the nominal stress range, equation 2.2

$$S = S_0 \cdot SCF \cdot \left(\frac{t_{fat}}{t_{ref}}\right)^k \tag{2.2}$$

where:

- S_0 : Nominal stress range
- SCF : Stress concentration factor
- $\left(\frac{t_{fat}}{t_{ref}}\right)^k$: Thickness correction factor

The fatigue thickness, t_{fat}, is defined as the average representative pipe wall thickness, given by $t_{fat} = t_{nom} - 0.5 \cdot t_{corr}$. Where t_{nom} is the nominal pipe wall thickness and t_{corr} is the corrosion allowance. Having a wall thickness that is t_{fat} larger than the reference wall thickness, the thickness correction factor is applicable. (DNV, 2005b) provide a reference wall thickness of, $t_{ref} = 25mm$.
The exponent k, is a function of actual structural design, and accordingly related to the S-N curve. For welds in pipelines and risers, (DNV, 2005a) provides values of $k = 0$ for hot spot at the root, and $k = 0.15$ for the weld toe.

Stress Concentration Factor

In cases of imperfect geometry of two neighboring joints, a SCF is applied to make up for possible stress magnifications. The SCF can be computed from detailed finite element, FE, analysis or by closed form expressions for the actual structural detail. At locations where the stress is increased due to local bending in consequence of an eccentricity, so-called hot spots, a stress concentration due to maximum allowable eccentricity should be included. The SCF for pipelines and risers is given by (DNV, 2005a) as the following analytical expression:

$$SCF = 1 + \frac{3(\delta - \delta_0)}{t} e^{-\sqrt{t/OD}} \tag{2.3}$$

where

- $\delta_0 = 0.1t$ is misalignment inherent in the S-N data
- OD : Outer diameter

Selection of S-N curves

(DNV, 2005a) recommends that the relevant S-N curves for risers are selected based on:

- Constructional details
- Fabrication process - welded, clad, forged, machined, etc.
- Base metal or weld
- Welds - hot spots on the inner surface and outer surface
- Weld details and tolerance, weld type
- Stress concentration factors from concentricity, thickness variations, out of roundness and eccentricity; angularity
- Environment - air, free corrosion or cathodic protection in seawater

2.1.2 The Miner Summation

Marine structures are subjected to stochastic loading, and the fatigue damage experienced is in general called cumulative damage. A method of calculating the cumulative damage is the Miner summation method.
The Miner summation method assume that the damage on the structure per load cycle is constant at a given stress range.

The damage, D, is given by equation 2.4:

$$D = \frac{1}{N} \tag{2.4}$$

In the given stress range, N is the constant amplitude endurance.
The Minor summation method state that for a spectrum with several different stress ranges, $S_{r,i}$, where each is contributing to a number of cycles, n_i, the damage sum will be given by equation 2.5:

$$D = \sum_i \frac{n_i}{N_i} \tag{2.5}$$

where N_i is the number of cycles to failure.

The failure criterion, D_f, is then given by equation 2.6:

$$D_f \geq 1 \tag{2.6}$$

An illustration of the procedure of the Miner summation method is presented in figure 2.4. Graph a) represents one stress range S_r with a number of cycles n. Taking the logarithm of the stress range, $logS_r$, and applying a S-N curve, graph b), the fatigue life, N, for the particular stress block is found. Applying equation 2.4 and 2.5, the damage sum of all the stress ranges can be calculated.

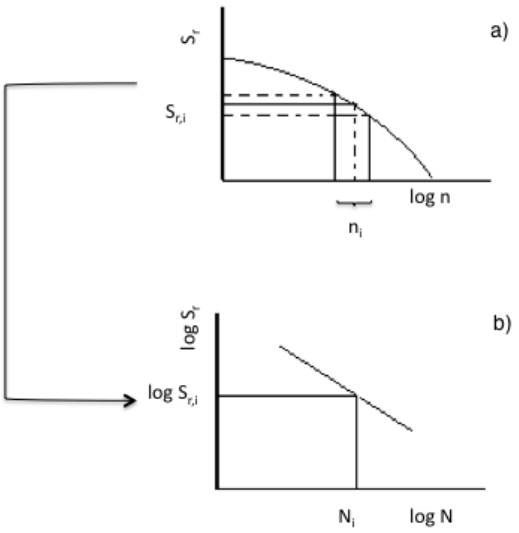

Figure 2.4: Procedure of the Miner Summation Method, a) stress range exceedance diagram and b) S-N curve.(Berge, 2004a)

2.2 Fatigue of Flexible Unbounded Pipe

In the design of flexible unbounded pipes, the study of fatigue life is of great importance. Flexible unbounded pipes are made out of separate unbounded polymeric and metallic layers that are able to move relative to each other. When computing the fatigue life, the expected life of the structural layers of the pipe is found. Figure 2.5 presents the different basic layers of a flexible unbounded pipe.

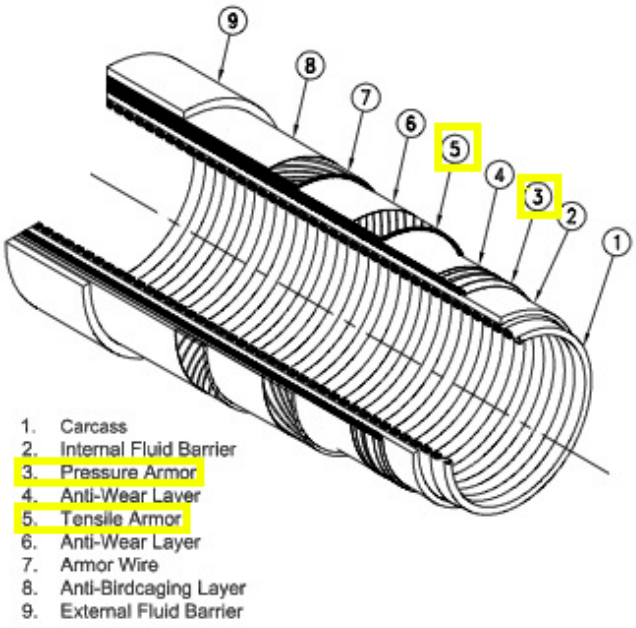

Figure 2.5: Basic Layers of Flexible Pipe, (Y.Zhang et al., 2003)

Table 2.1 gives a brief explanation the functions of the standard layers in a flexible pipe.

Layer	Function
Carcass, interlocked metallic layer	Supports hydrostatic pressure and fluid barrier against collapse
Internal pressure sheath, extruded polymer layer	Provides internal fluid integrity
Pressure-armor, interlocked metallic layer	Supports the internal pressure sheath and system internal-pressure loads in the radial direction $\rightarrow$ Hoop strength resistance
Cross-wound tensile armor, metallic wires	Gives tensile-stress resistance
Outer sheath, extruded polymer sheath	Provides external fluid integrity

Table 2.1: Description of structural layers

When applying flexible unbounded pipes in offshore environments, the top connection or the outlet of the guide tube, is most prone to fatigue damage. The principal loads affecting the pipe in such environments are axial tension, bending and internal pressure. In addition, the tensile armoring layers will be introduced to alternating tensions from both high frequency, HF, and low frequency, LF, motions of the floating vessel and hydrodynamic forces.
The tensile armor and the pressure armor layers, marked yellow in figure 2.5, limit the service life of the flexible pipe, hence the main focus in a fatigue life analysis is on these two layers of the pipe (Y.Zhang et al., 2003).
DNV presents a recommended practice for a typical riser fatigue assessment procedure, (DNV, 2005b). The basic procedure can be illustrated by a flow chart as given in figure 2.6.

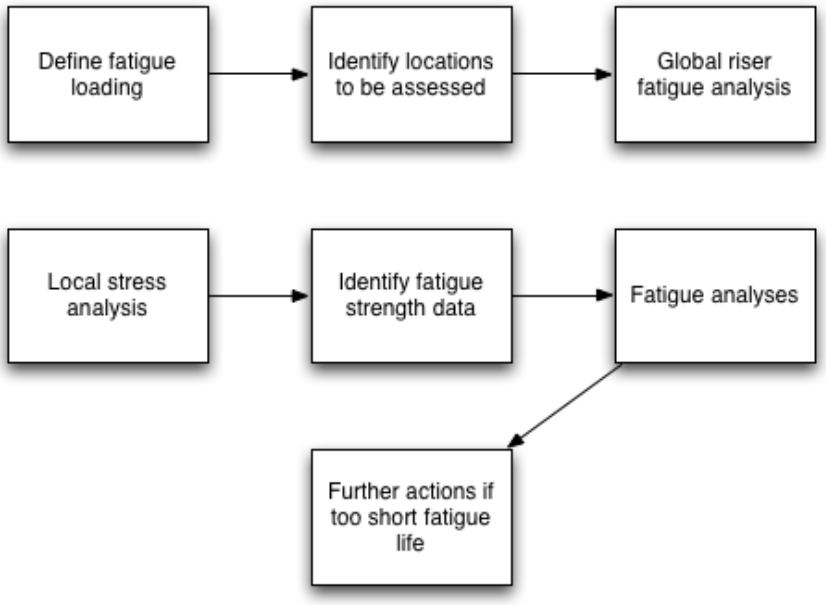

Figure 2.6: Fatigue assessment, (DNV, 2005b)

The following originate from (DNV, 2005b).

With reference to figure 2.6, the steps of the procedure are briefly explained.

The fatigue loading is based on operational limitations from wave frequency, WF, LF and vortex induced vibration, VIV, effects. When identifying the locations to be assessed in the analysis, structural discontinuities such as the intersection between bend stiffener and riser should be regarded. In the global riser fatigue analysis, short-term nominal stress range distributions for each identified location are computed.
The hot spot SCF is obtained from finite element analysis or parametric equations, and can be determined by a local stress analysis. When identifying the fatigue strength data, S-N curves are widely used. The S-N curves give the basic fatigue capacity depending on factors such as environment, construction details, fabrication and contents of the pipe, e.g. amount of CO_2 and/or H_2S.
In the fatigue analysis, the fatigue damage is computed from weighted short-term fatigue damage. There are different ways to go about to improve the fatigue capacity of the riser. Among these, a more refined stress analysis can be performed, change in detail geometry or in system details, or to apply fracture mechanics analysis.

Section 2.2.2 will present the procedure of fatigue assessment in tensile and pressure armor layers.

2.2.1 Failure Modes

Pipelines and risers are designed for a lifetime in the order of 20-25 years. At the Norwegian offshore sector, the average flexible riser has been in service for only around 50% of its planned service life,(Hokstad et al., 2009). Hence, it is important to have knowledge of possible failure modes for the decided pipe application. Flexible risers are likely to be affected by a number of conditions that may change the integrity of the riser. Due to the complex structure where different materials are interacting, several different failure modes are possible.

(Hokstad et al., 2009) presents typical failure modes for an unbounded flexible pipe, listed in table 2.2.

Global failure	Potential failure mechanisms
Collapse	- Collapse of carcass and/or pressure armor due to excessive tension - Collapse of carcass and/or pressure armor due to excess external pressure - Collapse of carcass and/or pressure armor due to installation loads or ovalisation due to installation loads - Collapse of internal pressure sheath in smooth bore pipe
Burst	- Rupture of pressure armors because of excess internal pressure - Rupture of tensile armors due to excess internal pressure
Tensile failure	- Rupture of tensile armors due to excess tension - Collapse of carcass and/or pressure armors and/or internal pressure sheath due to excess tension - Snagging by fishing trawl board or anchor, causing overbending or tensile failure
Compressive failure	- Birdcaging of tensile armor wires - Compression leading to upheaval buckling and excess bending
Overbending	- Collapse of carcass and/or pressure armor or internal pressure sheath - Rupture of internal pressure sheath - Unlocking of interlocked pressure armor layer or tensile armor layer - Crack in outer sheath
Torsional failure	- Failure of tensile armor wires - Collapse of carcass and/or internal pressure sheath - Birdcaging of tensile armor wires
Fatigue failure	- Tensile armor wire fatigue - Pressure armor wire fatigue
Erosion	- Of internal carcass
Corrosion	- Of internal carcass - Of pressure armor or tensile armor exposed to seawater, if applicable - Of pressure armor or tensile armor exposed to diffused product

Table 2.2: Failure modes for design of flexible unbounded pipes,(Hokstad et al., 2009)

From table 2.2, it is found that the failure modes for an unbounded flexible pipe mostly affect the carcass, pressure armor and tensile armor layers.

The following originate from (Hokstad et al., 2009):

The *carcass* may be exposed to failure modes such as overstretching, fatigue, radial collapse, wear, erosion, corrosion and damage from pigging and similar operations. Fatigue is not a common failure mode for the carcass, but it can be defined as a secondary damage as a result of initial damage in the production phase.

For the *pressure armor*, fatigue failure is a fundamental failure mode. When a pipe is introduced to cyclic bending, contact points of the pressure armor profile will slide cyclically generating substantial contact stress. The contact pressure will also vary cyclically as a consequence of the cyclic bending. For a Zeta profile of pressure armor, as illustrated in figure 2.13, problems occur since the contact stress leads to cross wire bending.
Fatigue failure of the pressure armor is usually due to sliding of the layers causing cyclic stresses in the cross-wire direction. In addition, fretting at the contact points affect the fatigue life of the pressure armors. Variation of curvature and side loads from a bend stiffener resulting in cyclic stresses longitudinal to the armor profile, may initiate fatigue cracking normal to the axis of the pressure armor.

For the *tensile armor*, probable failure modes can be overload in tension in combination with internal pressure. This can result in tensile failure overload in bending or compression, leading to birdcaging or wire disarray in torsion. The overload in tension can cause unwinding of the armor, birdcaging fatigue, corrosion fatigue, fretting fatigue, fatigue wear or induced cracking corrosion. The modes of failure are related to design an operational conditions, and not to the material properties.

Figure 2.7 illustrates a riser that has been subjected to birdcaging of the tensile armor wires.

Figure 2.7: Birdcaging of riser, given by SRT

2.2.2 Tensile and Pressure Armor Wires

The following originate from (oma, 2007):

For calculation of armor wire stresses in unbonded flexible pipes, the calculation will be a highly non-linear problem. The calculations are non-linear due to the complex cross-section of the pressure armor wires and contact forces between adjacent wires and adjacent layers. In addition, bending and combined frictional effects cause non-linear hysteretic behavior, which in turn cause relative movement between the structural layers of the pipe.
A methodology that has been suggested by (oma, 2007), include irregular-wave time-domain simulation with commercially available global analysis tools. Local analysis tools generate transfer functions for all stress components, and a post-processor combines the global time-histories of tension and curvature with the stress transfer functions. The result is combined wire stress time histories for strength or fatigue analysis.

Tensile Armor Wires

The tensile armor wires are applied to maintain the desired internal pressure and tensile load on the pipe. They are made of metallic wires that are laid helically in two or four layers with an angle of approximately 20^{o},(API, 2009). The design is important in terms of required axial strength and torsional properties of the pipe, (API, 2009). Figure 2.8 gives an illustration of the cross-section of an unbounded flexible pipe, where the tensile armors are marked red.

For tensile armor wires, the significant alternating stresses are caused by

1. Variation of effective tension in the pipe from HF and LF motions of the floater.
2. Variation of curvature in the pipe from HF and LF motions of the floater.
3. Variation of internal pressure in pipe.

Compared to the effect from curvature and effective tension, the variation of internal pressure is very low. Due to this, and the fact that the internal pressure has no significant effect on the mean stresses in the tensile wire, it is often neglected in a fatigue analysis, (Y.Zhang et al., 2003).
During pipe bending, torsional loads will contribute to additional alternating stresses. Similar to the variation of internal pressure, the torsional stresses are small in comparison to the axial stresses induced by change in curvature, and hence they can be neglected.

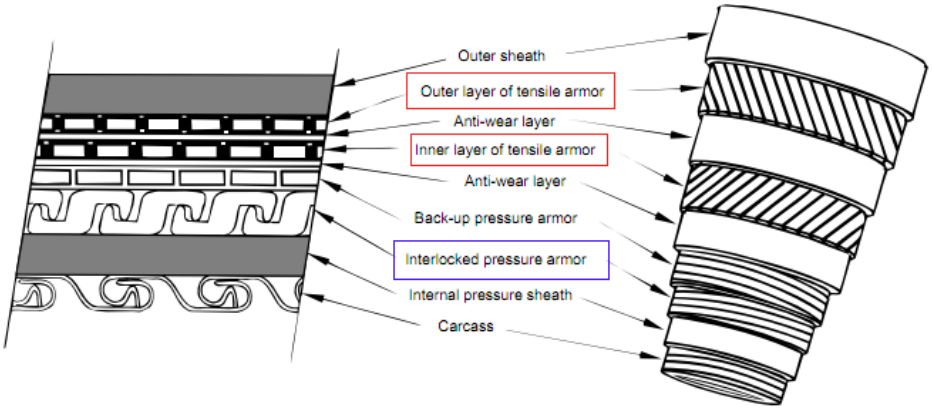

Figure 2.8: Cross section of unbounded flexible pipe, (API, 2008)

With reference to (Sævik, 2010b):
Fatigue of tensile armors due to bending loads can be described by the following:

- Low angles may lead to bending of each armor tendon.
- In addition to pure bending stress, friction stresses are presented.
- Fretting may occur as a result of metal to metal contact, but can be avoided by applying anti-wear layers.
- For corrosion fatigue cases, friction stresses are dominating.
- The armors will experience moderate contact pressure, e.g. $10MPa$.

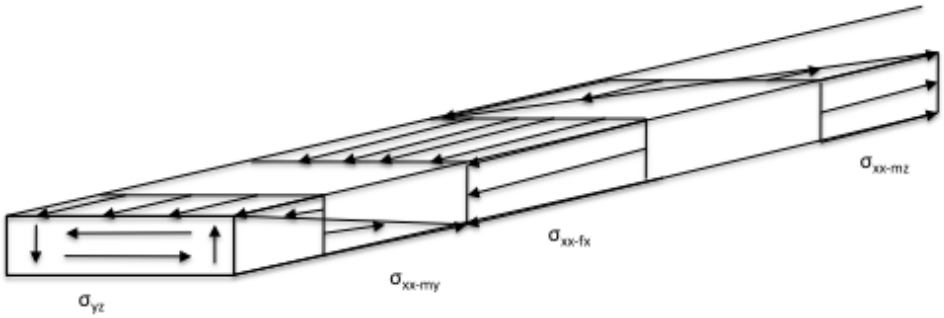

Figure 2.9: Stress components of armors, (Sævik, 2010b)

Figure 2.9 illustrates the stress components of a tensile armor.
The *axial stress*, σ_{xx-fx}, is constant over the entire armor cross-section. For tensile armors, the axial stress will be a result of the pressure axial force, F_x, friction, the riser tension and torsion moment.
The *normal curvature stress* is represented by σ_{xx-my} in figure 2.9. The maximum normal curvature stress is found at the outer and inner surface of the armor tendon at both compressive and tensile sides of the riser. The stress is caused by the bending moment, M_y, induced primarily due to riser bending.
The *transverse curvature stress* is illustrated as σ_{xx-mz}. The location of maximum transverse curvature stress is on the sides of the armor tendon at the neutral axis of the riser, and it is

caused by a bending moment, M_z, induced by global riser bending.
The final stress component illustrated in figure 2.9 is the *torsion stress*, σ_{yz}, caused by bending. Both normal curvature stress and the transverse curvature stress are bending stress components. They contribute to linear bending stress transfers functions at the corners of the tensile wire,(oma, 2007).

The following originate from (oma, 2007):
When a local analysis is carried out for an unbonded flexible pipe, the stress components of the tensile armor are evaluated. Axial and bending stress components are computed at each corner of the wire. By taking the sum of the axial stress component, the normal bending stress component and the transverse bending stress component, the total stress at each corner will be calculated.

The axial stress component is, as mentioned, affected by tension and friction. Hence, the axial stress component can be divided into two parts; one for axial stress due to torsion, and one part for axial stress due to friction. Considering the stress due to torsion, it will account for the overall pressure contribution. The stress will be linearly proportional to the global tension, based on the ratio between the axial stiffness of the wire and the axial stiffness of the riser.
The friction stress part is a non-linear function of curvature, tension, pressure and kinematic hardening.

Stick and Slip Regions

For an unbonded flexible pipe, stick and slip regions can be defined for the tensile wire layer. If the tensile wire does not move relative to the neighboring layer, it defines a stick region. The slip region represents movement or slips of the tensile wire on the top of the layer beneath. The critical curvature of the riser will separate the stick and slip regions.
The following originate from (Sødahl, 2009):

The tensile armor wires are helical elements that during cross-sectional bending will experience stick/slip behavior. Stick behavior will occur for low curvature when frictional forces prevent slip. If the frictional forces are exceeded, slip of the tensile wire will occur.
Slip in axial direction is determined as slip along a loxodromic curve.

Figure 2.10 illustrates relaxation of bending induced tension by slip from compression below neutral axis, NA, toward tensile region above NA.

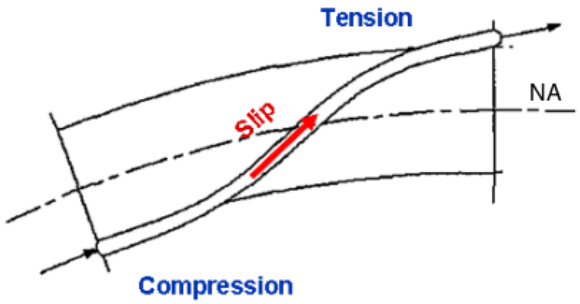

Figure 2.10: Slip in axial direction - along loxodromic curve, (Sødahl, 2009)

An axial slip initiation criterion states that slip occurs it the tension gradient exceeds the available friction:

$$\frac{dN_a}{ds} > f = q_i\mu_i + q_o\mu_o \tag{2.7}$$

where:

- N_a - axial force in helix element
- f - available friction force per unit length along helix element
- q_i - contact force per unit length along inner side of helix element
- q_o - contact force per unit length along outer side of helix element
- μ_i - friction coefficient for inner side of helix element
- μ_i - friction coefficient for outer side of helix element

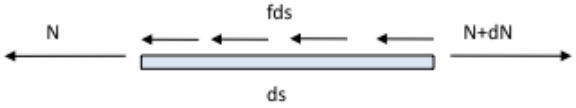

Figure 2.11: Axial slip initiation criterion, (Sødahl, 2009)

(oma, 2007) provides an example where the friction stress is a function of the riser global curvature. Tension, internal and external pressures are held constant. In the example, stress hysteresis curves are presented for frictional stress and riser global curvature, while the curves follow a pattern similar to a combined elasto-plastic and non-linear elastic material model. It is found that the slope of the stress development is constant in the stick region of the hysteresis curve, and non-linear in the slip region. Figure 2.12 illustrates a typical hysteresis curve for an example of the non-linear frictional stress component.

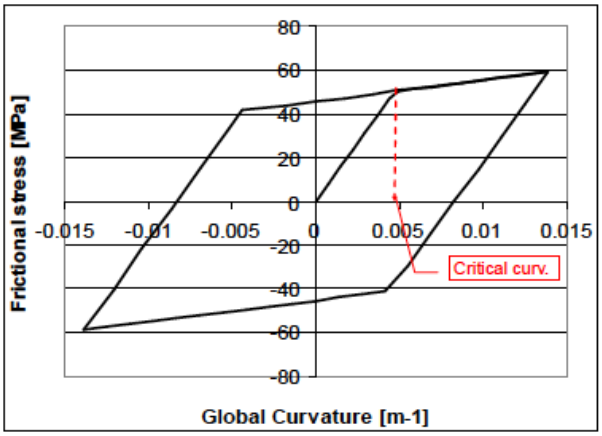

Figure 2.12: Typical hysteresis loop for non-linear frictional stress component, (oma, 2007)

In a physical point of view, the critical curvature can be assessed as a measure of the contact pressure between the tensile layer and its neighboring layers. The contact pressure is determined for a given tension and a set of internal and external pressure values. Thus, shifting the slip region to different critical curvatures corresponding to various tension levels can specify the frictional stress curve.

$$\text{Critical curvature corresponding to a specified tension level} \propto \frac{\text{Specified tension level}}{\text{Maximum tension}}$$

Pressure Armor Wires

The pressure armor wires are designed so that the requirements for hoop strength is achieved. They should account for gaps between the wires and also prevent loss of interlock. In a fatigue assessment, it is important to examine the alternating stresses affecting the pressure armor layers. The stresses are results from the relative motion of nearby pressure armor rings under high contact pressure at outer diameter, OD, and inner diameter, ID, of the layer.

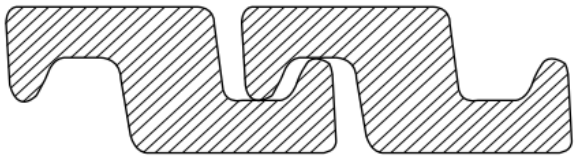

Figure 2.13: Typical pressure armor, Zeta profile, (API, 2008)

The following originate from (Sævik, 2010b):
For pressure armors, such as Zeta profile as illustrated in figure 2.13, the stress components can be illustrated as shown in figure 2.14. For the pressure armor, the stresses are assessed in three dimensions. Hence, σ_{yy}, σ_{zz} and σ_{yz} stresses occur along with σ_{xx}. The additional stresses will not be of importance for static loads, but they are governing for dynamic loads and fatigue. When considering the stress components described for the tensile armor in the previous section, additional information for the pressure armor must be accounted for.
For the pressure armor, the bend stiffener reaction forces also affect the bending moment resulting in normal curvature stress. The bending moment resulting in transverse curvature for a Zeta profile will also be influenced by rotation of the cross-section due to internal pressure. For pressure armors, additional local effects will cause torsion stress.

Fatigue of pressure armors due to bending loads can be described by the following, (Sævik, 2010b):

- Insignificant direct bending stresses will occur due to high lay angle
- Relative displacements between each winding will occur
- There will be high contact pressures with metal to metal contact, e.g. $100MPa$
- Metal contact may induce fretting fatigue or geometry change by wear
- Successful design at high internal pressures relies on moving the metal to metal contact area as far away from the pipe centre as possible, i.e. reduce contact pressure at metal to metal contact interface
- Dominating dynamic stress component due to alternating lift of the contact surface

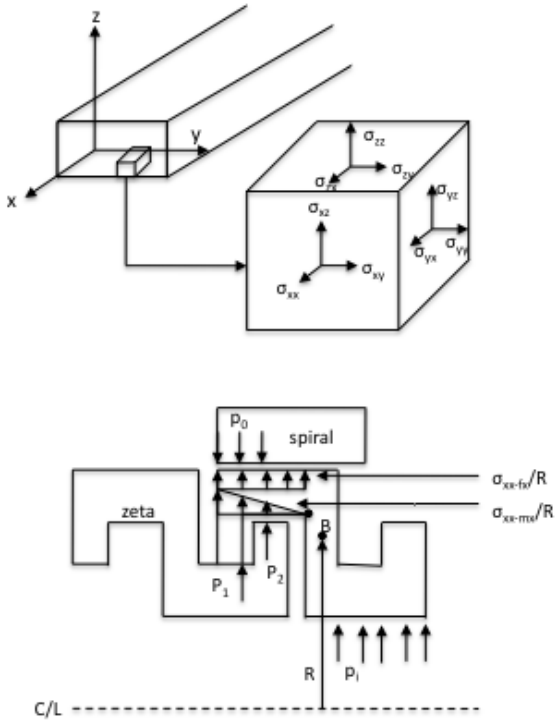

Figure 2.14: Stress components of pressure armors, (Sævik, 2010b)

2.2.3 Design Criteria for Steel Components

The following originate from (API, 2009):
Flexible pipes are designed to meet functional requirements under certain loading conditions. The loading conditions are defined by the purchaser of the pipe, and can be internal environment, external environment, system requirements and service life. (API, 2009) presents recommended annual probabilities of occurrence of the potential load cases for installation, and normal and abnormal loads for a 20-years service life, see table 2.3. Two load combinations should be examined when combining annual probabilities of waves and currents for 100-year conditions:

a) 100-year wave combined with 10-year current

b) 10-year wave combined with 100-year current

Type of load	Service condition		
	Installation	Service	
		Normal service	Abnormal service
Functional	Expected, specified or extreme value	Expected, specified or extreme value	Expected, specified or extreme value
External environment	Probability of exceedance according to season and duration of installation period	Yearly probability of exceedance $> 10^{-2}$	Yearly probability of exceedance between 10^{-2} and 10^{-4}
Possibility of abandonment	If abandonment is possible, the maximum weather in a period of three times the expected installation duration can be used. If abandonment is impossible, a more conservative approach shall be used or the duration of the operation reduced to a period where reliable weather forecast is available	The environmental load may be reduced such that the yearly probability of joint occurrence is $> 10^{-2}$ if combined with an accidental load	The environmental load may be reduced such that the yearly probability of joint occurance is $> 10^{-4}$ if combined with an accidental load
Accidental	As appropriate to installation method	As appropriate to normal operation conditions, i.e. annual probability $>10^{-2}$	Individual considerations. Yearly probability between 10^{-2} and 10^{-4}.

Table 2.3: Recommendations on annual probabilities for installation, and normal and abnormal operation for a 20-year service life,(API, 2009)

Ultimate Limit State

The following originate from (Paik & Thayamballi, 2011):
If the pipe does not collapse when exposed to the design loads, the ultimate limit state, ULS, is satisfied, (Wikipedia, 2011b). Structural design criteria for prevention of ULS are accordingly based on plastic collapse or ultimate strength. Considering a comparison of ultimate strength and the applied load effects, the safety margin of the structure can be assessed, as illustrated in figure 2.15. It is important to assess the ultimate load-carrying capacity together with the design load to gain a safe and economic structure. The ULS design criteria can be expressed by equation 2.8:

$$D_d < C_d \text{ or } \text{ safety measure} = C_d/D_d > 1 \tag{2.8}$$

where

- $\mathrm{D}_d = \gamma_0 \sum_i D_{ki}(F_{ki}, \gamma_{ki})$ = Design 'demand'
- $\mathrm{C}_d = C_k/\gamma_M$ = Design 'capacity'
- $\mathrm{D}_{ki}(F_{ki}, \gamma_{ki})$ = Characteristic measure of demand for load type i
- C_k : Characteristic measure of capacity
- $\gamma_M = \gamma_m \gamma_c$: Capacity-related safety factor
- γ_m and γ_c: Partial safety factor for material properties and the structure, respectively.
- γ_f : Partial safety factor related to loads
- γ_0 : Partial safety factor related to the seriousness of the particular limit state
- F_k : Characteristic measures of load

For ULS, C_d is the ultimate limit strength and D_d is related to load or demand measure.

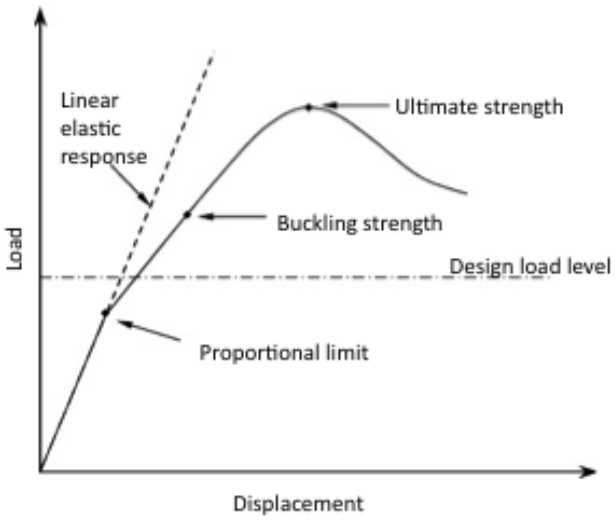

Figure 2.15: Structural design considerations based on ULS,(Paik & Thayamballi, 2011)

With reference to table 2.4, the recurrent operation is defined as an ULS condition.

Figure 2.16 illustrates an example of the sequence of steps in evaluating a limit state, ULS. Each limit state can be related to varius failure mechanisms. For each failure mechanism a relevant mathematical description, i.e. a failure criterion, has to be found.

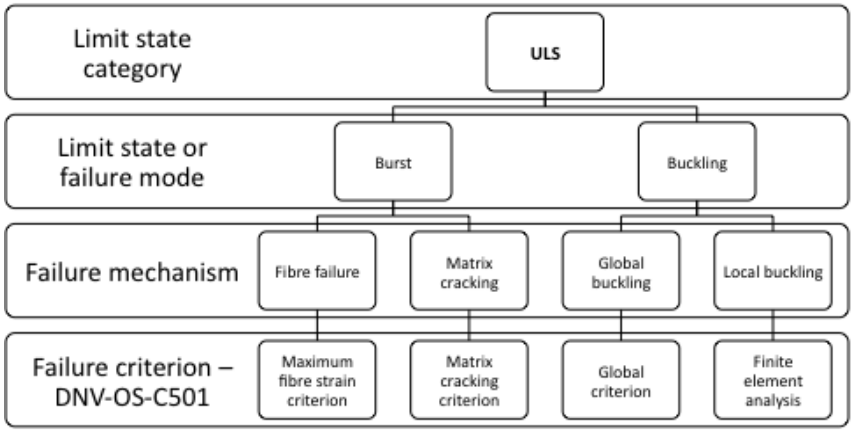

Figure 2.16: Evaluation of ULS, provided by SRT

Accidental Limit State

The following originate from (Paik & Thayamballi, 2011) and (API, 2008):
Accidental limit state, ALS, design for steel structures may be described by the three following objectives:

- to avoid loss of life in the structure or the surrounding area
- to avoid pollution of the environment
- to minimize loss of property or financial exposure

An important aspect of the ALS design is to make sure that the main safety functions of the structure are not damaged during any accidental occurrence or within a time period after the accident. When analyzing load cases for an accidental event, the analysis should be based on an assessment of the probability of the event occurring. For flexible pipes, accidental events can be impact from trawl boards and dropped objects, or broken mooring lines and loss of buoyancy. When evaluating the robustness of the pipe design in dynamic applications, extreme-event load cases are applied.
Two steps assess the integrity of the structure in ALS design:

1. Evaluation of the structural performance against design accident events
2. Computation of post-accident effects, e.g. damage to the environment

Extreme operation and abnormal operation from table 2.4 are defined as ALS conditions. The abnormal operation is additionally defined as a survival condition, even though the loading condition is still the same as for the extreme operation load case.

Fatigue

The following originate from (Paik & Thayamballi, 2011) and (API, 2008):
The fatigue life of a flexible pipe should be calculated in accordance with requirements based on service life. A criterion defined by (ISO, 2006) states that the predicted fatigue life should be at least 10 times the service life.
If the fatigue analyses result in stresses above the material endurance limit, then fatigue damage calculations must be performed. The fatigue calculations shall be carried out for tensile and pressure armor layers in dynamic application by applying Miner's method and design S-N curves. It is relevant to take into account the damage due to cycles with stresses below the endurance limit.
General design of an unbonded flexible pipe assumes that the outer sheath is never ruptured. For service life analysis in dynamic application it is still important to find the length of time to failure of the tensile and pressure armors when the outer sheath is ruptured and the annulus is flooded by seawater. A situation like this is described as an accidental situation, and the calculated service life determines the time before replacement of the pipe.

(ISO, 2006) presents a list of conditions that steel wires shall be subjected to under testing and evaluation, the S-N data should document these conditions:

a) Exposed to air, at atmospheric pressure, at temperature of 12^oC to 23^oC, with wires as rolled and degreased and tested to manufacturer's specifications

b) Exposed to seawater at atmospheric pressure, at a temperature of 12^oC to 23^oC, with wires as rolled and degreased and tested to manufacturer's specifications

c) Exposed to the predicted annulus environment for relevant transported fluids, with wires as rolled and degreased and tested to manufacturer's specifications

Design Criteria from ISO 13628-2

An unbounded flexible riser is built up by a combination of polymeric and metallic layers. The metallic, or steel layers are the pressure- and tensile-armor layers and the internal carcass. Other steel components are the end fittings. The pipe layers should be designed in accordance to (ISO, 2006).

The following sections originate from (ISO, 2006):

Pressure and Tensile Armors
For pressure and tensile armor layers, the utilization shall be calculated as utilization equals stress divided by structural capacity. The stress applied in the calculation is the stress in the actual layer, worked out from a design methodology specified in ch.6.2.1 of (ISO, 2006).

The stress calculation should involve the dynamic loads, and it should be based on the average stress in the layer. The average stress is found by calculations based on a uniform distribution of the total layer load over all the wires of the layer.

The structural capacity of the pressure and tensile armor layers should be either the yield strength, or 0.9 times the ultimate tensile strength of the material. The yield strength is defined by either the mean value minus two standard deviations from documented test data or as a minimum value certified by the supplier.

Tables 2.4 to 2.6 gives the design criteria for stress in pressure and tensile armor layers with reference to yield limit of the material. Tables originate from international standard (ISO, 2006).

Service condition			
	Normal operation		Abnormal Operation
	Recurrent operation	Extreme operation	
	Functional and environmental	Functional, environmental and accidental	Functional, environmental and accidental
Pressure armors	0.55	0.85	0.85
Tensile armors	0.67	0.85	0.85

Table 2.4: Pressure and tensile armor layer design criteria, Service condition

Installation		
	Functional and environmental	Functional, environmental and accidental
Pressure armors	0.67	0.85
Tensile armors	0.67	0.85

Table 2.5: Pressure and tensile armor layer design criteria, Installation

Hydrostatic pressure test – FAT and field acceptance	
Pressure armors	0.91
Tensile armors	0.91

Table 2.6: Pressure and tensile armor layers, Hydrostatic pressure test

Internal Carcass

The utilization of the internal carcass depends on three water-depth ranges. Buckling failure modes should be evaluated for the carcass and pressure armors, and the layers must meet the design requirements.
(ISO, 2006) defines design requirements for internal carcass as:

a) Collapse with minimum specified internal pressure, maximum external pressure, maximum pipe ovality, and pipe bent to an agreed bend radius. The external pressure shall be either the full external pressure acting on the outside of the internal pressure or the maximum annulus pressure if this exceeds the external pressure.

b) Fatigue in the carcass

c) Crack growth along the carcass strip due to bending-induced stresses in interlocked spirals. The carcass design shall be in such way that crack growth shall not occur.

d) Loads induced by thermal expansion and contraction, and/or swelling of the internal pressure sheath.

e) Erosion and corrosion.

The support provided by the pressure armor layer is accounted for by hydrostatic collapse calculations. Collapse-failure mode caused by pressure build-up between pressure sheath and neighboring sacrificial layers should be evaluated if relevant. According to (ISO, 2006), the design criteria for the internal carcass are defined for stress buckling load. For all conditions, i.e. service condition, installation and hydrostatic pressure test – FAT and field acceptance, the design criteria is divided into three water-depth ranges.

$$[0.67] \text{ for } D_{max} \leq 300m$$

$$\left[\left(\frac{D_{max} - 300}{600}\right) \times 0.18 + 0.67\right] \text{ for } m < D_{max} > 900m \tag{2.9}$$

$$[0.85] \text{ for } D_{max} \geq 900m$$

where D_{max} is the maximum water depth including tidal and wave effects.

Illustration of a cross-section of internal carcass is given in figure 2.17.

Figure 2.17: Cross-sectional illustrations of internal carcass, provided by SRT

Auxiliary Steel Components

The following sections originate from (ISO, 2006):
End-fittings, as illustrated in figure 2.18, on flexible pipes are designed to provide reliable termination of all pipes. The function of end-fittings is to prevent leakage, structural deformation and pullout of wires or extruded layers during service life. The design requirements, accounting for all physically possible load combinations, must apply for the pressure-containing parts of the end-fittings. The requirements are given by equation 2.10:

$$\sigma_t \leq n \times \sigma_y \tag{2.10}$$

$$\sigma_e \leq n \times \sigma_y$$

where:

- σ_t : Tensile hoop stress
- σ_e : Equivalent stress
- n : Permissible utilization factor

The permissible utilization factors for service condition, installation and hydrostatic pressure test are given in appendix E.1.

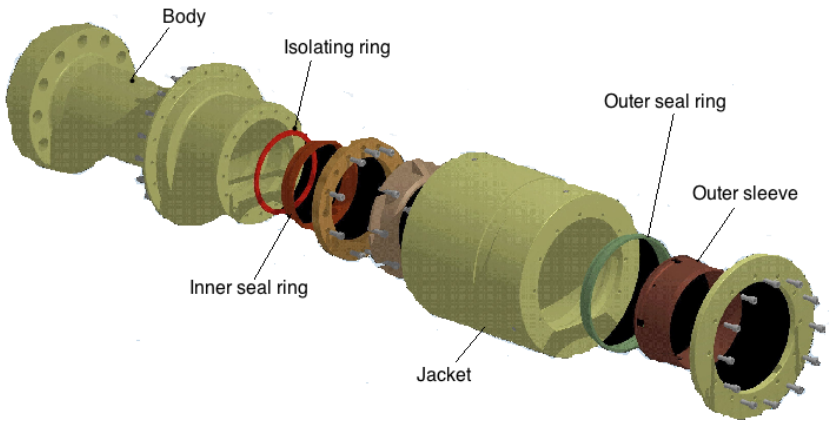

Figure 2.18: Layers of end-fitting, provided by SRT

3 Introduction to the Theory of Bflex v.2010

Bflex *(v2010)* is a software developed for stress analysis of tensile armors in flexible pipes exposed to pressure, tension and bending loads. The mathematical approach applied in the software is a combination of a FE approach and the Principle of Virtual Displacements. This combination together with co-rotated kinematics description enables geometric, material and contact non-linearity. This approach is applied when handling dynamic stresses due to bending of flexible pipes in fatigue calculations. In Bflex *(v.2010)*, a separate mathematical model is applied for initial conditions for static stresses from tension, torsion and internal and external pressure.

The armor tendons are helically wound around the pipe. Bending the pipe into a constant curve radius, two limit curves will appear. These are called loxodromic and geodesic curves, illustrated along a bent cylinder in figure 3.1. The difference between the two is that the geodesic curve has associated transverse slip while the loxodromic curve has no transverse slip. With reference to (Sævik, 1992), it is found that the displacements transverse to tendon during one dynamic cycle will be small. Thus, analytical description can be applied for the bending of the armor tendons if it is assumed that the initial path of the tendons is kept during bending. It is reasonable to assume that the relative displacements only occur in the longitudinal direction. This implies that a loxodromic curve can be assumed for elastic bending.

With this, it can be assumed that:

- The friction stress due to relative displacement between layers is only a result of longitudinal slip
- The elastic torsion and bending stresses can be found by differential geometry

(oma, 2010)

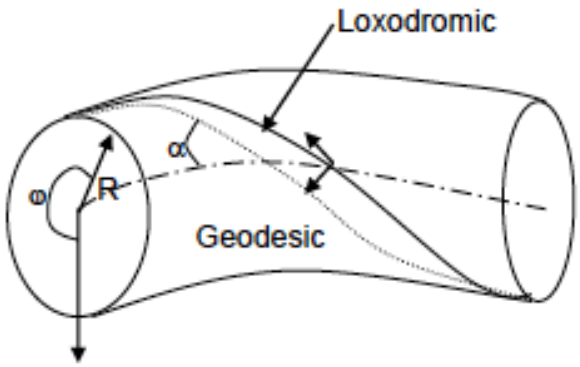

Figure 3.1: Loxodromic and geodesic curves along bent cylinder, (Sævik, 2010a)

Elastic Torsion and Bending Stresses

From figure 3.2 an illustration of a riser cross-section illustrated with vectors $\mathbf{g}_i$ of arbitrary length directed along the centre line and principal axes of a tendon.

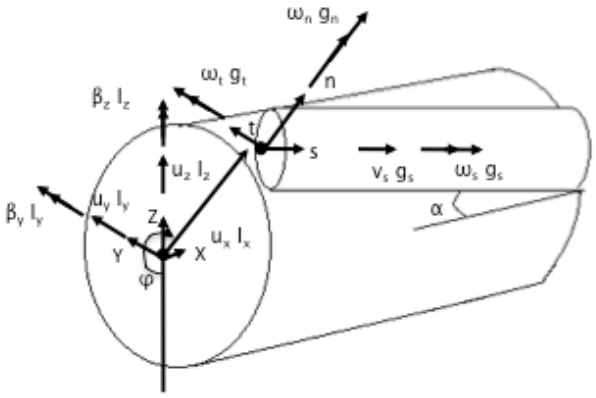

Figure 3.2: Kinematic quantities, (oma, 2010)

To find the total torsion and curvature components $\boldsymbol{\kappa}_i$ along the loxodromic curve, the Serret-Frenet formula is applied as:

$$\boldsymbol{\kappa}_s = -\frac{\boldsymbol{g}_t}{|\boldsymbol{g}_t|} \cdot \frac{\frac{d\boldsymbol{g}_n}{ds}}{|\boldsymbol{g}_n|} \tag{3.1}$$

$$\boldsymbol{\kappa}_t = -\frac{\boldsymbol{g}_n}{|\boldsymbol{g}_n|} \cdot \frac{\frac{d\boldsymbol{g}_s}{ds}}{|\boldsymbol{g}_s|} \tag{3.2}$$

$$\boldsymbol{\kappa}_n = -\frac{\boldsymbol{g}_t}{|\boldsymbol{g}_t|} \cdot \frac{\frac{d\boldsymbol{g}_s}{ds}}{|\boldsymbol{g}_s|} \tag{3.3}$$

By applying equation 3.1 – 3.3 and subtracting the initial torsion and normal curvature quantities found for a straight cylinder, the following results are obtained.

$$\omega_s = sin\alpha cos^3\alpha(cos\varphi\beta_y + sin\varphi\beta_z) \tag{3.4}$$

$$\omega_s = -cos^4\alpha(cos\varphi\beta_y + sin\varphi\beta_z) \tag{3.5}$$

$$\omega_s = cos\alpha(1 + sin^2\alpha)(sin\varphi\beta_y - cos\varphi\beta_z) \tag{3.6}$$

Equation 3.4 – 3.6 are given in terms of torsion and curvature quantities ω_i , and the global bending quantities β_y and β_z . φ is the angular coordinate starting at negative z-axis and α is the lay angle, see figure 3.1.

Bending of a pipe will result in shear stresses between armor tendons and supporting layers. This gives reason for an assumption of uncoupled axisymmetric and bending strains.
Bflex2010 divides the tensile armor model into two various formulations:

- A sandwich beam formulation (SBM), described in section 3.1
- A moment formulation (MM), described in section 3.2

The following sections originate from (Sævik, 2010a) and (oma, 2010).

3.1 Sandwich Beam Formulation (SBM)

The sandwich beam formulation is based on solving the equilibrium equations for the tendons and supporting beam structure. The approach is formulated in terms of the Potential Energy for each tendon, equation 3.7.

$$\prod = \frac{1}{2}\int_0^l EA\left(\frac{dv_s}{ds}\right)^2 + \frac{1}{2}k(v_s - v_p)^2 ds - Pv_p \tag{3.7}$$

- EA : Axial stiffness
- v_s : Actual longitudinal displacement along the tendon
- v_p : Tendon displacement if plane surfaces remain plane after bending deformation
- k : Shear stiffness
- P : External loading

The shear stiffness, k, is a non-linear stiffness parameter. It describes the friction stick-slip behavior.

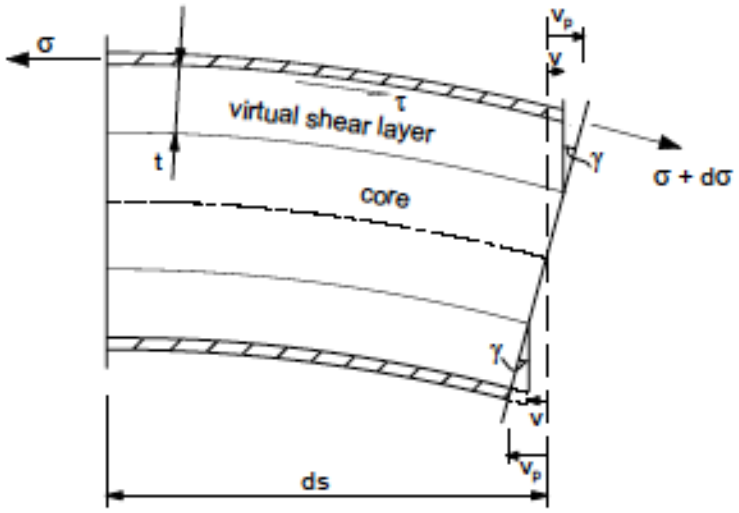

Figure 3.3: Sandwich Beam Theory, (Sævik, 2010a)

The sandwich beam method is illustrated in figure 3.3, where shear deformation γ over a thickness t, is defined by

$$\gamma = \frac{v_s - v_p}{t} \tag{3.8}$$

the shear stiffness, k, is then defined by

$$k = \frac{Gb}{t} \tag{3.9}$$

where G is the shear modulus and b is the width of the beam. The boundary conditions for each tendon will influence the result since the model includes each tendon, hence the end effects will be included.

3.2 Moment Formulation (MM)

The moment formulation is applied when the equilibrium equations are established based on a friction moment approach. The method is described on stress resultant level. This indicates that no single tendon end effect is handled since none of the boundary conditions for each tendon is taken into account.

The friction coefficient between the layers of the pipe is the governing parameter regarding both the global behavior of the pipe and the response in terms of stress in the tensile armor layer. The pipe will at first behave as a rigid pipe in compliance with Navier's hypothesis. At some point, slip will occur between the layers. This happens because the shear stress at the neutral axis of bending is exceeding the shear capacity governed by friction; see section 2.2.2, chapter 2.

If a cross-section is exposed to further bending into a given curvature, the cross-section will be divided into two parts. With reference to figure 3.4, part II represent the part of the cross-section that is in the slip domain after bending, and part I will still be in the stick domain. The tensile side of the cross-section is represented as the upper right part of figure 3.4. Considering one quarter of the cross-section and the tensile side, an angle φ_o define the transition between the regions, equation 3.10.

$$\varphi_0 = cos^{-1}\left(\frac{\beta_{yc}}{\beta_y}\right) + \frac{\pi}{2} \tag{3.10}$$

The critical curvature β_{yc} is defined at the initial slip with equilibrium along the helical path, equation 3.11:

$$\beta_{yc} = \frac{\mu\left(q_r^i + q_r^{i+1}\right)R}{EAcos^2\alpha sin\alpha} \tag{3.11}$$

Where EA is the stiffness of the tendon, μ is the friction coefficient and ${q_r}^i$ represent the radial load per unit length along the helix path acting on interface i of the tendon.

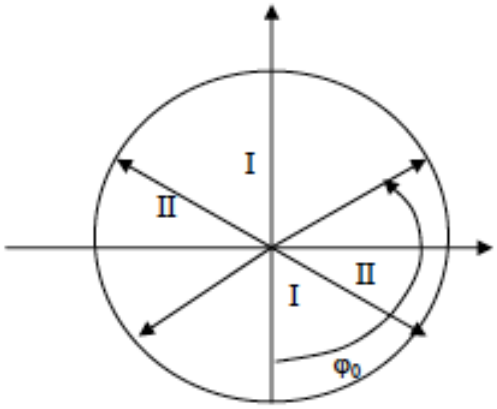

Figure 3.4: Slip Sones of a cross-section, (Sævik, 2010a)

With this, the stress distributions along region II and I can be expressed respectively by equation 3.12 and 3.13:

$$\sigma(\varphi) = \frac{\mu\left(q_r^i + q_r^{i+1}\right)R}{sin\alpha A}\left(\varphi - \frac{\phi}{2}\right) \tag{3.12}$$

$$\sigma(\varphi) = Ecos^2\alpha R\beta_y sin(\varphi - \varphi_0) + \frac{\mu\left(q_r^i + q_r^{i+1}\right)R}{sin\alpha A}\left(\varphi - \frac{\phi}{2}\right) \tag{3.13}$$

where:

- R : Layer radius
- A : Cross-sectional area
- α : Lay angle of tendon
- E : Young's modulus

The cross-section stress reaches its full value in case of full slip, equation 3.14:

$$\varphi = \varphi_0 = \pi \tag{3.14}$$

The full stress, ${\sigma_f}^i$, is given by equation 3.15:

$$\sigma_f^i = \frac{\pi}{2}\frac{\mu\left(q_r^i + q_r^{i+1}\right)R}{sin\alpha A} \tag{3.15}$$

By making use of the previous equations, a start slip bending moment from layer i can be defined:

$$M_c^i = \frac{R^2\mu\left(q_r^i + q_r^{i+1}\right)n_t}{2tan\alpha} \tag{3.16}$$

Where n_t is the number of tendons in the layer.

If full slip is assumed for the layers, then a friction moment M_f^i contribution from one tendon layer i with n_t tendons can be described by:

$$M_f^i = \frac{2R^2\mu\left(q_r^i + q_r^{i+1}\right)n_t}{\pi tan\alpha} \tag{3.17}$$

After calculating the bending moments and curvatures, a moment-curvature model can be constructed. Figure 3.5 illustrates an idealized moment-curvature model that is divided into three regions.

1. Region I - the stick region where plane surfaces remain plane
2. Region II - the stick-slip region where one section of the quarter pitch is in the stick domain whereas the other part is in the slip domain
3. Region III - where the entire length along the quarter pitch is in the slip domain

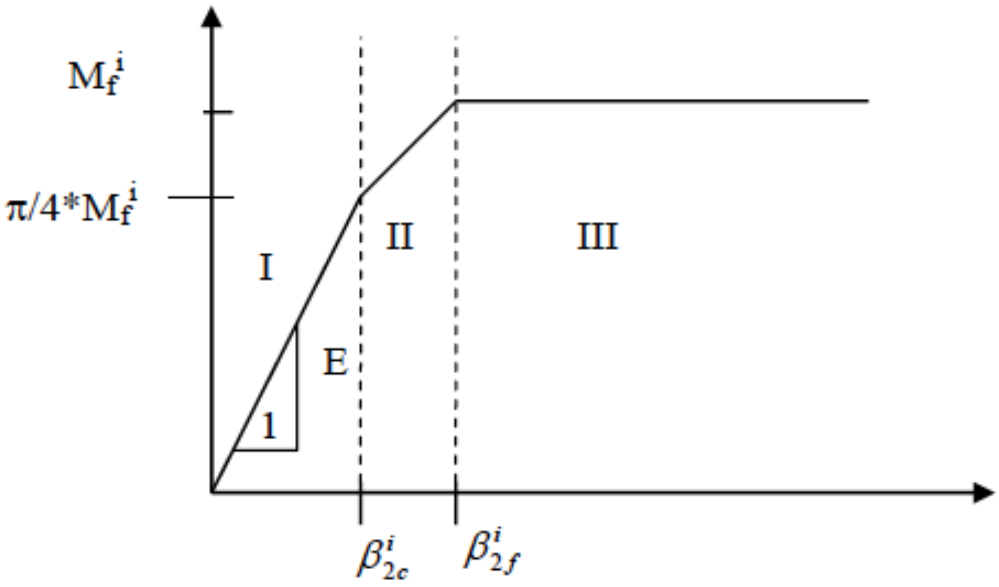

Figure 3.5: Moment-curvature model, (Sævik, 2010a)

Region II is defined by β_{2c}^i and β_{2f}^i, where the quantity β_{2f}^i depends on which cut-of level that is chosen for the moment level.

4 Analysis Methodology

The procedure of analyzing fatigue failure of a flexible riser in the bend stiffener area can be described by an analysis methodology as illustrated by the flow chart in figure 4.1.

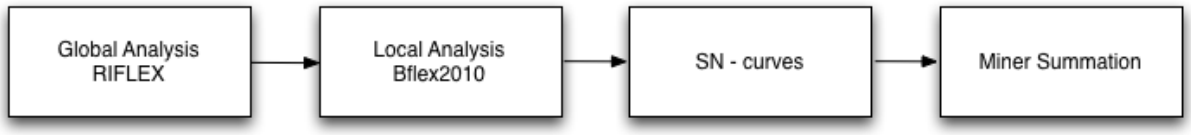

Figure 4.1: Analysis Methodology

Principally a global analysis is performed to obtain global loads on the riser configuration, and further on a local analysis is performed to find the stress distribution in the riser cross-sectional layers. The output obtained in the local analysis is applied in fatigue damage calculations where S-N curves and Miner summation method are used.

4.1 Global Analysis

For a typical riser configuration such as a free hanging catenary riser, a global analysis must be performed to obtain extreme interface loads acting on the configuration. For this to be performed, data of extreme environmental conditions must be known. The extreme environmental conditions include information of statistically calculated values, e.g. estimated significant wave heights, wave period and current speed in return periods of 10 years or 100 years. Given a *100-years* value of the wave height, it means the mean value of the estimated significant wave height which occur one time in a period of 100 years,(Myrhaug, 2007).
In the global analysis, the riser configuration will be introduced to different combinations of waves and currents from various headings.

In the design of offshore structures it is also important to observe how the sea state varies with the lifetime of the construction, so-called long term statistics. The number of storms or extreme wave heights experienced by the construction is helpful input parameters when performing a global analysis to establish long term distribution of fatigue loads. Scatter diagrams are common tools in computation of long term distribution of waves. The diagrams gives a statistical relationship between the significant wave height and the wave period, (Myrhaug, 2007).

Figure 4.2 gives a segment of a typical scatter diagram for individual wave heights with associated wave periods.

Period → Height ↓	0 – 2	2 – 4	4 - 6	6 - 8	8 - 10	10-12	12-14	14-16	16-18	18-20	20-22	22-24	Total
0.0-0.5	85171	166779	50632	10991	2167	425	110	25	13	7	5	0	316325
0.5-1.0	11867	208032	229458	111698	40289	11835	2862	547	132	49	17	0	616786
1.0-1.5	322	47777	164356	145537	73169	27184	7458	1481	271	55	32	0	467642
1.5-2.0	6	6545	64094	85930	53460	23925	7570	1592	266	41	25	0	243454
2.0-2.5	0	742	19753	38224	27785	14938	5669	1263	190	37	13	2	108616
2.5-3.0	0	82	5311	14769	12522	8057	3290	798	149	11	3	0	44992
3.0-3.5	0	6	1277	5433	5522	4149	1907	510	90	10	3	0	18907
3.5-4.0	0	1	309	2006	2350	1963	987	265	51	3	0	0	7935
4.0-4.5	0	0	69	733	1117	973	535	168	33	1	0	0	3629
4.5-5.0	0	0	12	234	513	507	321	60	11	0	0	0	1658
5.0-5.5	0	0	4	83	230	271	165	52	6	0	0	0	811
5.5-6.0	0	0	1	30	115	123	86	23	4	0	0	0	379

Figure 4.2: Typical Scatter Diagram, (A.Maia, 2005)

The global analysis can be performed in structural analysis programs such as RIFLEX, which is based on FE modeling of flexible riser structures. Results obtained from the global analysis can be applied in a local analysis of the riser. If the local analysis involves the top part of the riser or typically the bend stiffener area, important output parameters for further application are the maximum top tension and the bending angle of the riser.

4.2 Local Analysis - Bflex2010

The local analysis of the riser section can be performed in a taylor made software named Bflex,*(v2010)*. The theory behind this software is briefly described in chapter 3. A local analysis tool is required to predict local wire tension, curvatures, and contact pressure form variation of dynamic wire geometry. Additionally, bending restrictions from bend stiffeners must be accounted for.

The model in the local analysis will include a section of the riser, with all the structural layers, and a bend stiffener, see figure 4.3. The output from the global analysis is included in terms of tension and bending angle. In addition, values of the external and internal pressure of the riser, normally given for the specific field, are needed in the analysis.

The main result obtained from a local analysis are series of stress distribution, found for all critical fatigue locations in the riser layers. It is important to check that the stress in armoring and pressure wires are acceptable compared to relevant guidelines. The curvature achieved from Bflex *(v.2010)* should be the same as for the global analysis and acceptable according to design regulations [1].
Other variables of interest are pressure, temperature and material properties. These parameters are important when doing parametric studies concerning the effect on stress level in the bend stiffener area.

Figure 4.3: Illustration of a typical Bflex model

4.3 S-N Curve and Miner Summation Method

When both the global and the local analysis are performed, evaluation of fatigue failure is the next point of interest. When applying S-N curves for fatigue calculations, the focus is on the steel layers of the riser cross-section. From the local analysis, series of stress distribution have been obtained for the steel layers of the riser cross-section. Each steel layer has its own material property, and thus its own S-N curve.

Each stress range contributes to a number of wave cycles in the long term distribution. Comparing this number of cycles with the S-N curve for the selected steel layer, the damage sum can be computed. The total fatigue damage is calculated from summation of each damage sum using the Miner-Palmgren rule, equation 2.5 in section 2.1.2.

[1] Keep in mind that the curvature in the bend stiffener area will not be the same in the RIFLEX analysis and Bflex analysis since the riser is hinged in RIFLEX

5 Design of Bend Stiffener

The following sections originate from (Sødahl, 1991).
In the design of flexible pipes, problems involving the termination of flexible riser to a rigid structure are significant. One way to solve this problem is to introduce bend stiffeners at the supports. A bend stiffener will increase the bending stiffness of the flexible pipe to a greater value so that the pipe can be rigidly connected.
The design requirements essential for bend stiffener design are curvature and support forces. In terms of curvature, it is important that the critical curvature will not be exceeded during the lifetime of the riser. The bend stiffener should be optimized to give minimum support forces, i.e. axial- and shear force, and bending moment at the support.

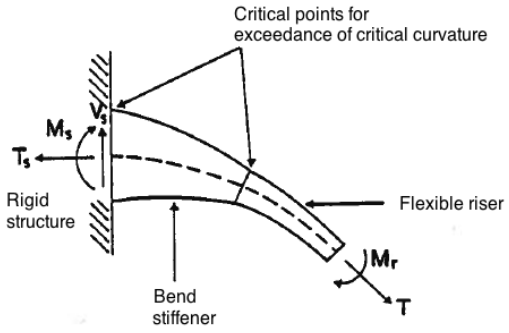

Figure 5.1: Bend stiffener used for connection to a rigid support, (Sødahl, 1991)

There are two areas of interest regarding sensitivity of exceeding the allowable curvature. As illustrated in figure 5.1, these areas are at the support and near the intersection point between the flexible riser and the bend stiffener. At the intersection point, a combination of a small axial force and a large force angle will be essential for exceeding of critical curvature. A large axial force may at the support give excess of the critical curvature. For a flexible unbounded pipe, the bend stiffener will commonly be introduced as a separate structure with varying diameter wrapped around the pipe, as illustrated in figure 5.2.

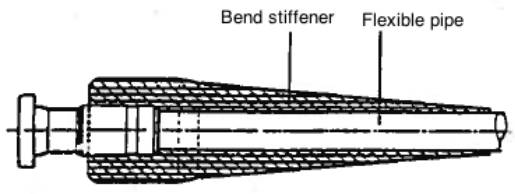

Figure 5.2: Type of bend stiffener, (Sødahl, 1991)

5.1 Methodology of Bend Stiffener Design

The basic principle of bend stiffener design is to find the length of the bend stiffener, and the bending stiffness distribution that does not exceed the critical curvature along the bend stiffeners for any load combination. As mentioned in the introduction to chapter 5, the bend stiffener should also be optimized to give minimum support forces.

In the design of bend stiffeners, the separate response model provides a good basis for the procedure. For a bend stiffener, the most important loadings are force, force angle and support rotations. Hence, loads from weight, buoyancy and hydrodynamic forces can be neglected in a local analysis. Additionally, the bending moment at the splitting point is negligible as it will not lead to any important loss of accuracy. External loadings are still considered in a final verification of the proposed bend stiffener design.

With a simplified design formulation, the loading on the local model will be reduced to time series of force, $T(t)$, and relative force angle, $\alpha_R(t)$. The relative force angle is given as:

$$\alpha_R(t) = \alpha(t) - \alpha_o(t) \tag{5.1}$$

where $\alpha_o(t)$ is the direction of the centerline at the support, with reference to illustration in appendix A. On the basis of the time series of T and α_R, a design space can be established. The design space is defined as all combinations of T and α_R, illustrated in figure 5.3:

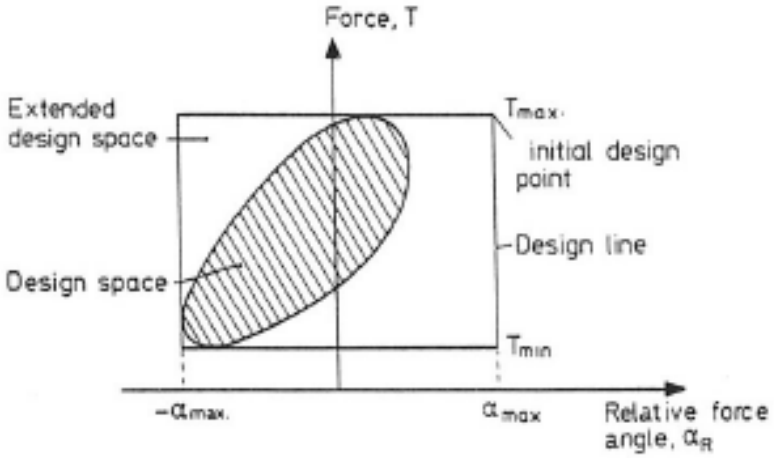

Figure 5.3: Design space, design line, and initial design point, (Sødahl, 1991)

where α_{max} is the maximum, absolute value of the relative force angle, and T_{min} and T_{max} are the minimum and maximum force.
By making use of a design line concept, the bend stiffener will be designed for all points along the design line and hence for the total design space. Additionally, due to symmetry, it will also be designed for an extended design space, figure 5.3. The design line concept gives a conservative design of the bend stiffener.
The design problem is reduced to finding the bending stiffness function so that the critical curvature is not exceeded for the design line. Furthermore, the length of the bend stiffener is important when considering the support moment. The supporting moment will be minimized if the bend stiffener is short. This can be illustrated by comparison of support moments of two bend stiffeners with constant radius of curvature, figure 5.4, where $R_2 > R_1$.

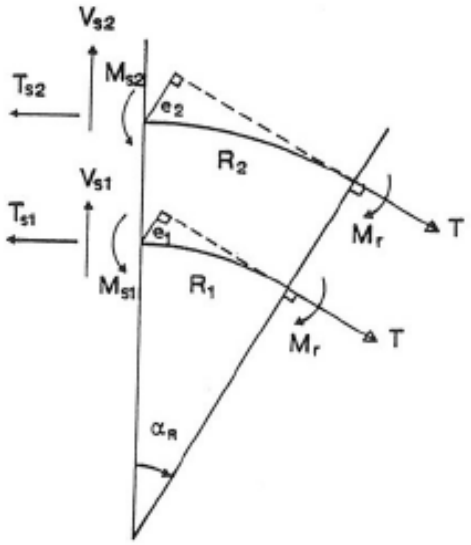

Figure 5.4: Comparison of support forces for two bend stiffeners with constant radius of curvature, (Sødahl, 1991)

In figure 5.4 :

- V : Shear force
- T : Force effective tension
- M_r : Bending moment at end of bend stiffener
- R : Radius of curvature
- α_R : Relative force angle

With reference to figure 5.4, the following is valid for the support moment M_s:

$$\frac{M_{S2}}{M_{S1}} = \frac{e_2 T + M_r}{e_1 T + M_r} \approx \frac{e_2}{e_1} = \frac{R_2}{R_1} \tag{5.2}$$

Equation 5.2 gives the relation that the support moment is proportional to the length of the bend stiffener. When loading along the bend stiffener, forces such as the support axial force and support shear force are not affected by the design of the bend stiffener, and hence they are neglected.

Further on, the design procedure is divided into an initial design and a final design.

5.1.1 Initial Design

For the initial design, the model is simplified by not including the riser part. With a simplification like this, there will be no interaction effect between the bend stiffener and the riser.
The basis for the initial design is the design equation expressing the bending stiffness distribution. The design equation gives constant radius of curvature along the bend stiffener for one specific design point.

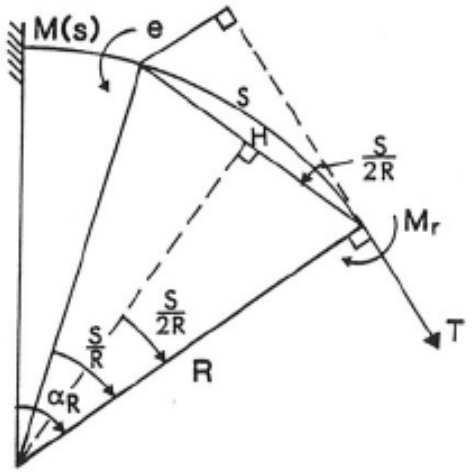

Moment equilibrium yields: $M(s) = eT + M_r$ where
$e = H\sin(s/2R) = 2R\sin^2(s/2R)$

Figure 5.5: Moment equilibrium of a bend stiffener, (Sødahl, 1991)

If considering the moment equilibrium, figure 5.5, the design equation can be found by evaluating the deflection of the centerline of the bend stiffener as a circle segment with radius R.

$$EI(s) = EI_r + 2TR^2 sin^2\Big(\frac{s}{2R}\Big) \tag{5.3}$$
$$0 \leq \mathrm{s} \leq S_B{=}\mathrm{R}\alpha_R$$

where:

- s : Length coordinate of bend stiffener
- S_B : Length of bend stiffener
- EI : Bending stiffness, where subscript r represent the riser

If a critical radius of curvature, R_c, is introduced at the initial design point (α_{max},T_{max}), the initial design, $EI_o(s)$, can be found by making use of equation 5.3. The result will be a favorable bend stiffener design with minimum length at the initial design point, where the length is given as:

$$S_{min} = R_c\alpha_{max} \tag{5.4}$$

5.1.2 Final Design

The final design is an improvement of the initial design, where the interaction between the riser and the bend stiffener is included. As for the initial design, the basis for the final design is the design equation expressing the bending stiffness distribution where the design equation gives constant curvature along the bend stiffener for one specific design point.

A common situation is that the initial design is unacceptable. A local maximum in the curvature near the intersection point can be due to exceedance of critical curvature along the bend stiffener. Thus, the degree of exceedance of the critical curvature for a given maximum force, T_{max}, will depend on the lower force value, T_{min}, in a force range at a fixed force angle α_{max}.

The initial design will give a bend stiffener that is to short and to stiff, so the procedure is stated as non-conservative. In the final design, a longer and more flexible bend stiffener is presented. The design equation is applied for a design radius of curvature $R_D > R_C$ and design force $T_D < T_{max}$, where the relative force angle is fixed at $\alpha_R = \alpha_{max}$.

The variables that need to be determined to obtain an ideal bend stiffener are R_D and T_D. By making use of the maximum curvature along the bend stiffener for all points on the design line as a function of R_D and T_D, expressed as $\kappa_{max}(R_D, T_D)$, the unknowns can be found numerically. The criteria for determining R_D and T_D are:

- Minimation of the length of the bend stiffener
- $\kappa_{max}(R_D, T_D) = \kappa_c = 1/R_c$

The following gives a typical iteration procedure described by (Sødahl, 1991):

1. Specify start value of radius for curvature $R_D^i = R_c$, as a parameter in the design equation 5.3.
2. For a fixed value of R_D^i, T_D^i is found. This gives the minimum value for κ_{max} according to the following procedure:
   i) Specify start value $T_D^i = T_{max}$
   ii) Calculate the bending stiffness function EI(s) for current estimates of T_D^i and R_D^i by use of the design equation 5.3.
   iii) Calculate κ_{max} for a finite number of points on the design line $T_{min} \leq T_j \leq T_{max}, j = 1, n$. this means that κ_{max} is based on n configurations calculated by the shooting method given the actual bending stiffness distribution EI(s).
   iv) If κ_{max} is minimum, T_D^i is identified as the design force that gives the best possible bending stiffness distribution EI(s) for the actual value of R_D^i (this is the best possible solution for any R_D^i if κ_{max} is identical to κ_c), go to 3.
   v) Calculate improved estimate of T_D^i, go to ii).
3. If $0 \leq \kappa_c - \kappa_{max} < \epsilon$ then Stop, final conservative solution is found within tolerance limit ϵ for maximum curvature. The final bending stiffness distribution is then given by the design values $T_D = T_D^i, R_D = D_D^i$.
4. Calculate improved estimate of R_D, go to 2.

The final solution obtained from the iteration procedure will give an optimum bending stiffness distribution. The bend stiffener will be longer and more flexible than the one obtained from the initial solution.

6 Design Basis for Analysis

6.1 Environmental Data

6.1.1 Wave and Current Data

In the global operation analysis, extreme values of current velocities are applied in 10- and 100-years conditions. The data applied originate from (A.Maia, 2005) and values for the different load cases applied are given in appendix C.1 – C.3 .

Current does not have any significant effect on the result in a dynamic fatigue analysis. Thus current is assessed as the most common south current surface velocity in the fatigue analysis, see appendix C.4.

The wave data applied in the analysis for long term distribution of fatigue loads, is based on a H_s-Tp scatter diagram, from Metocean data provided by Seaflex Riser Technologies, SRT, (A.Maia, 2005). The scatter diagrams are included in appendix B.1 and appendix B.2. Regarding the global operation analysis to establish extreme interface loads, an extreme wave parameter table, given by (A.Maia, 2005), is applied. The table represents waves approaching from all directions, and it is given in appendix B.3.

Regular sea is evaluated.

6.1.2 Hydrodynamic Coefficients

The hydrodynamic coefficients are given in table 6.1.

Coefficient	Value
Normal drag	1.2
Tangential drag	0
Normal added mass	1.0
Tangential added mass	0

Table 6.1: Hydrodynamic coefficients

6.1.3 Water Depth and Seabed Friction Coefficients

The water depth at the given field is set to 1750 m. Friction coefficients for the seabed are listed in table 6.2.

Components	Coefficients
Longitudinal	0.9
Transverse	0.35

Table 6.2: Seabed friction coefficients

6.2 FPSO Data

6.2.1 RAO Data

The data for the response amplitude operator, RAO, is provided by SRT.

The given RAO's for the vessel applies to the center of gravity, CoG. The RAO's are specified for four loading conditions of the vessel:

i) Ballast

ii) Intermediate 1

iii) Intermediate 2

iv) Fully loaded

For each of these loading conditions there will be three sets of RAO's defined:

- Extreme - used for extreme 100/10-year wave conditions
- Operation - used for abnormal 1-year wave condition
- Fatigue - used for fatigue conditions

The main difference between extreme, operation and fatigue is the level of damping for roll motion, with reference to figure 6.1. The damping will be largest for the extreme condition, intermediate for operation and lowest for fatigue.

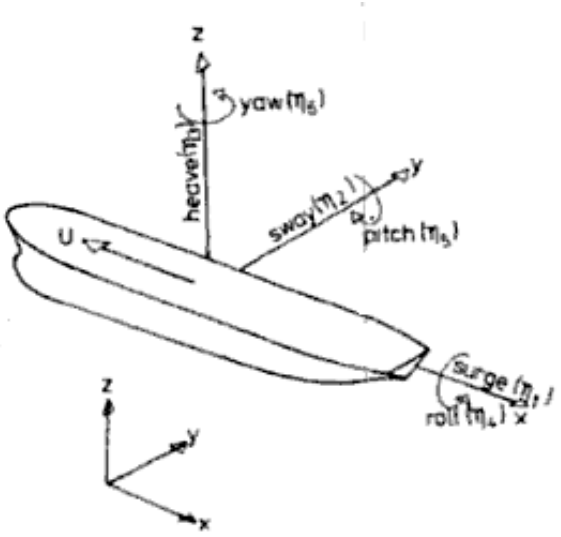

Figure 6.1: Illustration of the rigid body motions of a vessel, (Faltinsen, 1993)

6.2.2 Vessel Geometry

The basic vessel geometry is listen in table 6.3:

Description	Length [m]
Total length of FPSO	338.63
Length between perpendiculars	320.00
Bredth	53.60
Depth	24.40
Minimum operational draft	7.00
Medium operational draft	14.00
Maximum operational draft	21.00

Table 6.3: Vessel geometry, FPSO P-37

Medium operational draft is applied for the global extreme analysis.

An illustration of the main dimensions of the FPSO P-37 is given in figure 6.2.

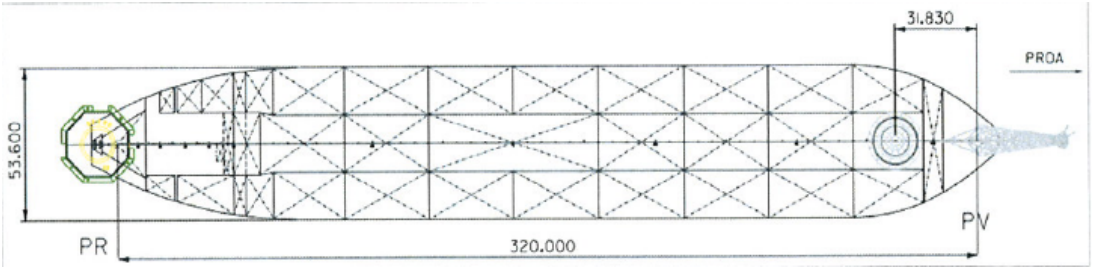

Figure 6.2: Illustration FPSO P-37 main dimensions

Tables describing different loading conditions are given in appendix D.

6.2.3 Turret Layout and Hang-Off Position

A simplified model of the riser system is developed in co-operation with SRT. The hang-off position of the riser is assumed to be 14 m below the water line. And the riser is set to a position following the FPSO in the x-direction. Sketches of hang-off position and turret layout are given in figure 6.3 and figure 6.4 respectivly.

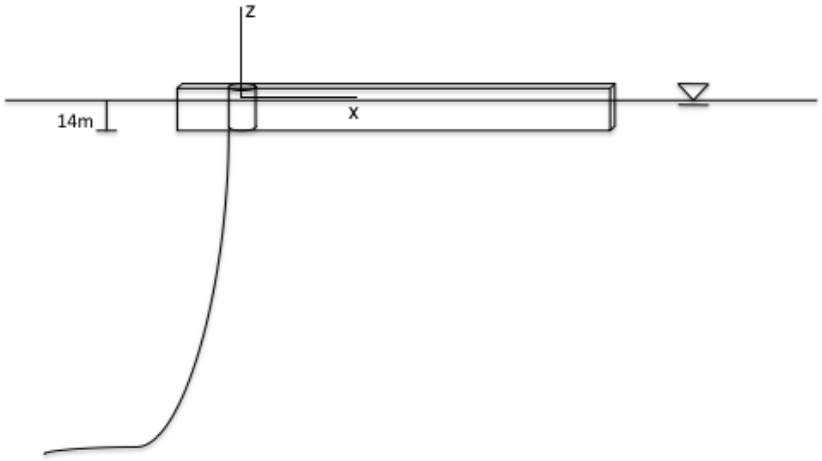

Figure 6.3: Illustration of hang-off point

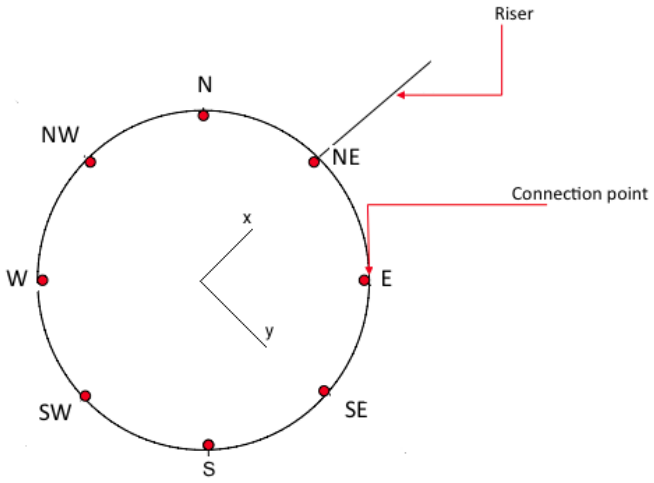

Figure 6.4: Illustration of turret layout

6.2.4 Vessel Offset

With reference to documentation given by SRT:
The vessel offset applied in the global extreme analysis is assumed as a centenary condition for an intact mooring system. The offset will be set to 9,9% of the water depth, with additional 1,5% of the water depth due to vessel positioning tolerance[1] and 7,5 m due to subsea equipment tolerance. The water depth is 1750 m, so the total offset is 207m.

Percent of water depth [%]	Offset [m]	Description
9.9	173.25	
1.5	26.25	Due to vessel positioning error
-	7.5	Due to subsea equipment error
Total	207	Total offset

Table 6.4: Vessel offset

In the fatigue analysis, offset is taken in accordance to one year offset and one year extreme wave height, H_s. This will be based on scatter diagrams given in appendix B.4.

Condition	Mooring system	Offeset [% of water depth]	Platform positioning error [% of water depth]	Subsea equipment positioning error [m]
Annual	Intact	5.6	1.5	7.5

Table 6.5: Vessel offset for fatigue analysis

The offset is calculated for each block in the fatigue analysis, by equation 6.1

$$\text{Offset} = \frac{\text{Annual offset}}{\text{Mean maximum wave height}} \cdot \text{Wave height of single block} \tag{6.1}$$

6.3 Riser System Design

6.3.1 Overview of Riser System

The riser system applied for the analysis is a simplification of a system used at the Jubarte field in Brasil. The orientation of true north, south, east and west are assumed to follow a vessel coordinate system with origo in the turret center, as illustrated in figure 7.2. The 11' riser will be extended in negative x-direction, accordingly northeast orientation.

[1] Installation tolerance which gives a range that needs to be considered

6.3.2 Riser System Configuration

A sketch of the riser configuration is illustrated in figure 6.5. Lengths and distances are given in table 6.6.

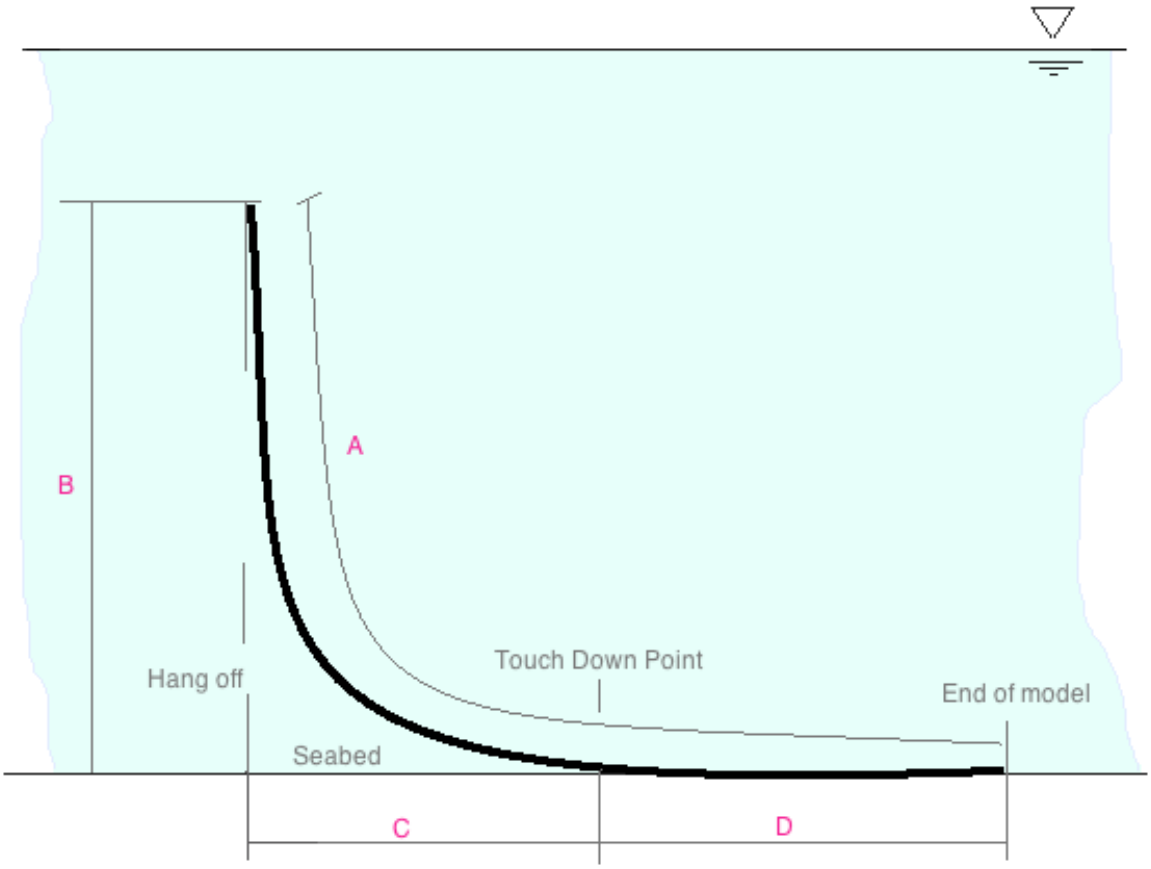

Figure 6.5: Illustration of a free hanging catenary riser configuration

Section, ref. figure 6.5	Length [m] of 11" riser	Description
A	2400	Total length of riser
B	1736	Vertical distance from seabed to hang-off
C	434.378	Horizontal distance from hang-off to TDP
D	565.622	Horizontal distance from TDP to end of model

Table 6.6: Riser lengths

6.3.3 Mechanical Properties

Mechanical properties for the 11" riser are listed in table 6.7.

Theoretical characteristics	Value	Unit
Diameter inside	279.40	mm
Diameter outside	450.70	mm
Volume internal	66.56	l/m
Volume external	159.54	l/m
Weight in air empty	398.74	kgf/m
Weight in air full of seawater	466.97	kgf/m
Weight in seawater empty	235.21	kgf/m
Weight in seawater full of seawater	303.44	kgf/m
Specific gravity in sea water empty	2.44	
Pressure nominal bursting	542	bars
Hydrostatic collapse pressure lay 0	234	bars
Damage pull in straight line	25643.60	kN
Minimum bending radius for storage	3.01	m
Bending stiffness at 20°	226.64	kN.m2
Axial stiffness	3.952	GPa
Torsional stiffness	33.03	MPa
Relative elongation at design pressure	0.029 %	
Relative elongation for 100 kN	0.003019 %	
Thermal exchange coefficient at 20°C	7.11	W/m.K

Table 6.7: Mechanical properties

From table 6.7, axial stiffness and torsional stiffness are found by the following equations, 6.2.

$$EA = \sum_{j=1}^{N_w} n_j EA_j cos^3\alpha_j \tag{6.2}$$

$$GI_t = \sum_{j=1}^{N_w} EA_j R_j^2 cos\alpha_j sin^2\alpha_j$$

where:

- EA : Axial stiffness
- n_j : Number of wires
- N_w : Total number of wires
- R_j : Radius to middle of wire
- α_j : Lay angle of wire
- GI_t : Torsional stiffness

The design properties are given in table 6.8.

Internal Diameter	11" Sweet service
Design pressure	310 bars
Design temperature	20 °C
Factory test pressure	465 bars
FTP/DP 1.50	

Table 6.8: Design properties

6.3.4 Riser Cross Section

The cross section of the riser is given in table 6.9.

Nº	Layer Description	UTS [MPa]	MYS [MPa]	Mass [Kg/m]	I.D. [mm]	Th. [mm]	SDP [MPa]
1	Interlocked Carcass	660	-	67.68	279.4	15.0	
3	Pressure Sheath RII SAN P40TL TPO			9.0	317.4	12.3	
4	Zeta Wire 12.0H FI 11	980	-	86.89	334.0	12.0	504
5	Anti-Wear Tape			1.62	358.0	1.5	
6	First Armor Lay. FI41 – 71 Flat wires: 14 x 6 at -25 deg.	1400	-	48.39	361.0	6.0	118
7	Anti-Wear Tape			1.69	373.0	1.5	
8	Second Armor Lay. FI41 – 73 Flat wires: 14 x 6 at 25 deg.	1400	-	49.84	376.0	6.0	140
9	Fabric Tape			0.78	388.0	1.3	
10	Anti-Wear Tape			1.76	390.6	1.5	
11	First Armor Lay. FI41 – 77 Flat wires: 14 x 6 at -25 deg.	1400	-	52.48	393.6	6.0	108
12	Anti-Wear Tape			1.83	405.6	1.5	
13	Second Armor Lay. FI41 – 80 Flat wires: 14 x 6 at 25 deg.	1400	-	54.59	408.6	6.0	134
14	High Strength Tape			2.74	420.6	3.35	
15	External Sheat HD-Flex (TP26+TP28) Yellow			15.35	427.3	11.7	

Table 6.9: Layer Description

6.3.5 Internal Fluid Density

The internal fluid density of the riser is given in table 6.10

Internal fluid	Density	Unit
Oil	800	kg/m3

Table 6.10: Internal fluid density

6.3.6 Bend Stiffener Material

Non-Linear Material

The non-linear material applied for the bend stiffener is polyurethane. Stress-strain curves for different temperature levels are given figure 6.6.

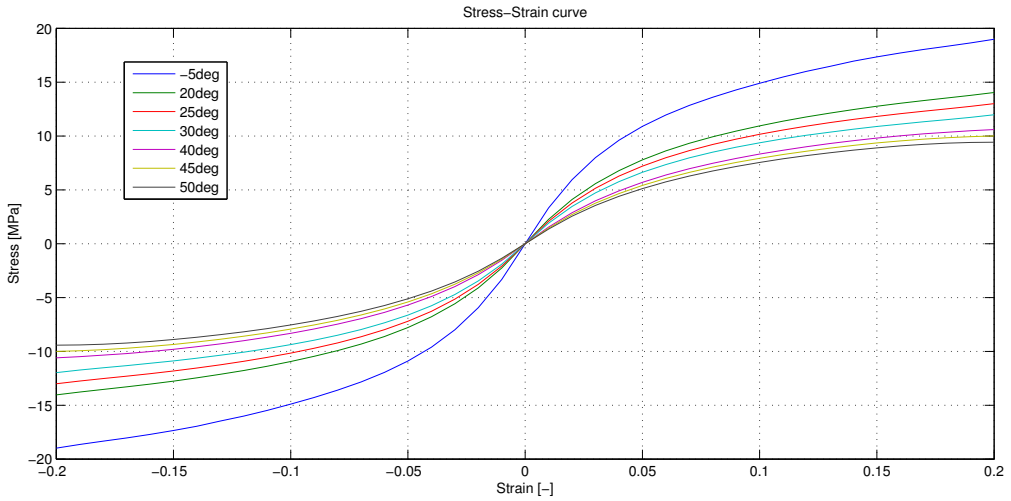

Figure 6.6: Stress-strain curves for bend stiffener with different temperature levels

A base case temperature level for the bend stiffener is chosen to be at 20°C.

Linear Material

The linear material applied for the bend stiffener is found from linear interpolation of the stress-strain curve values close to zero, given for 20deg.

Strain [-]	Stress [MPa]
-0.2	-36.22
0.0	0.0
0.2	36.22

Table 6.11: Input data for Bflex *(v.2010)* analysis

Table 6.11 gives the material properties for the bend stiffener to be applied in the Bflex *(v.2010)* analysis. The Young's modulus for the bend stiffener is found to be 181.1MPa.

$$\mathrm{E} = \frac{36.22 - (-36.22)}{0.2 - (-0.2)} = 181.1\mathrm{MPa} \tag{6.3}$$

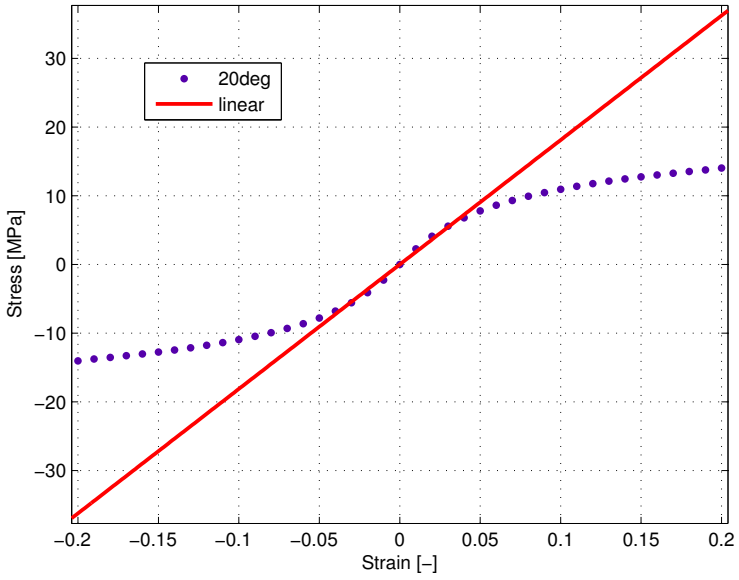

Figure 6.7: Stress-strain curve for bend stiffener with linear interpolation

6.4 S-N Curve Definition

The S-N curve applied in the fatigue analysis applies for a wet annulus environment with 0.2 bar CO_2. The data given in table 6.12 and 6.13 is provided by SRT.

Longitudinal Failure Mode						
No. of failure modes considered	No. of points in the fatigue S-N diagram	R-ratio	Method for taking the mean stress into account	Interpolation method in S-N diagram	SCF	Ultimate stress
1	2	0.1	1	1	1.0	1400

Table 6.12: Fatigue data for longitudinal failure mode, with reference to (Sævik et al., 2010)

Transverse Failure Mode					
No. of points in the fatigue S-N diagram	R-ratio	Method for taking the mean stress into account	Interpolation method in S-N diagram	SCF	Ultimate stress
2	0.1	0	1	1.0	1400

Table 6.13: Fatigue data for transverse failure mode, with reference to (Sævik et al., 2010)

The number of failure modes considered is only longitudinal failure mode, i.e. transverse cracks. The R-ratio is defined as:

$$R = \frac{\sigma_{min}}{\sigma_{max}} \tag{6.4}$$

The method applied for taking mean stress into account is the Goodman interpolation. The mean stress is calculated as $\sigma_{xx} + \sigma_{yy} + \sigma_{zz}$, where σ_{yy} og σ_{zz} only applies for the pressure armors. Both number of cycles to failure and stress are given in logarithmic scale, and the SCF is 1.0. The ultimate strength of the steel layer is 1400 MPa.

The stress ranges with corresponding number of cycles to failure are given in table 6.14.

Longitudinal Failure Mode		
Point no.	Stress range [MPa]	No. of cycles to failure
1	1	2.840E+21
2	1000	2.840E+03
Transverse Failure Mode		
Point no.	Stress range [MPa]	No. of cycles to failure
1	1	2.840E+21
2	1000	2.840E+03

Table 6.14: Fatigue data, with reference to (Sævik et al., 2010)

7 Global Analysis

7.1 Global Extreme Analysis

The global extreme analysis is performed for three different wave and current headings, i.e. near, far and transverse direction as illustrated in figure 7.2. Metocean data for 100– and 10–years values for regular waves and current are applied. The wave and current values are put on in combinations of 10–year wave with 100–year currents, and vica versa. Values applied for extreme wave parameters and current are found from (A.Maia, 2005), given in appendix B.3 and appendix C respectively.

Table 7.1 presents the six different load cases evaluated in the extreme analysis.

Load case no.	Floater position	Wave and current	Wave direction	Current direction	Wave height [m]	Wave period [s]
1	Far	10w100c	NE	SW	9.35	10.61
2	Far	100w10c	NE	SW	9.89	10.73
3	Near	10w100c	SW	NE	13.30	14.40
4	Near	100w10c	SW	NE	14.53	14.99
5	Transverse	10w100c	SE	NW	10.83	13.21
6	Transverse	100w10c	SE	NW	12.34	13.94

Table 7.1: Load cases for global extreme analysis, (A.Maia, 2005)

7.2 Results - Global Extreme Analysis

7.2.1 Static Analysis

A static analysis is performed, where the static equilibrium configuration for the single line is computed. Boundary conditions are known at both ends of the riser, and a feasible configuration is obtained. Typically, a static nominal angle is found to be approximately 4.2 deg. at the hang-off position. The static nominal angle is found by applying dummy elements in the RIFLEX analysis. One of the dummy elements follows the riser lay direction, while the other is orthogonal to this direction. When evaluating time series of the top-angle, the near and far load cases will be assessed with reference to the first dummy element, while a floater position in transverse direction is assessed with reference to the second dummy element.
Figure 7.1 illustrates the static riser configuration in xz-plane, with different floater positions. Floater positions are given in figure 7.2

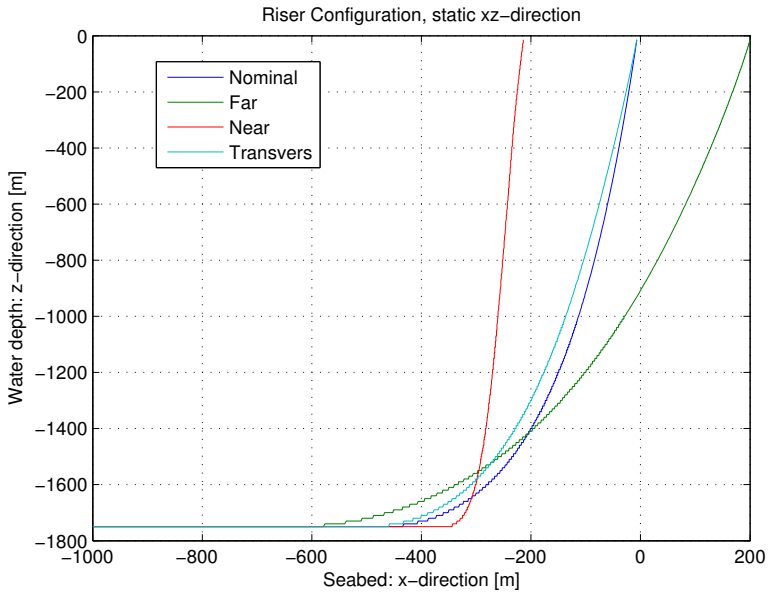

Figure 7.1: Static configuration with nominal, far, near and transverse floater position

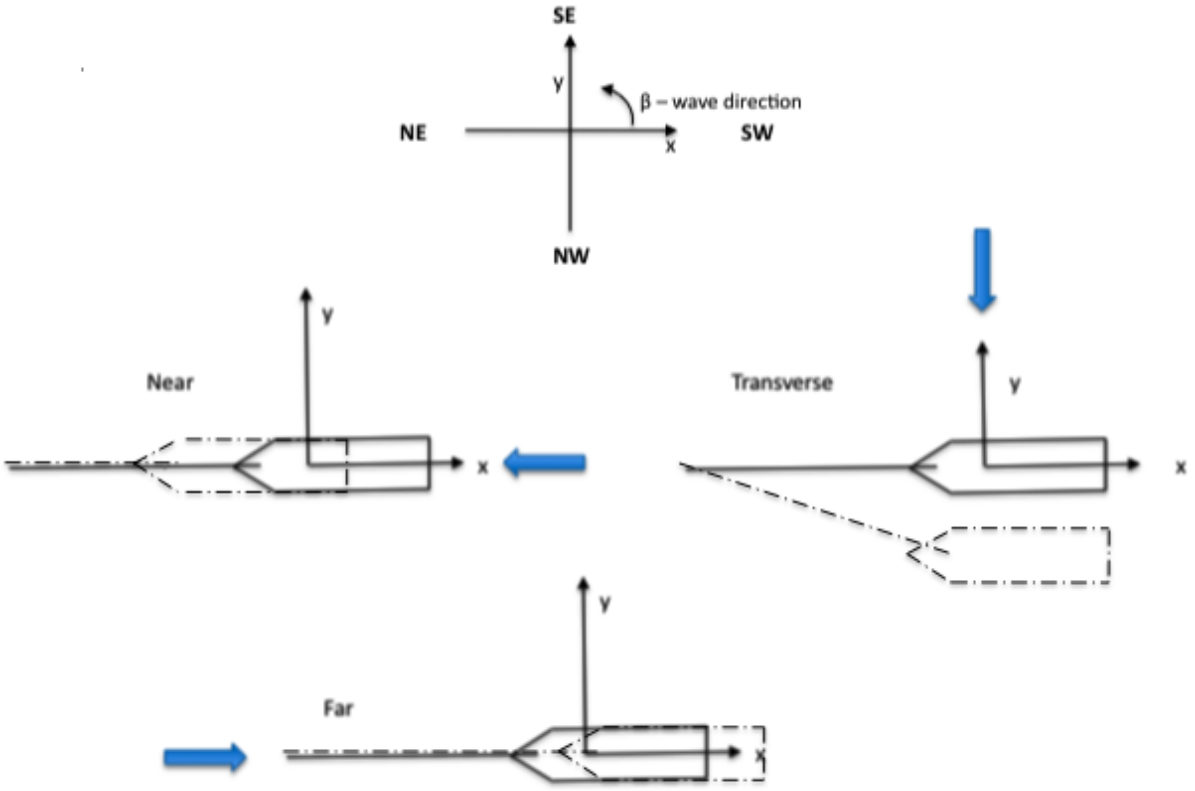

Figure 7.2: Illustration of vessel position for the different load cases

The blue arrow indicate wave propagation direction.

7.2.2 Dynamic Analysis

The dynamic analysis performed is a time domain analysis. It gives an indication on how the loads act on the configuration during a period of time. As mentioned in section 4.1, chapter 4, important output parameters from the global extreme analysis are the maximum top tension and the bending angle of the riser. It is also important to evaluate the curvature of the riser in critical areas, i.e. hang-off and TDP. The curvature obtained should not exceed the MBR, designed for the riser. MBR for storage is given in table 6.7 in section 6.3.3.

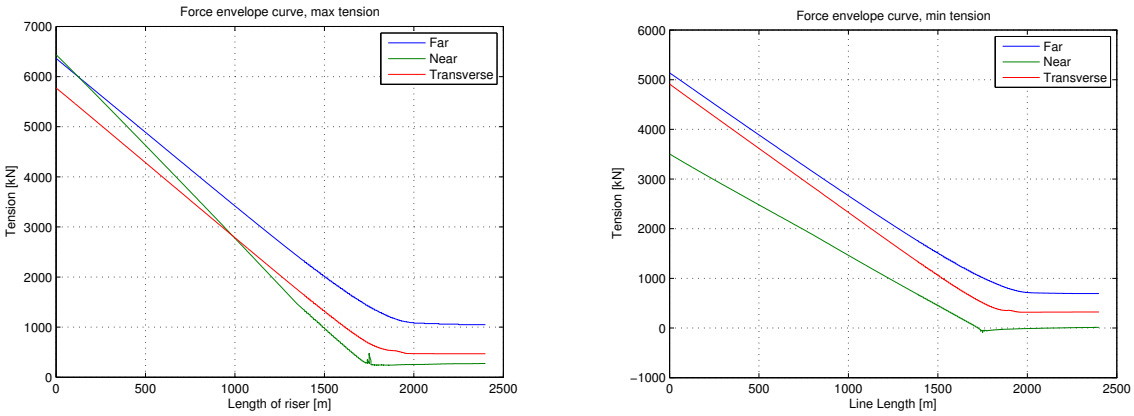

Figure 7.3: Max. and Min. force envelope curves for load case 1,3 and 5

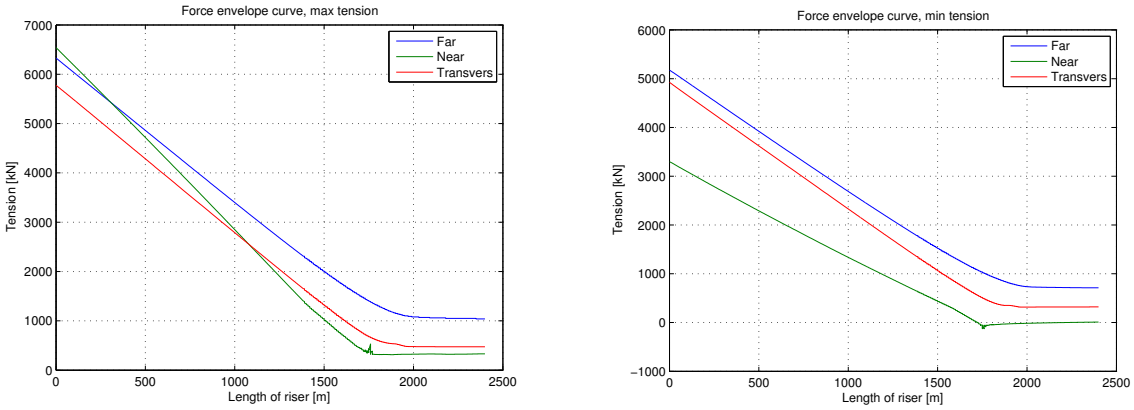

Figure 7.4: Max. and Min. force envelope curves for load case 2,4 and 6

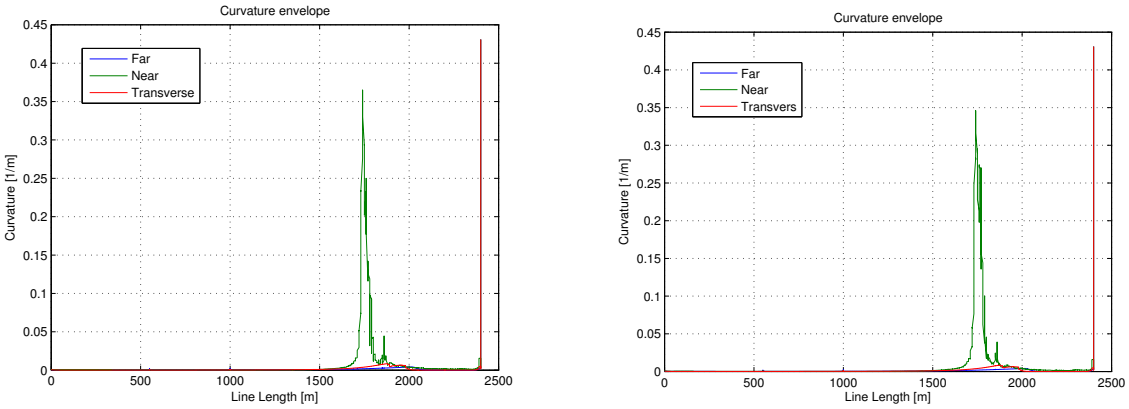

Figure 7.5: Curvature envelope curves for load case 1,3 and 5, and 2,4 and 6

From figure 7.3 and 7.4 it is found that load case 3 and 4 gives maximum top tension of the riser. When regarding the force envelope curves for minimum tension, it is important to evaluate the possibility of compression of the riser. Load case 3 and 4 indicate that compression may take place at the TDP. This is a common problem for free hanging catenary risers when the floater position is as represented by load case 3 and 4. Since the bend stiffener area is of interest in this thesis, compression at TDP will not be evaluated at this stage.

Figure 7.5 represents envelope curves for total curvature of the riser. The areas of a riser where the effect of curvature is most critical, is at hang-off and at TDP. From figure 7.5, it is found that there will be no significant curvature effect at hang-off. However, for load case 2 and 4, the curvature effect at TDP is substantial. Weather it is critical or not, can be calculated from equation 7.1. If the radius calculated is exceeding the MBR, then the riser configuration is suitable for its working area. It is important to keep in mind that numerical errors from the analysis may cause inaccurate results for the curvature.

$$Curvature = \frac{1}{Radius} \tag{7.1}$$

MBR for storage is given as $3.01m$, and the maximum curvature achieved from the global analysis is found in load case 4, as approximately $0.35m^{-1}$. This gives a radius of $2.857m$, equation 7.2, which is smaller than the MBR and hence not acceptable.

$$Radius = \frac{1}{0.35m^{-1}} = 2.857m < 3.01m \rightarrow \text{NOT OK!} \tag{7.2}$$

As for compression, curvature at TDP will not be evaluated further due to focus on the bend stiffener area.

Time Series

Time series are attained for axial tension and angle in the top of the riser for each load case. The values obtained from the time series are applied in bend stiffener design, chapter 8.

Table 7.2 represents some of the statistical values obtained of the time series, i.e. maximum and minimum results. Nominal angle is found to be 85.8130deg. and 90deg., in reference to dummy line one and two respectively.

Load Case	Max. Tension [kN]	Min. Tension [kN]	Max. Angle [deg]	Max. angle relative to nominal [deg]	Min. Angle [deg]	Min. angle relative to nominal [deg]
1	6362.5	5135.5	81.693	4.12	80.3	5.513
2	6327.5	5174.5	81.487	4.326	80.214	5.599
3	6436.0	3503.0	89.96	4.147	81.826	3.987
4	6538.2	3296.2	91.163	5.35	81.443	4.37
5	5770.2	4911.3	92.157	2.157	87.32	2.68
6	5773.3	4923.3	92.672	2.672	86.224	3.776

Table 7.2: Output from time series in global extreme analysis

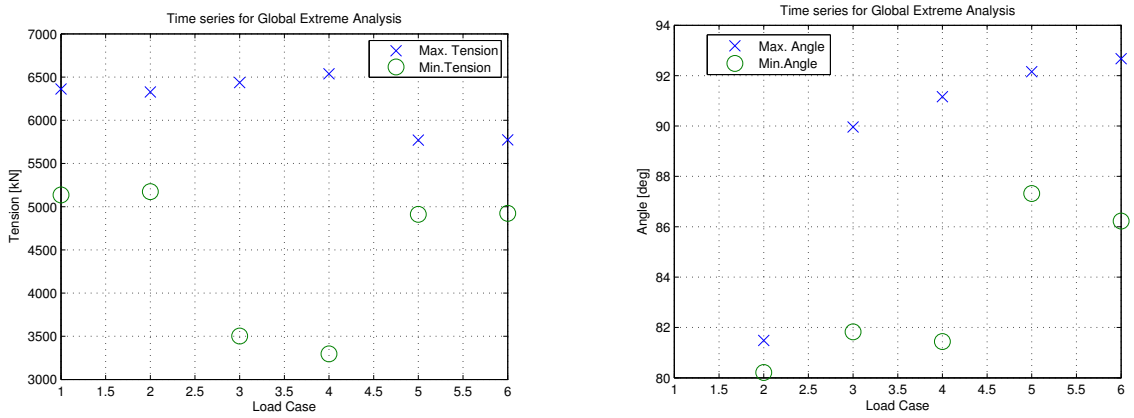

Figure 7.6: Time series for max/min tension and bending angle

8 Bend Stiffener

8.1 Introduction

The bend stiffener is designed with basis in the global extreme analysis results. SRT provides a design tool, Taper, which is a Microsoft Office Excel template. The template utilizes cross-sectional and material properties of the riser in combination with maximum tension and tension departure angle. Curvature and stress in armoring wires are assessed to be acceptable in accordance to relevant guidelines. The stresses will be evaluated in chapter 9.

8.2 Design Loads

The bend stiffener is designed with basis in the load case that gives maximum shear force during extreme analysis. The maximum shear force is found by evaluating time series of tension and angle in the root of the riser, i.e. at hang-off.

$$Max.shearforce = Tension \cdot sin(angle) \tag{8.1}$$

The maximum shear force found from the time series is $447.29kN$. This represents load case 2 from table 7.1 in section 7.1, where the maximum tension was $632.75kN$ in combination with an angle of 4.326 relative to static nominal angle.

8.3 Bend Stiffener Geometry

The geometry and properties found for the bend stiffener are given in table 8.1

Description	Data	Unit
Number of elements	20	-
Internal diamter	0.450	m
Stiffness of internal pipe	266	Nm^2
Length of taper	7	m
External diameter top	0.5	m
External diameter root	2.0	m
Tension (Max.Shear force)	447.29	kN
Departure angle of tension	4.350	deg
MBR for internal pipe	3.010	m

Table 8.1: Bend stiffener geometry

To achieve a satisfactory curvature, two cases are evaluated in Bflex*(v.2010)* for the extreme loads found in section 7.2.2, chapter 7.

The first case applies the load case with maximum fluctuation of the top angle in combination with maximum tension for this specific load case. The second case applies the same angle combined with the minimum tension for the specified load case, see table 8.2.

Case no.	Load case from global analysis	Angle [deg]	Tension [kN]
1	2	5.599	632.75
2	2	5.599	517.45

Table 8.2: Load cases for evaluation of curvature

The bend stiffener geometry is found by iteration of root diameter and length, so that a satisfactory distribution of the pipe curvature is provided. The bend stiffener design proposed, has a relatively large root diameter. From consultation with supervisor, it is decided to carry on with this design, even though the dimensions are a bit unusual.
Figure 8.1 illustrates the curvature distribution along the bend stiffener for both cases. It is desirable to have low values of curvature at the root of the bend stiffener and to distribute the curvature along the bend stiffener. It is also desirable to have minimum bending radius close to the middle of the bend stiffener. This is achieved for both cases, so the bend stiffener distributes a satisfactory curvature. A displaced contour of the bend stiffener is illustrated in figure 8.2.

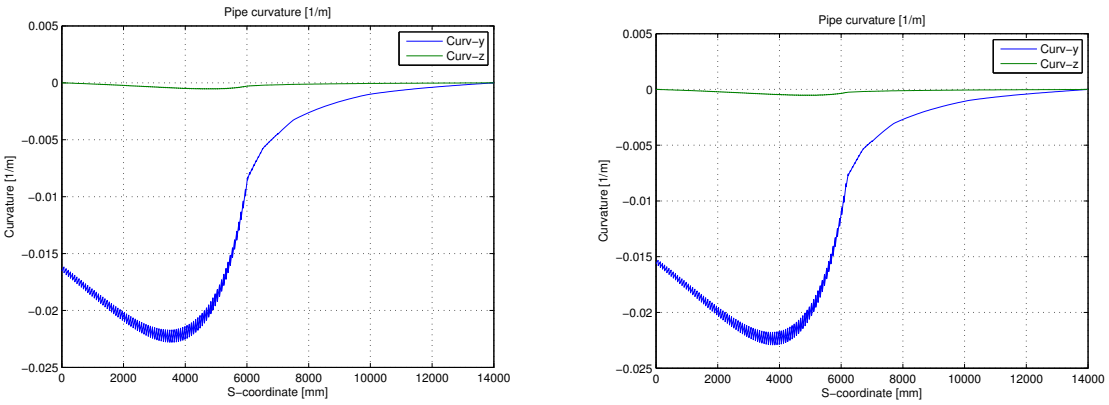

Figure 8.1: Curvature of case 1 and 2 respectivly

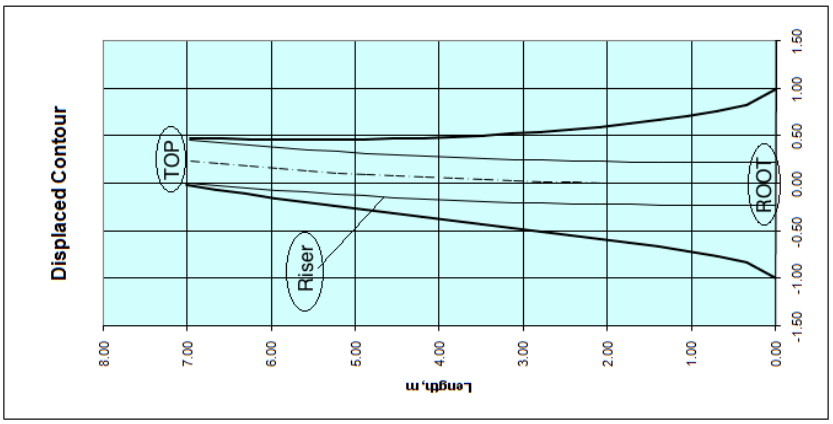

Figure 8.2: Displaced contour of bend stiffener with internal pipe

9 Cross Section Analysis

9.1 Introduction

The cross section analysis is performed for the armoring wires to verify that the stresses achieved are acceptable in accordance with relevant guidelines. A decision made in conversation with thesis supervisor Svein Sævik, is not to evaluate the pressure spiral due to shortage of information.

The local analyses are performed in Bflex*(v.2010)* with concentration on the first armor layer since this layer will be most affected.

9.2 Verification of Bend Stiffener

The bend stiffener must be verified for the extreme loads acting on the configuration. The stress in the armoring wires must be acceptable in accordance with relevant guidelines, e.g. (API, 2009). Table 2.4 in section 2.2.3, presents the pressure and tensile armor layers design criteria for service condition, where utilization factors are given for recurrent and extreme operation. The utilization factor for tensile and pressure armor layers in extreme operation are both given as 0.85, and the utilization is calculated as presented by equation 9.1, (API, 2009).

$$utilization = \frac{stress}{structural\ capacity} \tag{9.1}$$

The ultimate tensile strength for the four armoring layers are given in table 6.9, section 6.3.4. The first armor layer will be most affected by the stress distribution; hence the analysis will concentrate on this layer. The UTS for the first armor is given in table 6.9 as $1400MPa$. The stresses obtained from the Bflex*(v.2010)* analyses, must be evaluated in comparison with the UTS in extreme operation and should not exceed $1190MPa$, as shown in equation 9.2.

$$stress = 1400MPa \cdot 0.85 = 1190MPa \tag{9.2}$$

The two cases from section 8.3 are evaluated for the level of stress distribution in the bend stiffener area. In the local analysis, axial and bending stress components are computed at each corner of the armor wire. The bending stress can be divided into normal bending stress and transverse bending stress. By evaluation of each corner of the wire, the sum of axial stress, normal bending and transverse bending stress will be found for the corner.

The results for maximum values of stress found for case no.1 and no.2 are given in table 9.1. The total longitudinal stress for each corner of the armor wire, are presented in table 9.2.

Case no.	Axial stress [MPa]	Normal curvature stress [MPa]	Transverse curvature stress [MPa]
1	669.159	9.53338	35.2179
2	629.005	9.5912	35.4316

Table 9.1: Maximum stress from local analysis, bend stiffener verification

Case no.	Stress in corner no.1 [MPa]	Stress in corner no.2 [MPa]	Stress in corner no.3 [MPa]	Stress in corner no.4 [MPa]
1	679.427	677.959	660.36	658.892
2	639.289	637.905	620.106	618.722

Table 9.2: Total longitudinal stress of each corner in the armor wire

From table 9.1 and 9.2 it is found that the stresses obtained from axial stress and in the first and second corner have the highest contribution. While the bending stresses, i.e. curvature stresses, have no significant contribution to the total stress distribution. All stresses are less than the UTS given in (API, 2009), hence the bend stiffener is acceptable.

The distribution of longitudinal stress in corner 1 for load case no.1 and no.2 is illustrated in figure 9.1. It is noticeable that the maximum stress found for the armor wire occurs in the same section as where the maximum curvature was found.

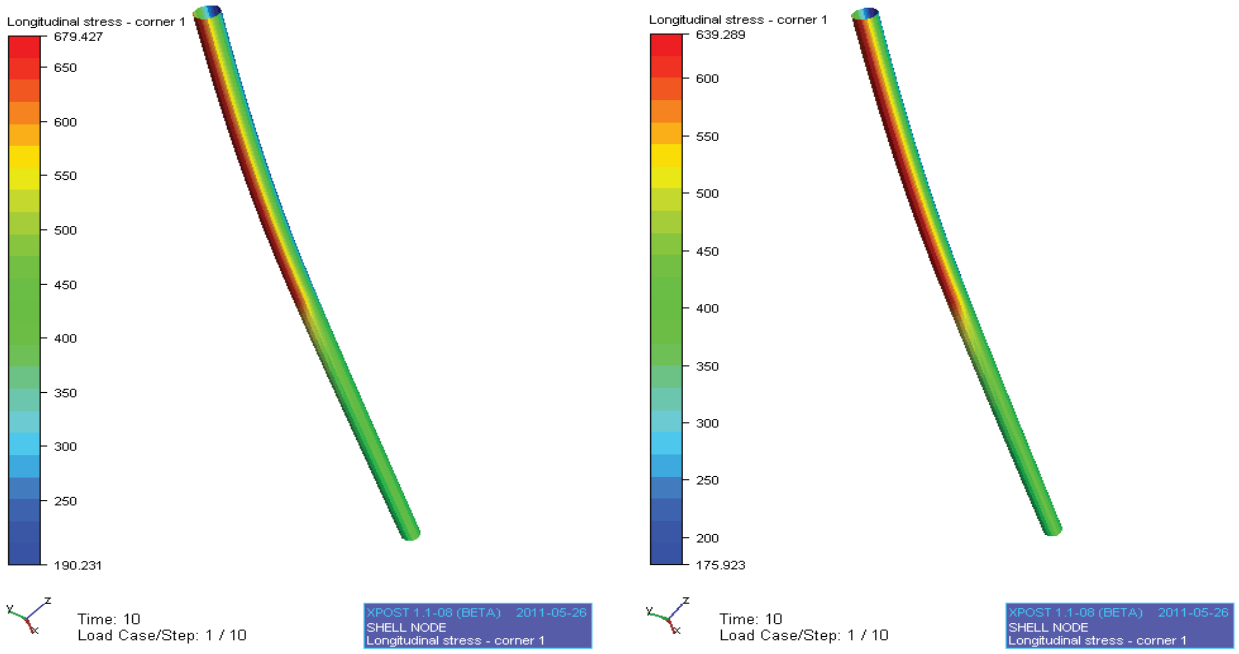

Figure 9.1: Longitudinal stress in corner 1 for case 1 and 2, respectively

10 Fatigue Analysis

10.1 Long Term Distribution of Fatigue Loads

To establish long term distribution of fatigue loads for the riser configuration, a global analysis is performed for various sets of wave- and current headings and values. The load cases established are found from a combination of wave scatter diagrams that presents individual wave heights with associated periods or direction. The wave scatter diagrams are found in metocean data, (A.Maia, 2005), given by SRT. Considering the size of a wave scatter diagram, performing analysis for each wave height and period or direction will be time consuming. Hence it is necessary to apply blocking of the wave scatter diagrams.

Waves with small wave heights may be of great importance when considering the total fatigue damage of the pipe, this is mainly due to the high quantity of small waves. It is also important to evaluate the probability of each wave height when performing blocking of the wave scatter diagrams.

Table 10.1 gives the selection of blocks applied in the fatigue analysis. The table is based on *Table 1 - Wave Period and Direction Distribution (in time percentage)* in (Calemos, 2004), see appendix B.4.

The first six blocks of waves with similar wave height in table 10.1 are considered individually with associated wave direction. This is done due to the high probability of occurrence of each wave direction. The period applied for the first six blocks is taken as an average of wave periods between 3.31s to 7.77s. The following six blocks are also considered individually. The period applied for these blocks is found by evaluating the RAO-data. A period of 9.9s presents the highest result of a period range of 8.41s to 9.9s in the RAO-data, and will be a conservative choice of wave period for these six blocks.

Block 13-16 represents combined cases where the probability of occurrence is relatively low. The period's chosen for each block is found from evaluation of the RAO-data, and conservative values are chosen for both wave period and wave height. The direction applied for each block is the mean direction for the different cases.

The current velocities applied in the fatigue analysis are based on the most common south current surface velocity, given in appendix C.4. Vessel heading is held constant, while waves and current direction vary.

Block	**Wave Height, H_{max} [m]**	**Wave Period, T [s]**	**Direction**	**Offset [m]**	No. of waves	**%**
1	2	5.54	N	30.01	458318	8.05220
2	2	5.54	NE	30.01	1480232	26.0062
3	2	5.54	E	30.01	868046	15.2507
4	2	5.54	SE	30.01	654875	11.5055
5	2	5.54	S	30.01	1157135	20.3297
6	2	5.54	SW	30.01	456468	8.01970
7	4	9.9	N	60.2	27878	0.48980
8	4	9.9	NE	60.2	108633	1.90910
9	4	9.9	E	60.2	81438	1.43080
10	4	9.9	SE	60.2	78445	1.37820
11	4	9.9	S	60.2	167027	2.93450
12	4	9.9	SW	60.2	128385	2.25560
13	6	11.42	N	90.24	455	0.00800
14	6	11.42	S	90.24	20826	0.36590
15	7	11.42	Mid. NE-N	105.35	2453	0.04310
16	8	11.42	S	120.4	1183	0.02080
				Total	**5691834**	**99.9998**

Table 10.1: Selection of blocks in scatter diagram for fatigue analysis

10.2 Time Series

When evaluating the long term distribution of fatigue loads, time series are applied. For each block in table 10.1, time series for top tension and angle are examined. The time series are applied in the local analysis in Bflex *(v.2010)*. Figure 10.1 illustrate maximum and minimum tension and angle of the blocks from the global long term analysis.

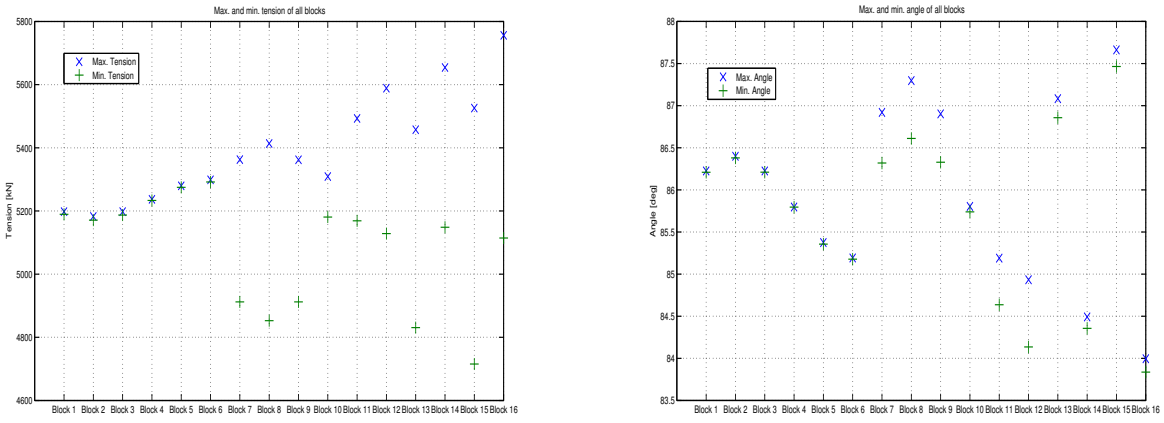

Figure 10.1: Max. and Min. tension and angle for all blocks

10.3 Introduction to Local Fatigue Analysis

The local fatigue analysis is performed to relate global loadings to stresses and strains in the pipe layers. The analysis is based on the long term distribution of fatigue loads found in section 10.2. The Bflex *(v.2010)* module Lifetime is applied for all the 16 blocks presented in table 10.1.

Each block has been analyzed with maximum change in top-angle, where both maximum and minimum angle, relative to nominal angle, are included to get the total range. In addition, maximum top-tension for each block is considered. The values applied are listed in table 10.2.

Block no.	Maximum tension [kN]	Maximum angle, relative to nominal [deg]	Minimum angle, relative to nominal [deg]
1	5198.0	0.411	-0.396
2	5182.6	0.586	-0.566
3	5197.9	0.411	-0.397
4	5236.8	-0.017	0.018
5	5279.7	-0.439	0.457
6	5298.7	-0.622	0.636
7	5362.5	1.106	-0.506
8	5413.6	1.484	-0.797
9	5362.1	1.089	-0.515
10	5308.9	-0.01	0.074
11	5492.8	-0.624	1.177
12	5588.7	-0.88	1.678
13	5457.3	1.27	-1.044
14	5654.2	-1.322	1.457
15	5525.6	1.849	-1.652
16	5756.0	-1.818	1.977

Table 10.2: Input for fatigue analysis

The S-N data applied in the fatigue analysis is given by SRT, and described in table 6.12 – 6.14, in section 6.4. The base case temperature level applied is 20^oC, see figure 6.6 in section 6.3.6.

10.4 Results of Fatigue Analysis

The results obtained for each block are evaluated with reference to the failure criterion given by equation 2.6 in section 2.1.2. Longitudinal failure mode is evaluated.
Figure 10.2 illustrates the fatigue damage for longitudinal failure mode for the first tensile armor wire layer for each block, values are given in table 10.3. With a safety-factor of 10, fatigue damage in block no.15 and no.16 will exceed the damage criterion of $D_f \geq 1$. The maximum fatigue damage is found at node no.673 for each block, and total fatigue damage at this node is found to be 0.64088346.

$$0.64088346 \cdot 10 = 6.4088346 \geq 1 \rightarrow \text{Not Ok!} \tag{10.1}$$

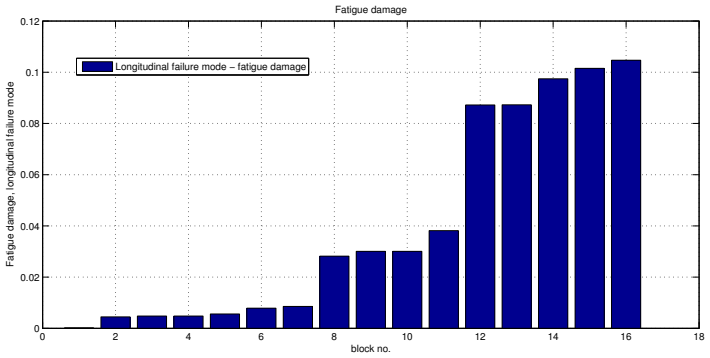

Figure 10.2: Fatigue damage of each block

Block no.	Max. fatigue damage at node no.673	Damage with safety factor of 10	OK [Y/N]
1	0.000173988	0.00173988	Y
2	0.00446369	0.0446369	Y
3	0.0047955	0.047955	Y
4	0.0047955	0.047955	Y
5	0.00562567	0.0562567	Y
6	0.00788616	0.0788616	Y
7	0.00854735	0.0854735	Y
8	0.0282015	0.282015	Y
9	0.0300614	0.300614	Y
10	0.0300614	0.300614	Y
11	0.0381493	0.381493	Y
12	0.0872111	0.872111	Y
13	0.0872904	0.872904	Y
14	0.0974315	0.974315	Y
15	0.101515	1.101515	N
16	0.104674	1.104674	N
Total Damage	0.64088346	6.64088346	N

Table 10.3: Results from fatigue analysis

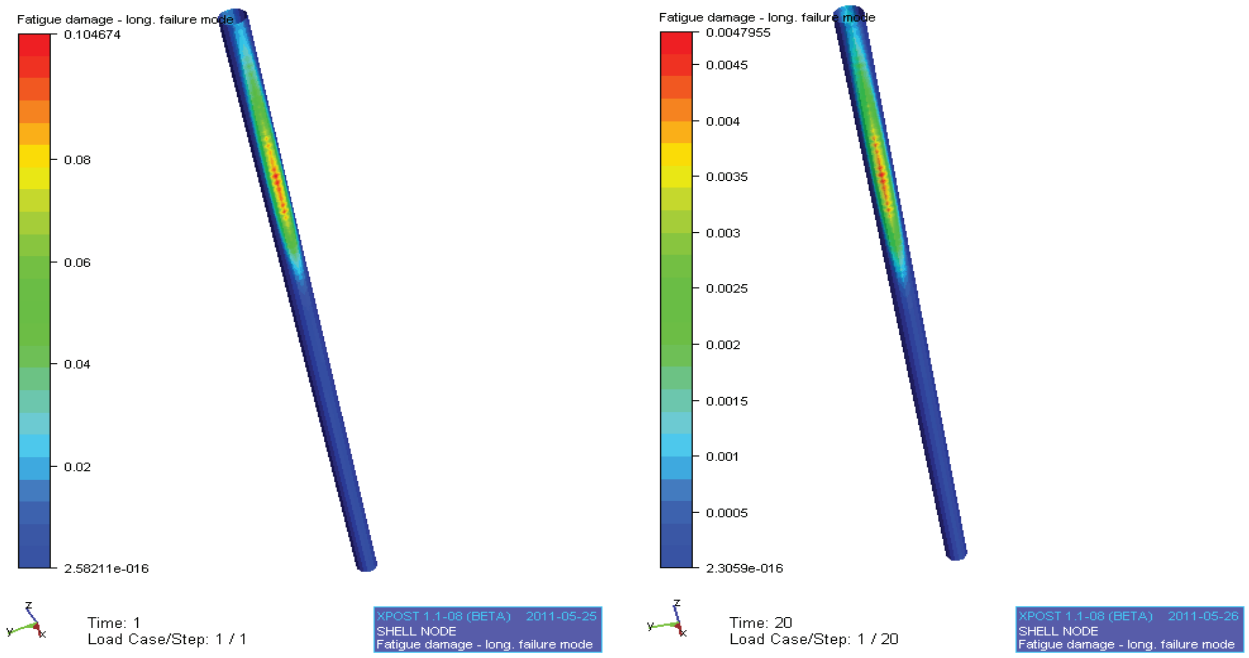

Figure 10.3: Fatigue damage of block no.16 and no.4

Figure 10.3 illustrates the distribution of fatigue damage for block no.16 and no.4. The red area indicates the highest effect of fatigue damage. The highest fatigue damage occurs in the bend stiffener area, at approximately the same section as where the largest curvature and stresses are achieved.

The stress distribution in the tensile armor wires should also be evaluated in the local fatigue analysis. All stresses found are acceptable in accordance with relevant guidelines. The effect of stress level from axial stress, and longitudinal stress at each corner of the wire, is highest in the bend stiffener area. Block no.16 has the highest stress distribution in the tensile armor wire, and block no.4 has the lowest. Values are listed in table 10.4.

Block no.	Axial stress [MPa]	Corner 1 [MPa]	Corner 2 [MPa]	Corner 3 [MPa]	Corner 4 [MPa]
16	605.668	609.031	608.662	602.674	602.305
4	383.682	383.71	383.767	383.625	383.654

Table 10.4: Stress distribution in tensile armor wire for block no.16 and no.4, respectively

Figure 10.4 illustrate the longitudinal stress distribution results for block no.4 and no.16. The red area indicates the highest level of stress, i.e. the stress is concentrated in the bend stiffener area.

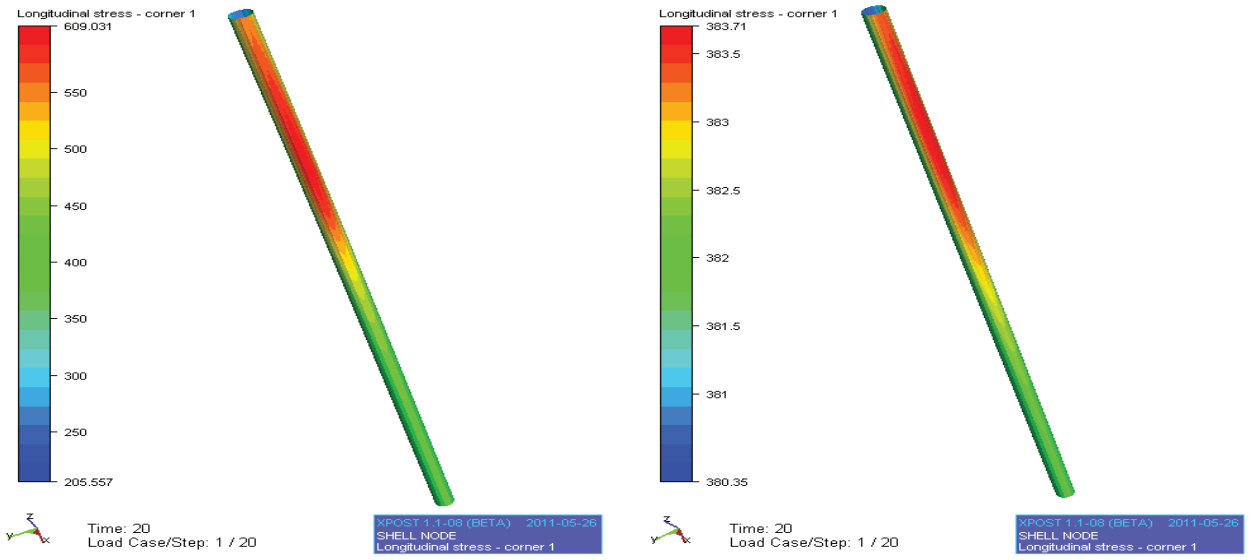

Figure 10.4: Longitudinal stress distribution of tensile armor wire corner for block no.16 and no.4, respectively

11 Parametric Study

11.1 Temperature Variation

This part of the parametric study deals with variation of temperature, and what affect this has on the stress level in the bend stiffener area. The temperature in the annulus is increased from the base case temperature of 20^{o}C to a temperature of 50^{o}C, which coincides with a reduction of the Young's modulus of the bend stiffener. The stress – strain curve applied in the material data for the bend stiffener is given in figure 11.1.

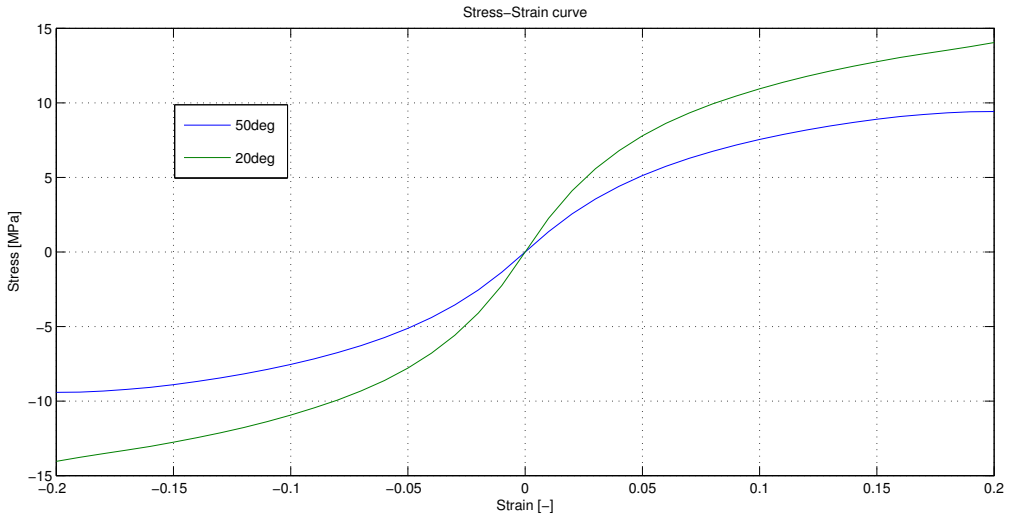

Figure 11.1: Stress – Strain curve at 50^{o}C and 20^{o}C

Temperature variation is evaluated for the two cases presented in section 9.2, chapter 9.

11.1.1 Results of Temperature Variation

When changing the temperature in the annulus to a higher temperature, the stress level in the bend stiffener area changes. Axial stress and longitudinal stress at all four corners of the first tensile armor wire is evaluated. The results are presented in table 11.1.

The axial stress and longitudinal stress of the first and second corner of the wire in case no.1 will decrease with higher temperature in the annulus. The remaining results obtained show an increase of the stress level at the bend stiffener area.

	Case no.	Axial stress [MPa]	Corner 1 [MPa]	Corner 2 [MPa]	Corner 3 [MPa]	Corner 4 [MPa]
50deg	1	669.122	679.342	677.88	660.363	658.901
	2	629.092	639.376	637.992	620.192	618.808
Increase(+)/Decrease(-) from base case [%]						
Difference from base case	1	(-) 0.0053	(-)0.0125	(-)0.01165	(+)0.000454	(+)0.00137
	2	(+)0.0138	(+)0.01361	(+)0.01364	(+)0.013869	(+)0.013899

Table 11.1: Stress distribution in tensile armor wire for case 1 and 2

The variation of stress due to change in temperature is illustrated for case 1 and 2 respectively, in figure 11.2 and 11.3. The larges stress variation is found in case no.2 for longitudinal stress in corner no.4.

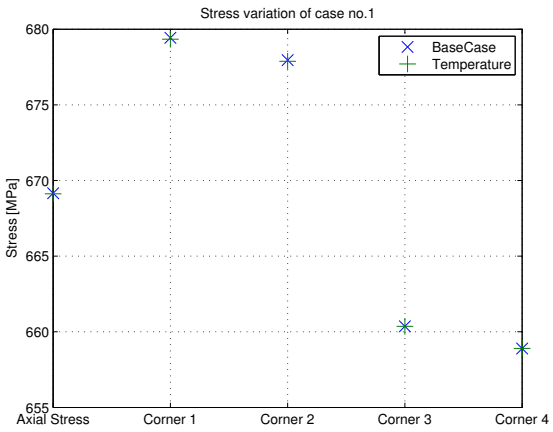

Figure 11.2: Variation of stress due to change in temperature, case no.1

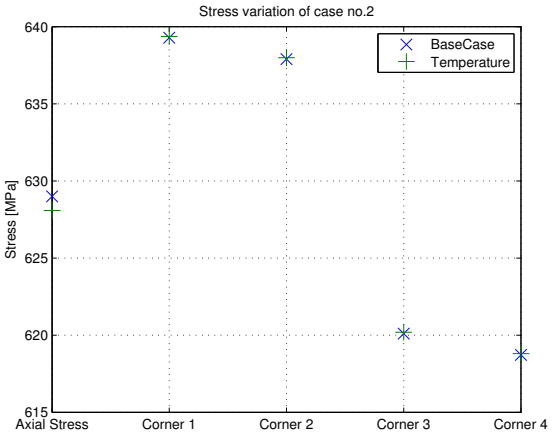

Figure 11.3: Variation of stress due to change in temperature, case no.2

11.1.2 Effect on Fatigue Damage

To evaluate the effect of varying temperature on resulting fatigue damage, the temperature in the annulus has been changed for each block in the local fatigue analysis.

Figure 11.4 presents the fatigue damage before temperature change, blue columns, and fatigue damage after temperature change, red columns, values are given in table 11.2.
The fatigue damage has increased for every block, and the maximum damage for each case is found at node no. 673. The total fatigue damage at this node is found to be 6.7417673, which is higher than 1.0. Hence; the total fatigue damage does not fulfill the damage criterion.

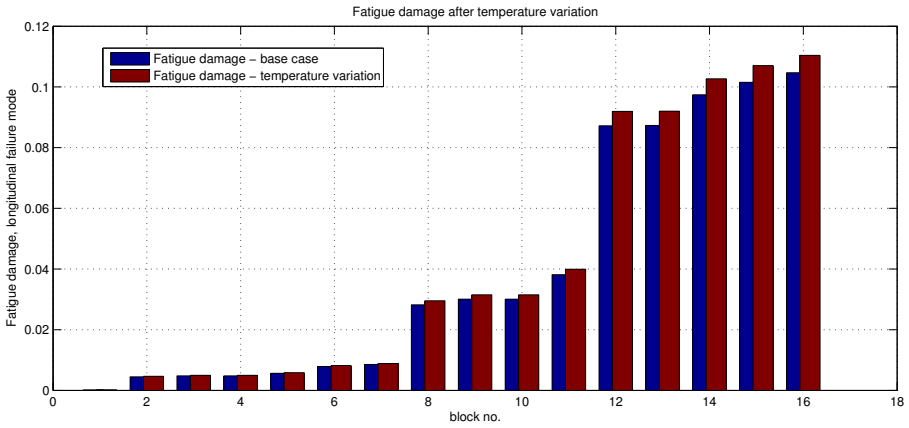

Figure 11.4: Comparison of fatigue damage

Block no.	Max. fatigue damage at node no.673	Damage with safety factor of 10	Change from base case [%]	OK [Y/N]
1	0.000180018	0.00180018	3.4658	Y
2	0.0046344	0.046344	3.8244	Y
3	0.00497772	0.0497772	3.7998	Y
4	0.00497772	0.0497772	3.7998	Y
5	0.00583666	0.0583666	3.7505	Y
6	0.00818057	0.0818057	3.7333	Y
7	0.00887074	0.0887074	3.7835	Y
8	0.0295481	0.295481	4.7749	Y
9	0.0314887	0.314887	4.74795	Y
10	0.0314887	0.314887	4.74795	Y
11	0.0399345	0.399345	4.6795	Y
12	0.0919274	0.919274	5.4079	Y
13	0.0920105	0.920105	5.40735	Y
14	0.102689	1.02689	5.3961	N
15	0.10704	1.0704	5.4425	N
16	0.110392	1.10392	5.4627	N
Total Damage	0.67417673	6.7417673	5.1949	N

Table 11.2: Results from fatigue analysis with temperature variation

Figure 11.5 illustrates the fatigue damage of the first armor layer in the riser, without and with temperature change. The result range is narrowed to get a more detailed impression of the fatigue damage.

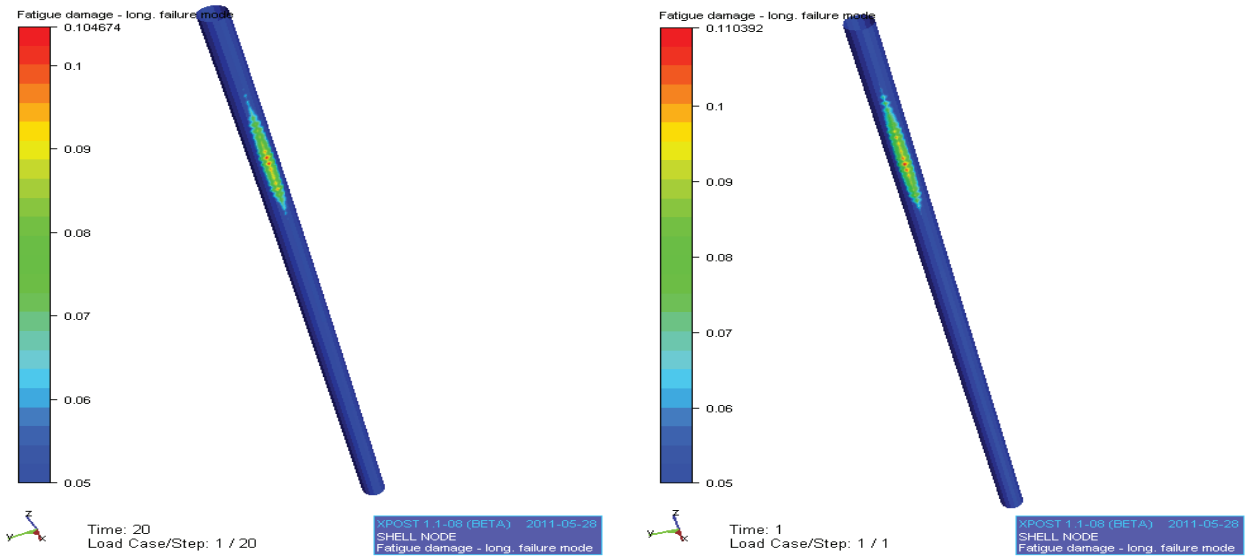

Figure 11.5: Fatigue damage of block 16, base case and temperature change

11.2 Linear vs. Non-linear Material Properties

The linear material is evaluated for the extreme cases from table 8.2, section 8.3.
Material values for analysis are given in table 6.3 in section 6.3.6.

The change of material from non-linear to linear for the bend stiffener gives a relatively small decrease in all stresses evaluated for case no.1. For case no.2, the axial stress and the total longitudinal stress in the corners on the tensile side of the wire have decreased from the results found in the base case. While at the corners on the compression side of the wire, there is an increase of the total longitudinal stress.

	Case no.	Axial stress [MPa]	Corner 1 [MPa]	Corner 2 [MPa]	Corner 3 [MPa]	Corner 4 [MPa]
Linear	1	669.061	679.156	677.702	660.299	658.846
	2	628.984	639.207	637.828	620.139	618.761
Increase(+)/Decrease(-) from base case [%]						
Difference from base case	1	(-) 0.01465	(-)0.03989	(-)0.03791	(-)0.00924	(-)0.006981
	2	(-)0.00334	(-)0.01283	(-)0.01210	(+)0.00532	(+)0.00630

Table 11.3: Stress distribution in tensile armor wire with linear material properties, for case 1 and 2

The largest decrease is found for longitudinal stress in the first corner of the tensile armor wire for both cases. Illustrations of the stress distribution for case no.1 and no.2 respectively, are given in figure 11.6.

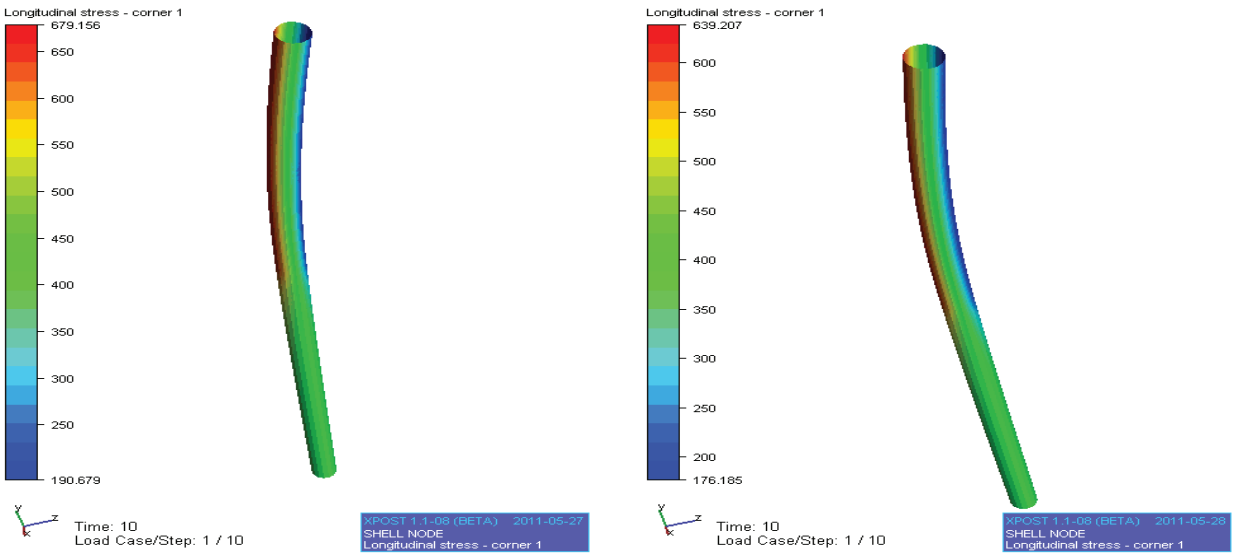

Figure 11.6: Longitudinal stress distribution at corner no.2 with linear material of bend stiffener, for case no.1 and no.2 respectively

12 Conclusion and Discussion

With the development of offshore oil and gas fields at deep waters come problems and challenges for the designer. In riser design, types of loading and load effects different from shallow water must be accounted for. In addition, it is important to evaluate the effect on the riser from complex reservoirs with high pressure and temperature.
Of vital interest is the fatigue life of the riser, and most risers are designed for at service life of 20–25 years. Yet at the Norwegian offshore sector, the average flexible riser has only been in service for roughly 50% of its planned service life. Thorough fatigue analyses need to be performed to obtain a desirable design life.

This thesis contains global analyses, both for evaluation of extreme loads and long term distribution of fatigue loads, of a free hanging catenary riser operating in 1750 m water depth.
From the global analysis with extreme environmental conditions, top tension and curvature of the riser are evaluated. It is known that the most critical areas of a free hanging catenary riser is at TDP and hang-off. From the extreme analysis, it is found that maximum tension occurs for near position of the vessel. Usually, far positioning of the vessel should contribute to maximum tension since this is the case where the riser is stretched out the most and hence large values of top tension should take place. The riser is exposed to compression and high curvature values at TDP when the static offset of the floater is at near position. This is known as a common problem encountered at deep waters for free hanging catenary risers when the floater is at near position. That the curvature achieved at TDP is critical in comparison with the MBR may not be exact. By evaluation of the envelope plots of curvature, peaks giving high curvature may be due to numerical errors from the analysis. With curvature results as found in this analysis, the free-hanging riser configuration will not be a proper choice for the given oil field and environment. However, optimization of the configuration should be carried out to obtain desired response on the riser. A method can be to shorten the riser, i.e. making it more taut and relocating the TDP, which leads to less bending and curvature at the TDP. An other option is to install a tether at the TDP that tightens up the riser.
The extreme analysis does not show any significant effect of curvature at hang-off. However, this area is prone to fatigue damage and should be evaluated more thorough by local analyses.

Based on the extreme loads found from the global analysis, a bend stiffener has been proposed for the riser. The bend stiffener should protect the riser from excessive bending, and this is verified by evaluation of curvature and stresses in a local analysis. The local analysis has been performed for two cases where maximum bending angle found from the global extreme analysis are applied for both. For the load case with maximum bending angle, maximum tension and minimum tension are found. The two local analysis cases is then divided into maximum bending angle in combination with maximum tension, and maximum bending angle in combination with minimum tension. The curvature should be distributed along the bend stiffener, with small bending radius close to hang-off and at the intersection between the riser and the bend stiffener.
The stress acting in the riser cross-section during bending has been evaluated in terms of axial-, normal curvature-, and transverse curvature stress. In addition, total longitudinal stress in the four corners of the riser tensile armor wires has been assessed. It is found that the bending stresses, i.e. normal and transverse curvature stresses, do not have any significant contribution to the total stress distribution. The maximum total longitudinal stresses obtained after bending of the tensile armor wires, are found at the armor wire corners on the tension side of the armor wire, while the lowest values of stress are found on the compression side.

To verify that the stresses are acceptable, the maximum allowable stress value is found from combination of structural capacity and utilization. The stresses found for the tensile armor layer in the local analysis are compared with the maximum allowable stress.
All stresses found are within the limit of the UTS, and the curvature is distributed desirably for both of the assessed cases. The dimensions established for the bend stiffener have been discussed with the supervisor. Compared to bend stiffeners that are in work, the bend stiffener found in this thesis has unusual dimensions in terms of diameter. From conversation with SRT, it was suggested a root diameter of 1.2m, which is 0.8m less than the diameter found in this thesis. In addition, the diameter of 2m is four times larger than the riser diameter. When evaluating a bend stiffener with less than 2m root diameter, the curvature distribution was not satisfactory. Large curvature results were found at the root, which is not a desirable outcome. So, the design proposed with a root diameter of 2m is applied for further analyses.

With basis in the global analysis where long term distribution of fatigue loads were established, a local stress analysis has been performed. The local analysis applies tension and bending angles found from time series in the global analysis. The bending angles were found to be relatively small. This may be due to a combination of the large water depth and small floater motions.
From the local analysis, the fatigue damage of the tensile armor wires was found. 16 different blocks with, with 7 different headings of wave height and period have been assessed. The blocks were established from scatter diagrams where number of waves and probability of occurrence are given. The input applied is chosen conservatively with focus on probability of occurrence. When performing blocking of the wave scatter diagrams, it was important to keep in mind that waves with small wave heights may be of great importance for fatigue damage due to the high quantity. When evaluating the results found in the fatigue analysis, it was important to keep in mind that fatigue damage may take place even though the nominal maximum stress values are below the yield stress limit of the material and less than the UTS. The resulting stresses found for each block evaluated was less than the UTS, still evaluation of fatigue damage was carried out.
The largest fatigue damage found in the analyses was obtained for the last case, block no.16 with $H_{max} = 8m$ and $T = 11.42s$. The fatigue damage has been evaluated in terms of the fatigue damage criterion of $D_f \geq 1$ and a safety-factor of 10 is applied. This is a common safety-factor applied in real projects for fatigue damage calculation of the layers in a flexible riser. The total damage should then be found to be lower than a value of 0.1. For the individual blocks, maximum fatigue damage is found at node no.673, and the damage criterion is fulfilled for all blocks except no.15 and no.16. The total fatigue damage at node no.673 is found to be 0.64088346, and with a safety-factor of 10, this will exceed the damage criterion. The reason for the high excess of fatigue damage can be that the FPSO and RAO's are not optimized in proportion to the metocean data. An other aspect is that the riser configuration is not optimized for the environment, i.e. metocean, water-depth, etc. To obtain better and desirable results, optimization of the configuration should be worked out, and an additional option can be to apply a different S-N curve for the armor layer. It is noticeable that the maximum fatigue damage, found for the tensile armor wire, appears in the same area as the maximum stress and curvature found in the earlier stages of the report.

When increasing the temperature in the annulus, from a relatively cold fluid to hot fluid, stresses and fatigue damage have been evaluated. Axial stress and longitudinal stress of the tensile armor wires have been assessed, and the results are varying. Overall, it seems like the increase of temperature in the annulus has a negative effect on the stresses obtained in the riser. The majority of the stresses found have increased from base case with approximately 0.014%.
An increase of the temperature in the annulus represents a decrease of the Young's modulus of the bend stiffener, this means that the material of the bend stiffener will be less stiff. This can lead to an increase of the response, i.e. $\Delta\sigma$, in the bend stiffener area. Hence; increased fatigue damage may occur. The total fatigue damage has increased with 5.19% compared to base case. As for the base case, the maximum fatigue damage is found at node no.673, and the total fatigue

damage at this node does not fulfill the damage criterion. For the individual blocks, excess of fatigue damage is experienced for three of the 16 blocks, i.e. block no.14, no.15 and no.16. This indicates that a temperature change from base case of 20^oC to 50^oC will have an effect on the fatigue damage of the riser in the bend stiffener area. But as for the base case, the high excess of fatigue damage can be due to insufficient optimization and no-good S-N curve data for the armor layer.
It is also important to keep in mind that the increase of temperature in the annulus may have an effect on the fatigue life of the plastic layers in the riser as they have different material properties and limitations. With an other bend stiffener design, e.g. more slender and smaller bend stiffener, the temperature dependence may be of even more importance for the results found for stress distribution and fatigue damage of the armor layers.

The local analysis is also performed to compare the effect on the stress level in the bend stiffener area by changing from non-linear to linear material properties of the bend stiffener. The linear material properties applied for the bend stiffener are made from interpolation of the stress-strain curves for the base case. Hence, it is important to keep in mind that the results may not be accurate. The variation of material properties has a relatively small effect on the stress distribution in the bend stiffener area. Most of the results evaluated for this part of the parametric study, show a decrease in the stress level. By adjusting from non-linear to linear material of the bend stiffener, the stiffness of the bend stiffener is reduced. A stiff material may lead to large bending moments at the intersection between the riser and the bend stiffener. As a result of that, large stresses may occur. When the material is changed, the bending moment will be distributed in more desirable manner and lower values of stress may occur.
For the second case examined, the total longitudinal stress on the compression side of the wire was subjected to an increase of the stress level. This might be due to less local bending of the wire, which in turn cause a reduction of compression and tension on the sides of the wire. Even though the stress level has increased and decreased, the design criterion is still accepted.

In spite the results obtained, it is not given that a reduction of the bend stiffener stiffness, due to temperature variation of change of material properties, will contribute to larger fatigue damage and/or extreme response. This will depend on the stress level distribution between the riser and the bend stiffener.

It is important to keep in mind that the riser configuration assessed in this thesis is a simplified model, where simplifications have been made for most of the input data. The configuration has not been optimized. Hence; uncertainties in the results should be accounted for.

13 Recommendations for Further Work

The riser configuration applied in this thesis is a free hanging catenary riser, which is a typical configuration chosen for deep-water offshore fields. The results obtained from the global extreme analysis presents compression of the riser and excess curvature at TDP. This is not a desirable outcome, but the configuration can be optimized to provide better results.
To prevent undesirable results at TDP, other types of configurations should be considered to obtain the best suited configuration for the given offshore field. Configurations such as a lazy wave configuration can be a proper choice for comparison of the riser feasibility. The configuration does not necessarily mean a "full" lazy wave, but a configuration with a few buoyancy elements clamped along the riser in critical sections, e.g. TDP. This may help to prevent compression and excess of the critical curvature at TDP. The buoyancy elements will help counteracting with the environmental loads affecting the riser in deep water environments. Alternatively, a lazy-s configuration or a hybrid riser could be evaluated for the given offshore field. The lazy-s configuration applies a mid-water arch, MWA, which helps eliminating dynamic forces that are causing friction and fatigue of the riser at the seabed. A hybrid riser applies a vertical pipe connected to the seafloor in combination with flexible jumpers. The hybrid riser system will contribute to a reduction of the water depth, thus reduce critical outcomes near the seabed.
Different floater concepts should be assessed for the specific offshore field. Other types of floaters may be more suitable for this environment, so analyses should be made for e.g. a semi-submersible or circular hull FPSO's. It is also important to keep in mind the riser hang-off position, e.g. placing of turret internal or external, use of balcony, etc. By moving the turret closer to the center of the FPSO, the pitch movement experienced at hang-off will be reduced. Hence, dynamic movement of the riser at hang-off will also be decreased.
By performing extreme analyses for different floater concepts in combination with various riser configurations, the best feasible system can be found.

Riser systems may experience VIV, which can contribute to significant fatigue of the riser. Evaluation of VIV is of particular importance for deep-water top-tensioned risers, and should be assessed in a fatigue analysis.

The bend stiffener design proposed in this thesis has an unusual geometry in terms of the root diameter of 2m, compared to a diameter of 1.2m suggested by SRT. The design can be optimized further to find a more suitable bend stiffener. Ways to do this can be to reduce the length of the bend stiffener and narrow the root diameter, while curvature and stresses are kept acceptable in accordance to relevant guidelines.
When verifying the bend stiffener design, only curvature and stresses in armoring wires were assessed in this thesis. In the thesis description it was stated that the stress in the pressure spiral should also be acceptable in accordance with relevant guidelines, hence analysis to verify this should be worked out.

In the thesis, a parametric study has been performed. The temperature in the annulus of the riser has been increased, and the material properties have been varied from non-linear to linear material. To gain even more knowledge of the effects locally in the bend stiffener area, a decrease in the annulus temperature can be evaluated based on stress level and fatigue damage. In addition, variation of the ambient temperature should be assessed.
In the study where linear material properties are applied for the bend stiffener, the first task to do should be to verify that the properties are exact and usable. Further on, the stresses should be evaluated again to gain a more accurate result. It is also of importance to get knowledge on how linear material properties of the bend stiffener affect the resulting fatigue damage of the riser.

References

(2007). *Methodology for Calculating Irregular Wave Stress Time Histories of Tensile Wires in Flexible Risers*, OMAE2007-29104. ASME, American Society of Mechanical Engineer.

(2010). *Comparison between theoretical and experimental flexible pipe bending stresses*, OMAE2010-20352. ASME, American Society of Mechanical Engineer.

A.Maia (2005). Metocean data. Tech. rep., Petrobras.

API (2008). Recommended practice for flexible pipe. Tech. Rep. Fourth Edition, American Petroleum Institute.

API (2009). Specification for unbonded flexible pipe. Tech. rep., American Petroleum Institute.

Bai, Y., & Bai, Q. (2005). *Subsea Pipelines and Risers*. Elsevier.

Berge, S. (2004a). *Fatigue and Fracture Design of Marine Structures - Fracture Design of Welded Structures*, (pp. 4.13–4.19). Faculty of Engineering Science and Technology -2- NTNU Trondheim, Norway.

Berge, S. (2004b). *Fatigue and Fracture Design of Marine Structures -1- Fracture Design of Welded Structures*, (pp. 4.12–4.19). Faculty of Engineering Science and Technology - NTNU Trondheim, Norway.

Calemos (2004). Service life - fatigue analysis. Tech. rep., Petrobras.

Campbell, M. (1999). The complexities of fatigue analysis for deepwater risers. Tech. rep., 2H Offshore Engineering.
URL `http://www.2hoffshore.com/documents/papers/pap029.pdf`

DNV (2005a). Recommended practice - dnv-rp-c203 - fatigue design of offshore steel structures. Tech. rep., Det Norske Veritas.

DNV (2005b). Recommended practice - dnv-rp-f204 - riser fatigue. Tech. rep., Det Norske Veritas.

Faltinsen, O. (1993). *Sea loads on ships and offshore structures*, (p. 41). Cambridge Univ Pr.

Hokstad, P., Håbrekke, S., Johnsen, R., Sangesland, S., & Haagensen, P. (2009). Ageing and life extension for offshore facilities. Tech. rep., SINTEF.

ISO (2006). Unbonded flexible pipe systems for subsea and marine applications. Iso 13628-2, ISO.

Martin Tarr (2011). Stress and its effect on materials.
URL `http://www.ami.ac.uk/courses/topics/0124_seom/index.html`

Myrhaug, D. (2007). *Marin Dynamikk - Uregelmessig Sjø*, (pp. 36–47). Faculty of Engineering Science and Technology - NTNU Trondheim, Norway.

Paik, J. K., & Thayamballi, A. K. (2011).
URL http://www.scribd.com/doc/22464962/Principles-of-Limit-State-Design#open_download

Rahman, A. (2011).
URL http://www.scribd.com/doc/38987359/Flexible-Riser-Abdul-Rahman

Sævik, S. (1992). *On Stresses and Fatigue in Flexible Pipes.* Ph.D. thesis, NTH.

Sævik, S. (2010a). *BFLEX2010 - Theory Manual.* MARINTEK.

Sævik, S. (2010b). Flesxible riser analysis and technology. Lecture note.

Sævik, S., Økland, O. D., Baarholm, G. S., & Gjøsteen, J. K. (2010). *Bflex 2010 User Manual.* MARINTEK, 3.0.5 ed.

Sødahl, N. R. (1991). *Methods for Design and Analysis of Flexible Risers.* Ph.D. thesis, NTH, University in Trondheim.

Sødahl, N. R. (2009). Cross-section analysis - fatigue analysis of flexible risers and umbilicals. www.tekna.no.
URL http://www.tekna.no/ikbViewer/Content/777787/S%F8dahl%20Cross%20sectional%20analysis%20-%20fatigue%20%20rev0.pdf

Wikipedia (2011a).
URL http://en.wikipedia.org/wiki/Fatigue_(material)

Wikipedia (2011b).
URL http://en.wikipedia.org/wiki/Limit_state_design

Y.Zhang, B.Chen, L.Qui, T.Hill, & M.Case (2003). State of the art analytical tools improve optimization of unbounded flexible pipes for deepwater environments.

Appendices

Appendix A

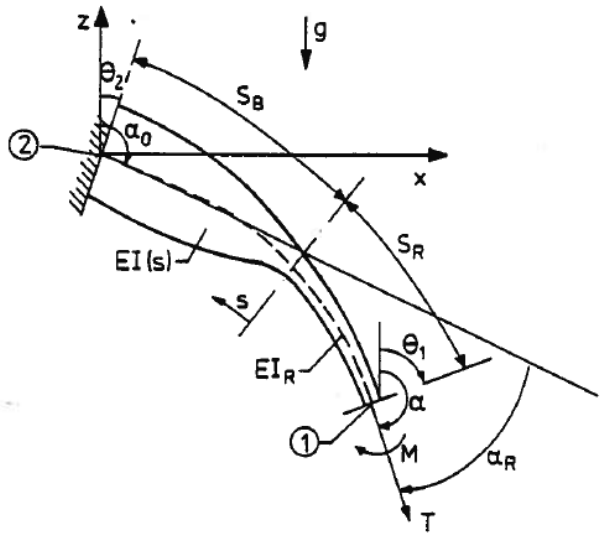

Figure A.1: The local response model, (Sødahl, 1991)

The local response model comprises two parts; bend stiffener of length S_B and initial riser part of length S_R. The bend stiffener will have varying cross sectional properties, where both the axial force and the bend stiffeners are important concerning lateral deformation. Large deformations and rotations will be present. Since bend stiffener is defined as the most critical area of excedance of maximum allowed curvature, a fine mesh is needed to give a good description of the varying curvature along the bend stiffener.
In the local response model, the bending stiffness of the riser is held constant, while the bending stiffness of the bend stiffener is increasing towards the clamped end.

For more information concerning the local response model, see (Sødahl, 1991).

Appendix B

B.1 Distribution of Individual Wave Heights and Associated Periods

(A.Maia, 2005):

Period → / Height ↓	0 – 2	2 – 4	4 - 6	6 - 8	8 - 10	10-12	12-14	14-16	16-18	18-20	20-22	22-24	Total	%	Tmed
0.0-0.5	85171	166779	50632	10991	2167	425	110	25	13	7	5	0	316325	17.27	3.31
0.5-1.0	11867	208032	229458	111698	40289	11835	2862	547	132	49	17	0	616786	33.70	5.38
1.0-1.5	322	47777	164356	145537	73169	27184	7458	1481	271	55	32	0	467642	25.53	6.91
1.5-2.0	6	6545	64094	85930	53460	23925	7570	1592	266	41	25	0	243454	13.30	7.77
2.0-2.5	0	742	19753	38224	27785	14938	5669	1263	190	37	13	2	108616	5.93	8.41
2.5-3.0	0	82	5311	14769	12522	8057	3290	798	149	11	3	0	44992	2.46	8.96
3.0-3.5	0	6	1277	5433	5522	4149	1907	510	90	10	3	0	18907	1.03	9.50
3.5-4.0	0	1	309	2006	2350	1963	987	265	51	3	0	0	7935	.43	9.90
4.0-4.5	0	0	69	733	1117	973	535	168	33	1	0	0	3629	.20	10.32
4.5-5.0	0	0	12	234	513	507	321	60	11	0	0	0	1658	.09	10.68
5.0-5.5	0	0	4	83	230	271	165	52	6	0	0	0	811	.04	11.31
5.5-6.0	0	0	1	30	115	123	86	23	1	0	0	0	379	.02	10.98
6.0-6.5	0	0	0	8	39	69	35	12	0	0	0	0	163	.00	12.14
6.5-7.0	0	0	0	3	21	26	16	2	0	0	0	0	68	.00	11.16
7.0-7.5	0	0	0	0	5	18	15	2	0	0	0	0	40	.00	11.93
7.5-8.0	0	0	0	2	3	3	7	0	0	0	0	0	15	.00	11.60
8.0-8.5	0	0	0	0	2	3	1	0	0	1	0	0	7	.00	10.34
8.5-9.0	0	0	0	0	0	2	2	0	0	0	0	0	4	.00	12.00
9.0-9.5	0	0	0	0	1	2	1	0	0	0	0	0	4	.00	11.25
9.5-10.0	0	0	0	0	1	1	2	0	0	0	0	0	4	.00	11.50
10.0-10.5	0	0	0	0	0	2	0	0	0	0	0	0	2	.00	13.00
10.5-11.0	0	0	0	0	0	0	0	0	0	0	0	0	.00	-	-
11.0-11.5	0	0	0	0	0	0	0	0	0	0	0	0	.00	-	-
11.5-12.0	0	0	0	0	0	1	0	0	0	0	0	0	1	.00	12.00
Total	97366	429964	535276	415681	219311	94475	31041	6800	1213	215	98	2	1831442	100.00	
%	5.32	23.48	29.23	22.70	11.97	5.16	1.69	.37	.07	.01	.00	.00			
Mean Height	.31	.64	1.06	1.39	1.60	1.81	2.01	2.10	2.02	1.62	1.49	2.17			

Figure B.1: Distribution of Individual Wave Heights and Associated Periods, (A.Maia, 2005)

B.2 Distribution of Individual Wave Heights and Associated Directions

(A.Maia, 2005):

Hs	Dir >	N	NE	E	SE	S	SW	W	NW	Total	% Hs	Mean Dir
0	0.5	1	0	0	0	2	0	0	0	3	0.02	139.2
0.5	1	16	84	72	57	50	10	3	1	293	2.15	98.3
1	1.5	276	922	681	504	574	142	14	12	3125	22.96	93.4
1.5	2	502	1368	849	626	981	335	31	4	4696	34.51	95.2
2	2.5	377	658	481	387	732	378	8	2	3023	22.21	114.7
2.5	3	146	237	207	265	374	255	0	1	1485	10.91	139.4
3	3.5	53	52	56	111	162	170	0	0	604	4.44	169.3
3.5	4	7	10	10	37	69	91	0	0	224	1.65	186.1
4	4.5	0	1	0	12	34	52	0	0	99	0.73	197.5
4.5	5	0	0	0	2	13	24	0	0	39	0.29	204.9
5	5.5	0	0	0	1	4	8	0	0	13	0.1	203.3
5.5	6	0	0	0	0	1	1	0	0	2	0.01	206.3
6	6.5	0	0	0	0	0	2	0	0	2	0.01	211
6.5	7	0	0	0	0	0	0	0	0	0	0	0
Total		1378	3332	2356	2002	2996	1468	56	20	13608		
% Dir		10.13	24.49	17.31	14.71	22.02	10.78	0.41	0.15			
Mean Hs		1.95	1.79	1.81	1.97	2.06	2.46	1.68	1.49			

Figure B.2: Distribution of Individual Wave Heights and Associated Directions, (A.Maia, 2005)

B.3 Extreme Wave Parameters

(A.Maia, 2005), table with waves approaching from all directions:

DIRECTION	PARAMETER	RETURN PERIOD (YEARS)				
		1	10	30	50	100
N	Hs: SIGNIFICANT WAVE HEIGHT (m)	4.44	4.74	4.87	4.93	5.01
	TP: PEAK PERIOD ASSOCIATED TO Hs (s)	8.81	9.20	9.38	9.46	9.56
	TZ: ZERO UP-CROSSING PERIOD (s)	6.54	6.82	6.94	7.00	7.07
	HMAX: MAXIMUM WAVE HEIGHT (m)	8.54	9.10	9.34	9.44	9.58
	THMAX: PERIOD ASSOCIATED TO HMAX (s)	10.42	10.56	10.61	10.63	10.66
NE	Hs: SIGNIFICANT WAVE HEIGHT (m)	4.55	4.88	5.02	5.09	5.17
	TP: PEAK PERIOD ASSOCIATED TO Hs (s)	9.13	9.47	9.62	9.68	9.77
	TZ: ZERO UP-CROSSING PERIOD (s)	6.76	7.00	7.11	7.16	7.22
	HMAX: MAXIMUM WAVE HEIGHT (m)	8.73	9.35	9.62	9.73	9.89
	THMAX: PERIOD ASSOCIATED TO HMAX (s)	10.47	10.61	10.67	10.69	10.73
E	Hs: SIGNIFICANT WAVE HEIGHT (m)	3.72	4.34	4.60	4.72	4.87
	TP: PEAK PERIOD ASSOCIATED TO Hs (s)	9.35	9.90	10.14	10.25	10.40
	TZ: ZERO UP-CROSSING PERIOD (s)	6.92	7.31	7.49	7.57	7.67
	HMAX: MAXIMUM WAVE HEIGHT (m)	7.13	8.29	8.78	9.00	9.28
	THMAX: PERIOD ASSOCIATED TO HMAX (s)	10.05	10.36	10.48	10.53	10.60
SE	Hs: SIGNIFICANT WAVE HEIGHT (m)	4.81	5.72	6.11	6.30	6.53
	TP: PEAK PERIOD ASSOCIATED TO Hs (s)	10.90	10.28	11.45	11.53	11.63
	TZ: ZERO UP-CROSSING PERIOD (s)	8.03	8.30	8.42	8.48	8.55
	HMAX: MAXIMUM WAVE HEIGHT (m)	9.13	10.83	11.57	11.90	12.34
	THMAX: PERIOD ASSOCIATED TO HMAX (s)	12.40	13.21	13.57	13.73	13.94
S	Hs: SIGNIFICANT WAVE HEIGHT (m)	5.14	6.19	6.64	6.84	7.10
	TP: PEAK PERIOD ASSOCIATED TO Hs (s)	12.65	13.54	13.93	14.11	14.35
	TZ: ZERO UP-CROSSING PERIOD (s)	9.28	9.91	10.18	10.31	10.48
	HMAX: MAXIMUM WAVE HEIGHT (m)	9.65	11.58	12.39	12.75	13.22
	THMAX: PERIOD ASSOCIATED TO HMAX (s)	12.65	13.58	13.97	14.14	14.37
SW	Hs: SIGNIFICANT WAVE HEIGHT (m)	6.37	7.16	7.49	7.64	7.84
	TP: PEAK PERIOD ASSOCIATED TO Hs (s)	13.93	14.78	15.15	15.32	15.55
	TZ: ZERO UP-CROSSING PERIOD (s)	10.18	10.78	11.05	11.17	11.33
	HMAX: MAXIMUM WAVE HEIGHT (m)	11.89	13.30	13.90	14.17	14.53
	THMAX: PERIOD ASSOCIATED TO HMAX (s)	13.72	14.40	14.69	14.82	14.99
W-NW	Hs: SIGNIFICANT WAVE HEIGHT (m)	3.21	3.57	3.72	3.79	3.88
	TP: PEAK PERIOD ASSOCIATED TO Hs (s)	7.91	8.22	8.37	8.43	8.51
	TZ: ZERO UP-CROSSING PERIOD (s)	5.89	6.11	6.21	6.26	6.32
	HMAX: MAXIMUM WAVE HEIGHT (m)	6.21	6.90	7.19	7.32	7.49
	THMAX: PERIOD ASSOCIATED TO HMAX (s)	9.77	9.98	10.07	10.11	10.16

Figure B.3: Extreme Wave Parameters - waves approaching from all directions, (A.Maia, 2005)

B.4 Wave Period and Direction Distribution

Height (m)	Wave Period (s)	Number of Waves	N	NE	E	SE	S	SW
2	3,31 to 7,77	5 324 106	8.0522%	26.0062%	15.2507%	11.5055%	20.3297%	8.0197%
4	8,41 to 9,9	356 832	0.4898%	1.9091%	1.4308%	1.3782%	2.9345%	2.2556%
5	10,32 to 11,31	8 769	0.0072%	0.0221%	0.0168%	0.0393%	0.0899%	0.1610%
6	10,98 to 11,31	1 689	0.0008%	0.0023%	0.0015%	0.0060%	0.0210%	0.0487%
7	11,16 to 12,14	336		0.0002%	0.0001%	0.0007%	0.0040%	0.0112%
8	11,60 to 11,93	80		0.0001%		0.0001%	0.0007%	0.0028%
9	10,34 to 12,00	18					0.0002%	0.0005%
10	10,25 to 11,50	12				0.0001%		0.0003%
12	12,00 to 13,00	4						0.0002%
		5 691 846	8.550%	27.940%	16.700%	12.930%	23.380%	10.500%

Table 1 – Wave Period and Direction Distribution (in time percentage)

Figure B.4: Wave Period and Direction Distribution, (Calemos, 2004)

Appendix C

C.1 Northeast Direction

Vertical Profile of Extreme Current [m/s], with northeast direction on surface by return period:

	Return period [Years]		
	10	100	Direction
Surface	1.26	1.45	NE
100m	1.18	1.29	NE
350m	1.02	1.20	NE
500m	0.59	0.65	N
1000m	0.64	0.69	N
1250m	0.48	0.53	N
10m to bottom	0.48	0.53	N

Table C.1: Vertical Profile of Extreme Current [m/s], with northeast direction on surface by return period, (A.Maia, 2005)

C.2 Southwest Direction

Vertical Profile of Extreme Current [m/s], with southwest direction on surface by return period:

	Return period [Years]		
	10	100	Direction
Surface	0.98	1.18	SW
100m	0.90	1.09	SW
350m	0.68	0.82	NW
500m	0.65	0.72	N
1000m	0.59	0.64	N
1250m	0.46	0.50	N
10m to bottom	0.46	0.50	N

Table C.2: Vertical Profile of Extreme Current [m/s], with southwest direction on surface by return period, (A.Maia, 2005)

C.3 Southeast Direction

Vertical Profile of Extreme Current [m/s], with southeast direction on surface by return period:

	Return period [Years]		
	10	100	Direction
Surface	1.29	1.44	SE
100m	0.78	0.83	SE
350m	0.58	0.63	N
500m	0.79	0.88	N
1000m	0.46	0.52	N
1250m	0.46	0.52	N
10m to bottom	0.46	0.52	N

Table C.3: Vertical Profile of Extreme Current [m/s], with southeast direction on surface by return period, (A.Maia, 2005)

C.4 Fatigue Current Profile

Depth.(m)	Range of Surface Velocity (m/s)	0,0 0,1	0,1 0,2	0,2 0,3	0,3 0,4	0,4 0,5	0,5 0,6	0,6 0,7	0,7 0,8	0,8 0,9	0,9 1,0	1,0 1,1	1,1 1,2	1,2 1,3	1,3 1,4
50m	Mean Intensity	0,07	0,16	0,25	0,36	0,45	0,55	0,65	0,75	0,84	0,94	1,09	1,14	1,24	1,34
	Mean Direction	178	182	184	185	185	186	187	187	188	185	179	177	175	166
100m	Mean Intensity	0,19	0,22	0,24	0,32	0,39	0,16	0,49	0,52	0,46	0,43	0,74	0,84	0,55	-
	Mean Direction	195	211	200	164	160	164	168	162	163	159	140	138	134	
150m	Mean Intensity	0,11	0,11	0,17	0,30	0,39	0,44	0,47	0,45	0,43	0,37	0,47	0,39	0,29	-
	Mean Direction	146	146	148	165	169	181	183	178	178	172	174	174	174	
250m	Mean Intensity	0,11	0,12	0,15	0,17	0,21	0,24	0,24	0,22	0,22	0,18	0,22	0,17	0,20	-
	Mean Direction	186	204	194	164	160	163	167	166	163	152	156	164	190	
350m	Mean Intensity	0,12	0,13	0,16	0,14	0,15	0,16	0,16	0,17	0,15	0,12	0,15	0,16	0,17	-
	Mean Direction	108	108	116	127	149	160	142	150	158	159	160	121	121	
450m	Mean Intensity	0,09	0,11	0,11	0,13	0,13	0,13	0,13	0,14	0,12	0,12	0,13	0,10	0,07	-
	Mean Direction	106	106	009	098	115	125	125	122	120	118	110	108	132	
550m	Mean Intensity	0,17	0,17	0,15	0,15	0,14	0,13	0,15	0,15	0,14	0,15	0,12	0,09	0,07	-
	Mean Direction	061	068	057	066	079	098	088	091	086	071	113	145	170	
650m	Mean Intensity	0,22	0,20	0,19	0,19	0,18	0,18	0,18	0,19	0,17	0,18	0,18	0,16	0,12	-
	Mean Direction	038	038	042	046	051	045	044	046	050	047	045	040	036	
750m	Mean Intensity	0,24	0,23	0,22	0,19	0,16	0,18	0,17	0,18	0,17	0,17	0,17	0,21	0,18	-
	Mean Direction	041	042	043	049	059	061	062	062	066	054	054	072	067	
900m	Mean Intensity	0,25	0,25	0,23	0,19	0,17	0,18	0,17	0,16	0,14	0,13	0,15	0,18	0,19	-
	Mean Direction	039	042	045	050	057	066	064	072	076	068	068	059	065	
1050m	Mean Intensity	0,27	0,26	0,22	0,23	0,21	0,19	0,18	0,17	0,13	0,12	0,10	0,08	0,12	-
	Mean Direction	043	048	068	057	059	067	069	088	075	070	087	131	099	
1220m	Mean Intensity	0,14	0,13	0,13	0,11	0,11	0,13	0,12	0,12	0,11	0,11	0,09	0,05	0,08	-
	Mean Direction	114	097	113	124	109	116	123	120	140	167	202	199	209	
Frequency		283	881	1246	1969	3240	3868	3915	2699	1588	801	342	179	77	3

Figure C.1: Fatigue Current Profile : South Surface Direction, (Calemos, 2004)

Appendix D

Draft - 21.00 m		
Description	Value	Unit
LCG	10.38	m
TCG	0.00	m
VCG	13.94	m
Displacement	308718	t
Trim	0.22	m
LCB	9.991	m
TCB	0.00	m
VCB	10.208	m
Ixx ($Roll$)	1.072E08	t.m^2
Iyy ($Pitch$)	2.072E09	t.m^2
Izz(Yaw)	2.115E09	t.m^2

Table D.1: Loading condition 1, draft 21m

Draft - 14.00 m		
Description	Value	Unit
LCG	13.35	m
TCG	0.00	m
VCG	10.66	m
Displacement	200226	t
Trim	0.14	m
LCB	13.002	m
TCB	0.00	m
VCB	6.835	m
Ixx ($Roll$)	6.908E07	t.m^2
Iyy ($Pitch$)	1.397E09	t.m^2
Izz(Yaw)	1.420E09	t.m^2

Table D.2: Loading condition 2, draft 14m

Draft - 7.00 m		
Description	Value	Unit
LCG	15.16	m
TCG	0.00	m
VCG	14.23	m
Displacement	96746	t
Trim	0.03	m
LCB	15.269	m
TCB	0.00	m
VCB	3.420	m
Ixx ($Roll$)	4.807E07	t.m^2
Iyy ($Pitch$)	7.958E08	t.m^2
Izz(Yaw)	8.004E08	t.m^2

Table D.3: Loading condition 3, draft 7m

Appendix E

E.1 End-fitting Permissible Utilization Factors

Item	Service conditions		
	Normal operation		Abnormal operation
	Recurrent operation	Extreme operation	
	Functional and environmental	Functional, environmental and accidental	Functional, environmental and accidental
Permissible utilization	0.55	0.85	0.85

Table E.1: End-fitting permissible utilization factors, service condition, (ISO, 2006)

Installation		
	Functional and environmental	Functional, environmental and accidental
Permissible utilization	0.67	0.85

Table E.2: End-fitting permissible utilization factors, installation, (ISO, 2006)

Hydrostatic pressure test – FAT and field acceptance	
Permissible utilization	0.91

Table E.3: End-fitting permissible utilization factors, hydrostatic pressure test, (ISO, 2006)

Appendix F

F.1 Axial Stress

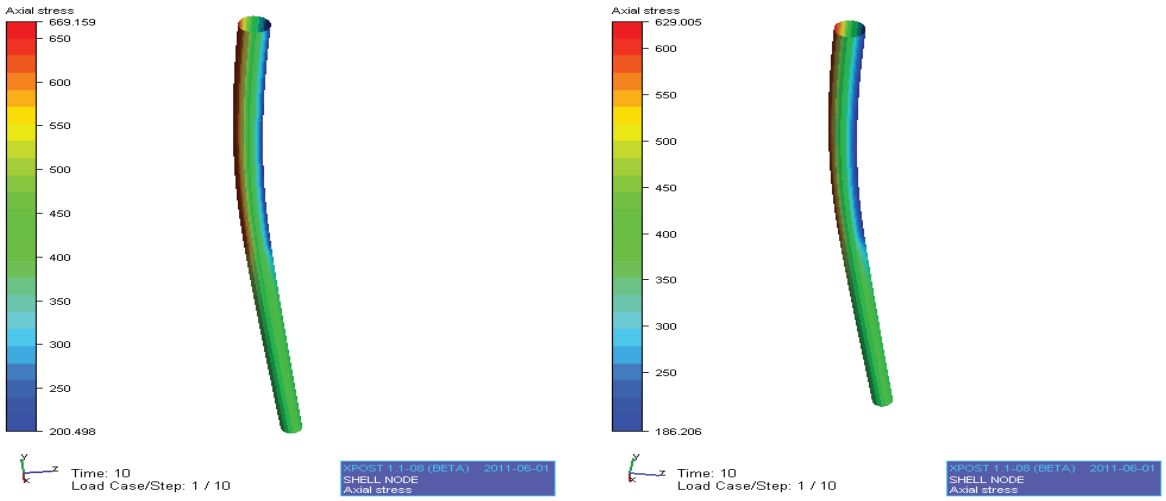

Figure F.1: Base case axial stress in case no.1 and no.2, respectively

F.2 Total Longitudinal stress at corner 2

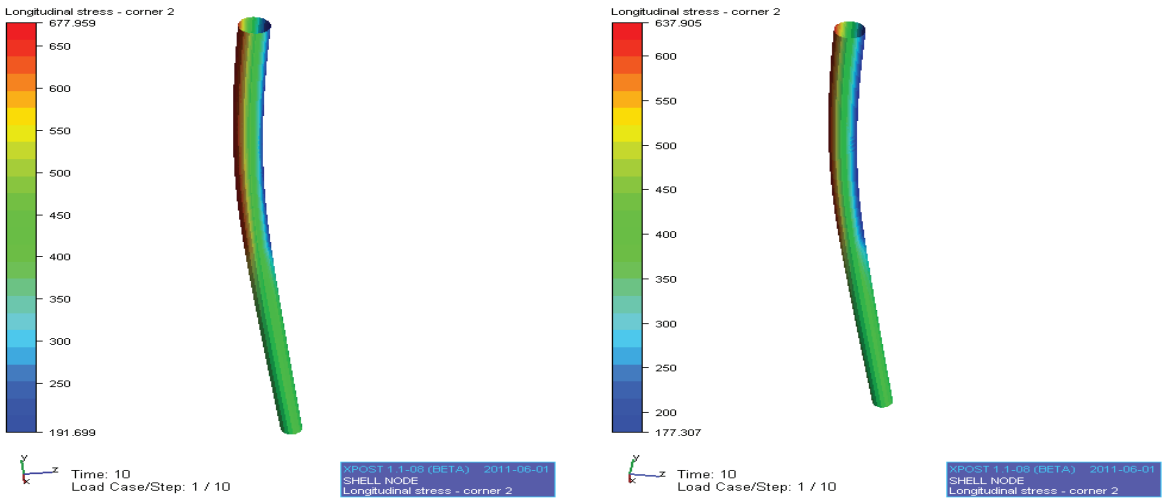

Figure F.2: Base case total longitudinal stress at second corner for case no1. and no.2, respectively

F.3 Total Longitudinal stress at corner 3

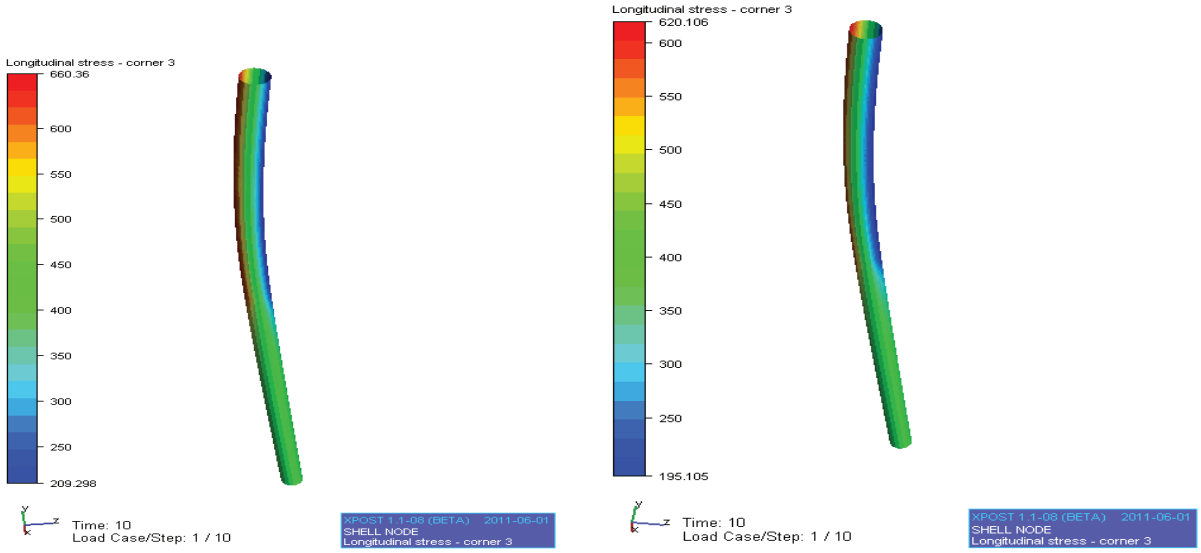

Figure F.3: Base case total longitudinal stress at third corner for case no1. and no.2, respectively

F.4 Total Longitudinal stress at corner 4

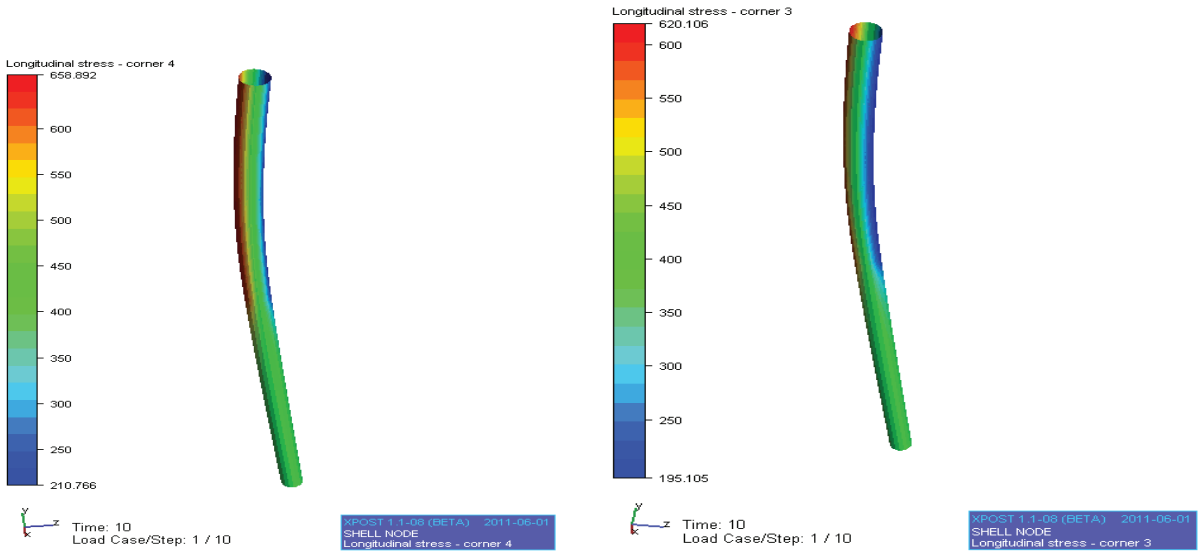

Figure F.4: Base case total longitudinal stress at fourth corner for case no1. and no.2, respectively

Appendix G

G.1 Stress Distribution

G.1.1 Axial Stress

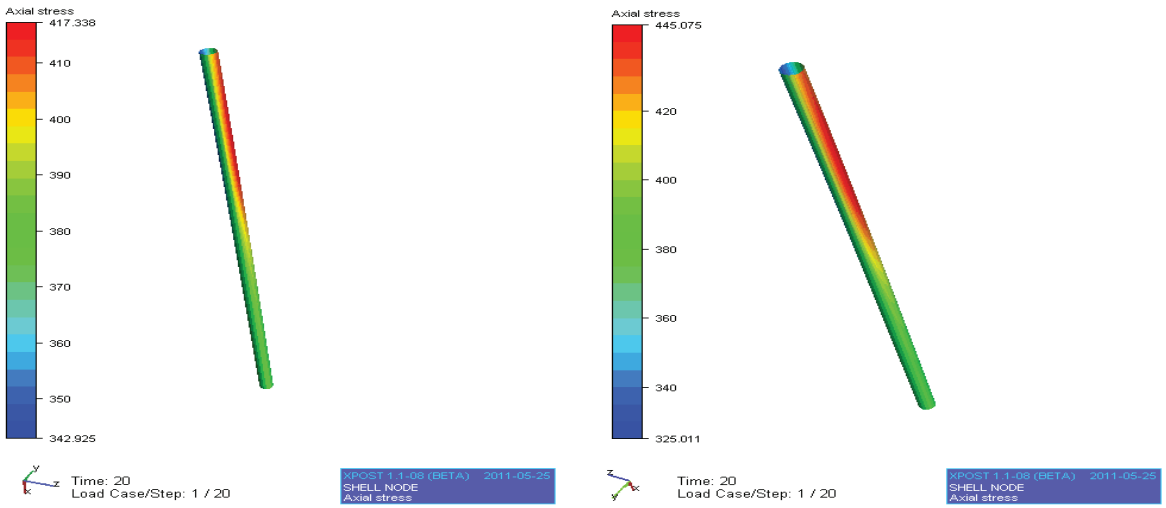

Figure G.1: Axial stress for block no.1 and no.6, respectively

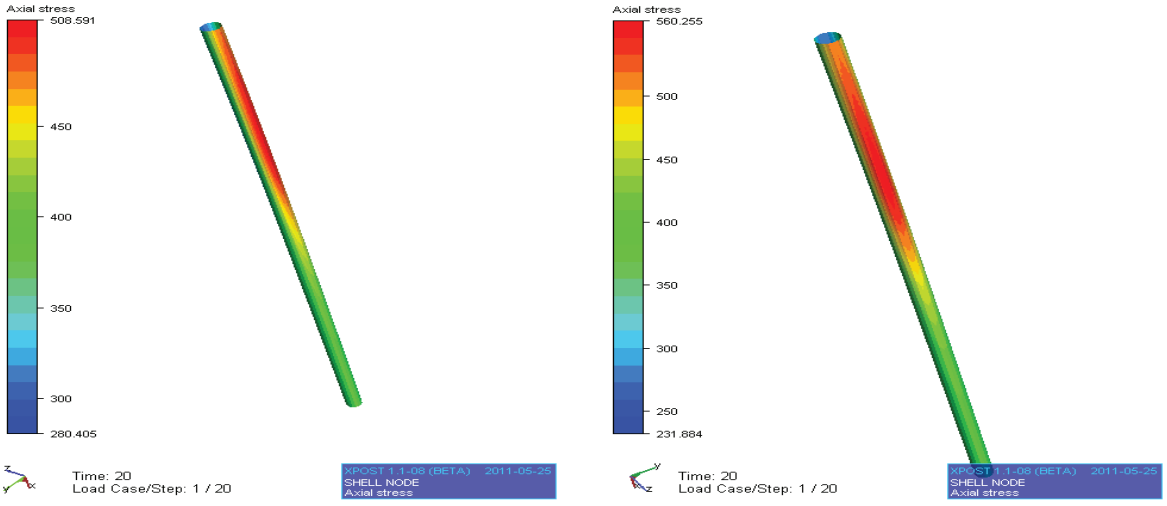

Figure G.2: Axial stress for block no.11 and no.15, respectively

G.1.2 Total Longitudinal stress at corner 1

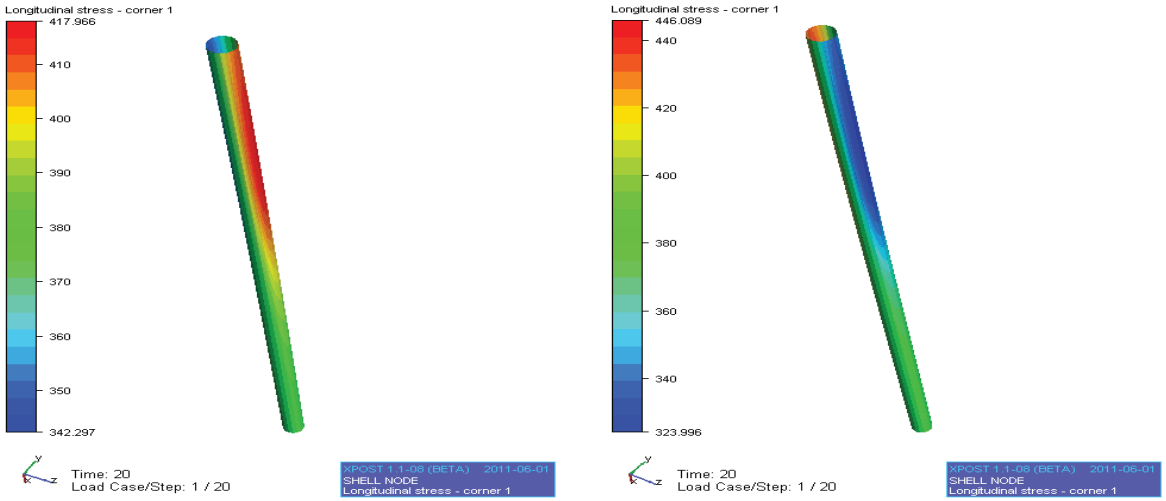

Figure G.3: Total longitudinal stress at the first corner of the wire for block no.1 and no.6, respectively

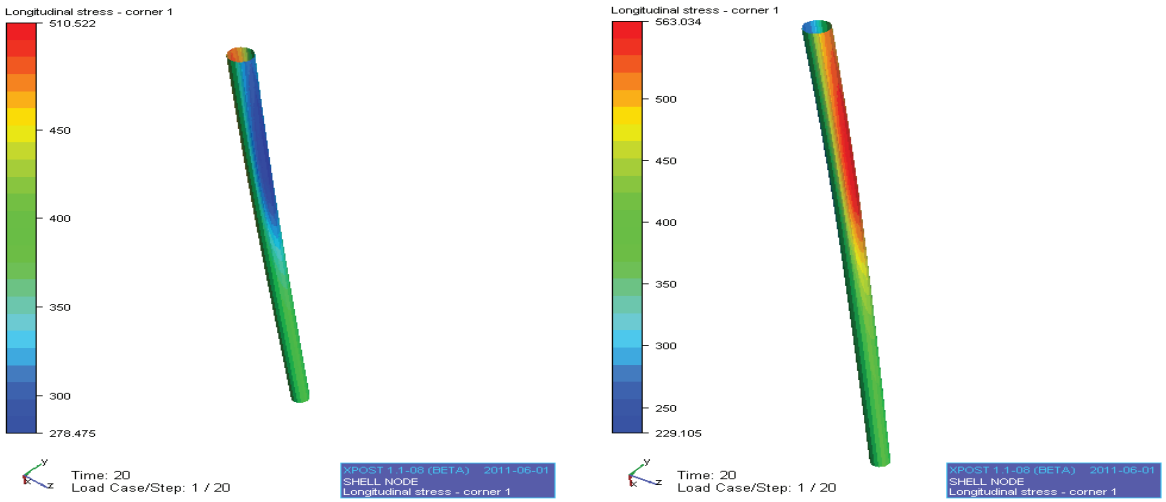

Figure G.4: Total longitudinal stress at the first corner of the wire for block no.11 and no.15, respectively

G.1.3 Total Longitudinal stress at corner 2

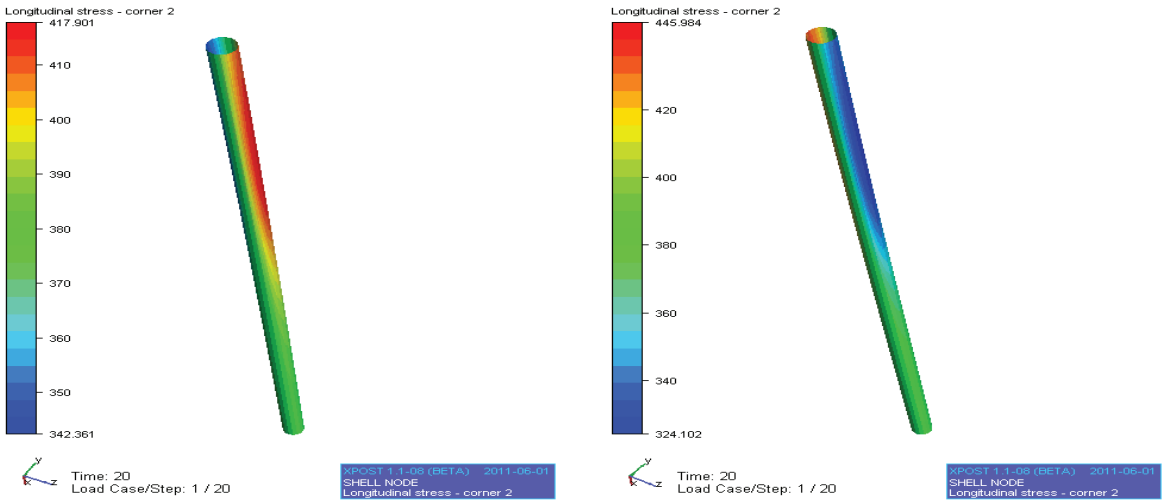

Figure G.5: Total longitudinal stress at the second corner of the wire for block no.1 and no.6, respectively

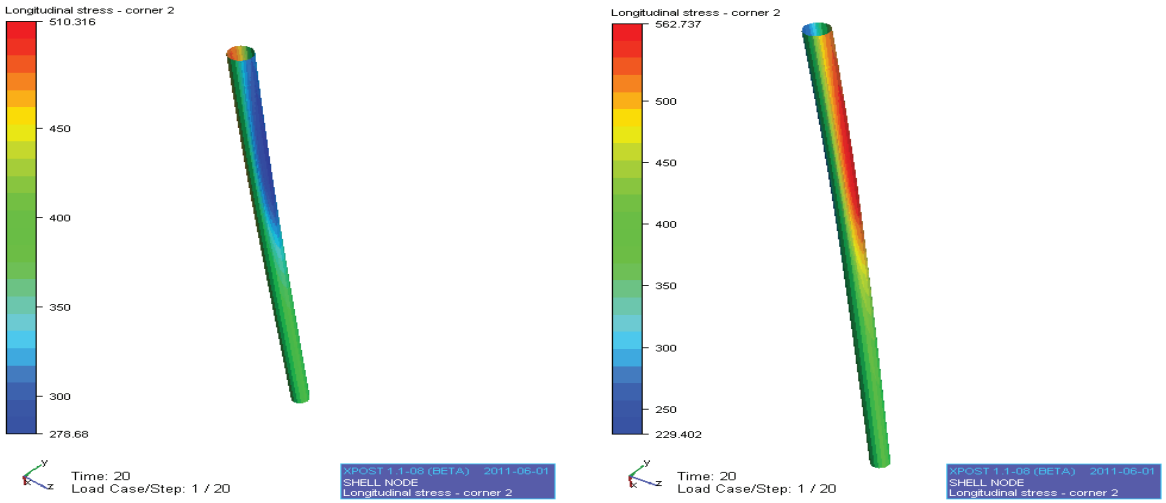

Figure G.6: Total longitudinal stress at the second corner of the wire for block no.11 and no.15, respectively

G.1.4 Total Longitudinal stress at corner 3

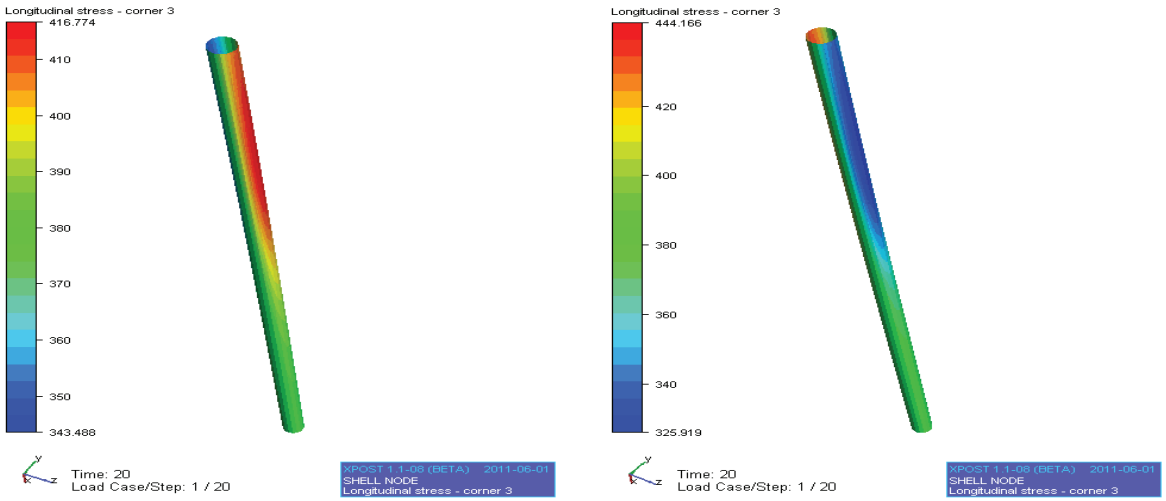

Figure G.7: Total longitudinal stress at the third corner of the wire for block no.1 and no.6, respectively

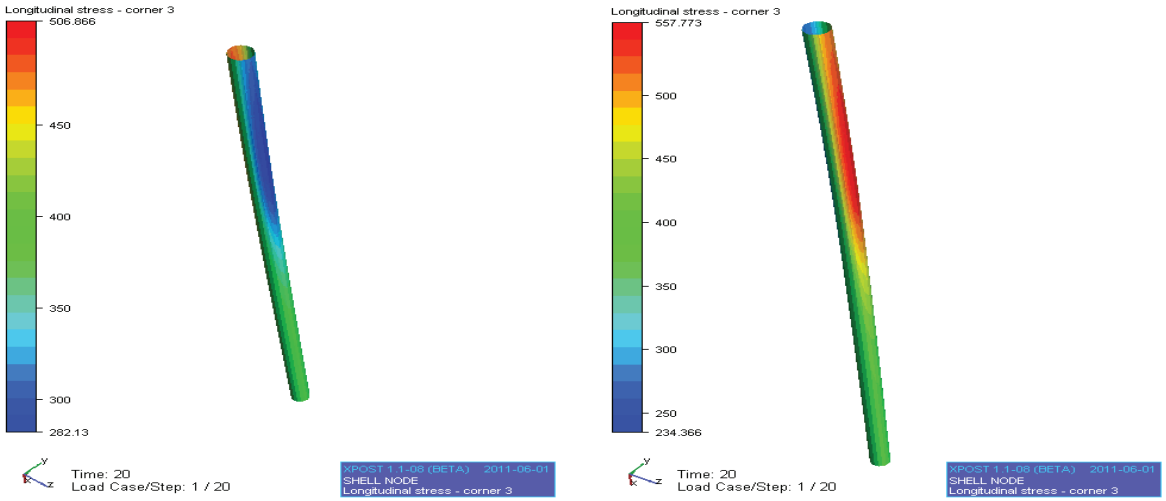

Figure G.8: Total longitudinal stress at the third corner of the wire for block no.11 and no.15, respectively

G.1.5 Total Longitudinal stress at corner 4

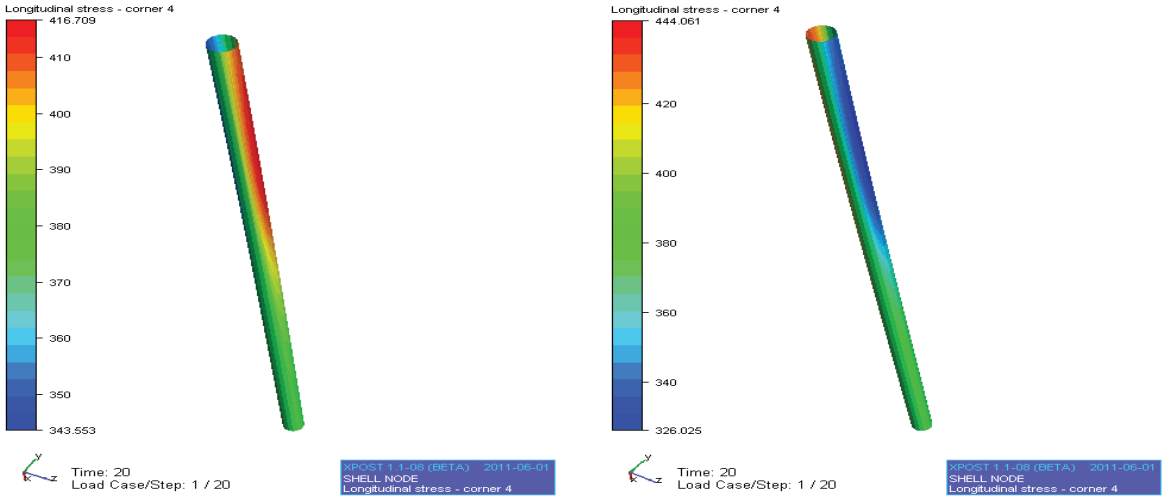

Figure G.9: Total longitudinal stress at the fourth corner of the wire for block no.1 and no.6, respectively

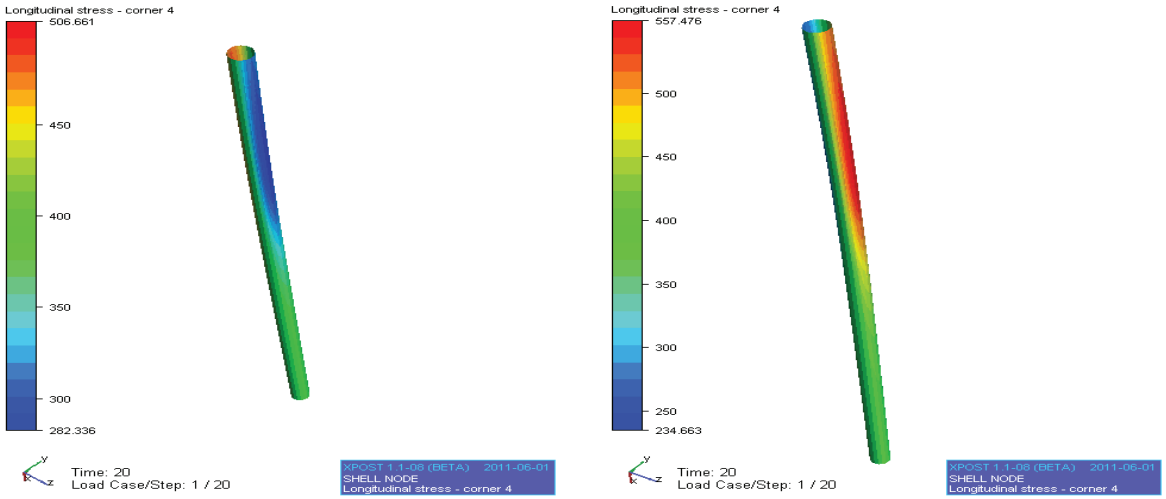

Figure G.10: Total longitudinal stress at the fourth corner of the wire for block no.11 and no.15, respectively

G.2 Fatigue Failure

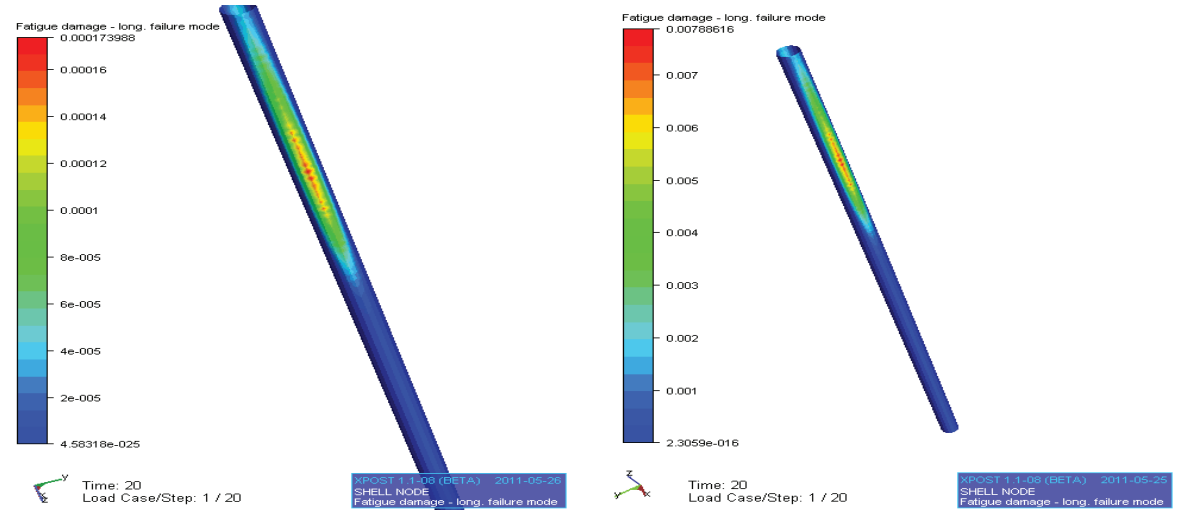

Figure G.11: Fatigue damage of block no.1 and no.6, respectively

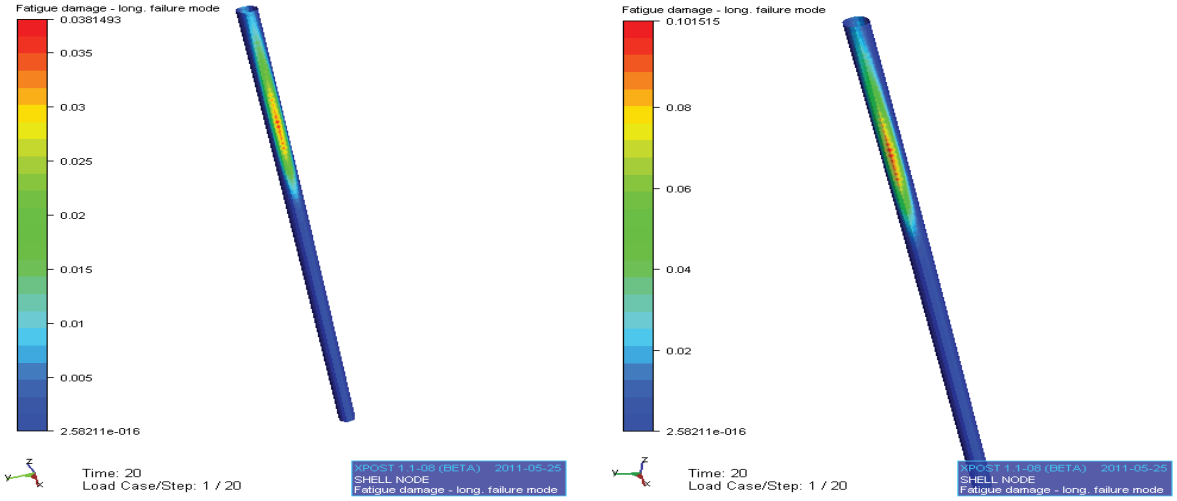

Figure G.12: Fatigue damage of block no.11 and no.15, respectively

Appendix H

H.1 Temperature Variation

H.1.1 Axial Stress

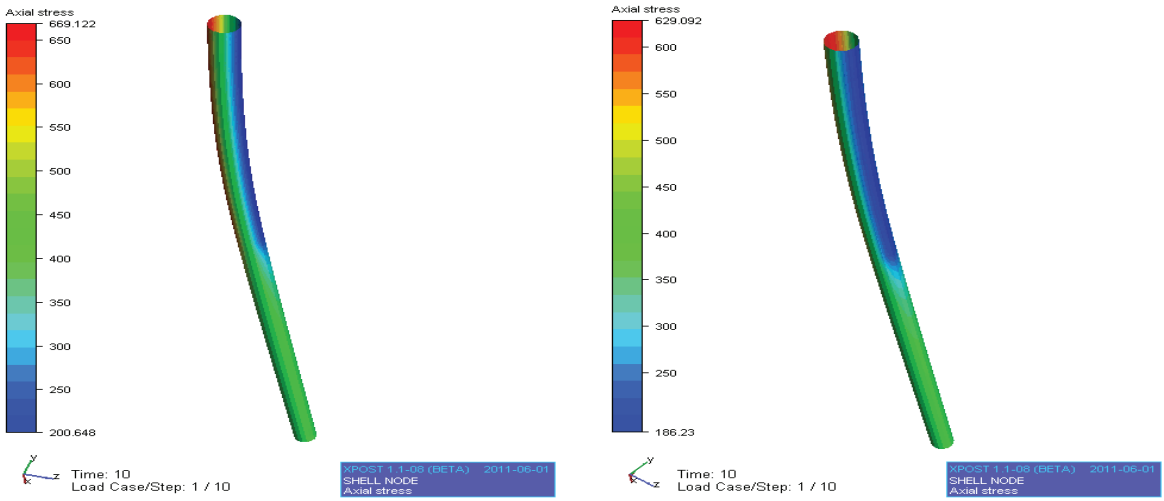

Figure H.1: Axial stress for temperature variation in case no.1 and no.2, respectively

H.1.2 Total Longitudinal Stress at corner 1

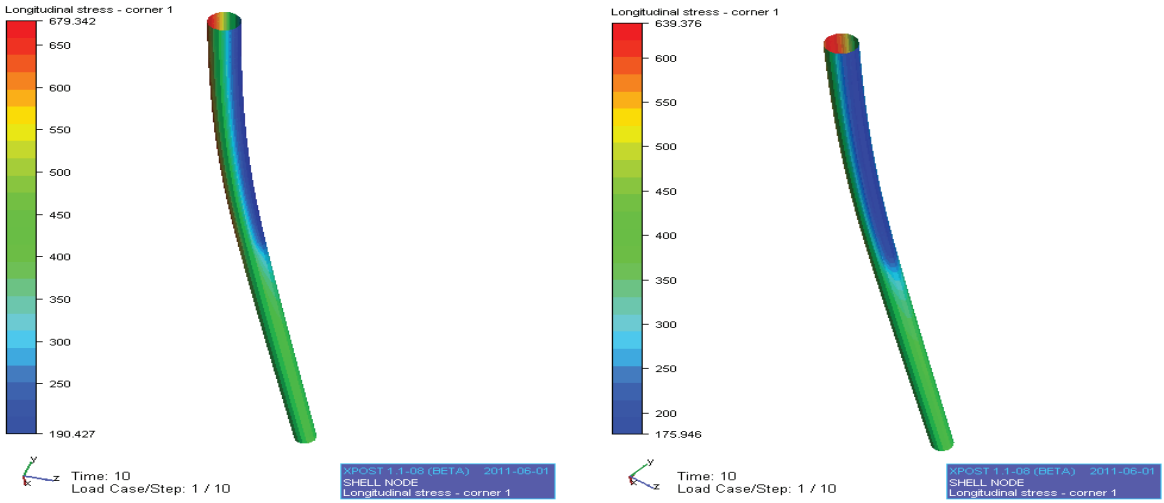

Figure H.2: Total longitudinal stress at first corner for temperature variation in case no.1 and no.2, respectively

H.1.3 Total Longitudinal Stress at corner 2

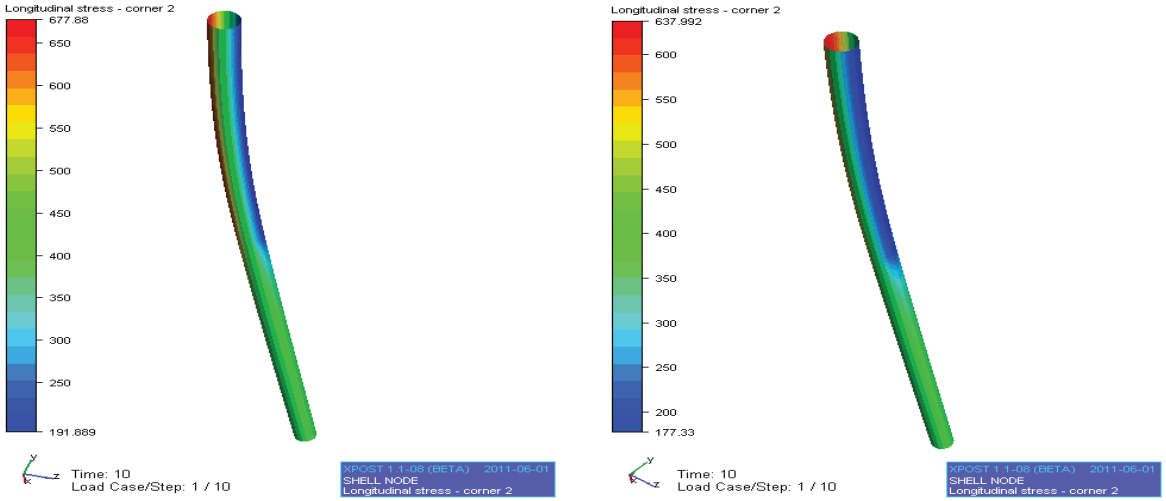

Figure H.3: Total longitudinal stress at second corner for temperature variation in case no.1 and no.2, respectively

H.1.4 Total Longitudinal Stress at corner 3

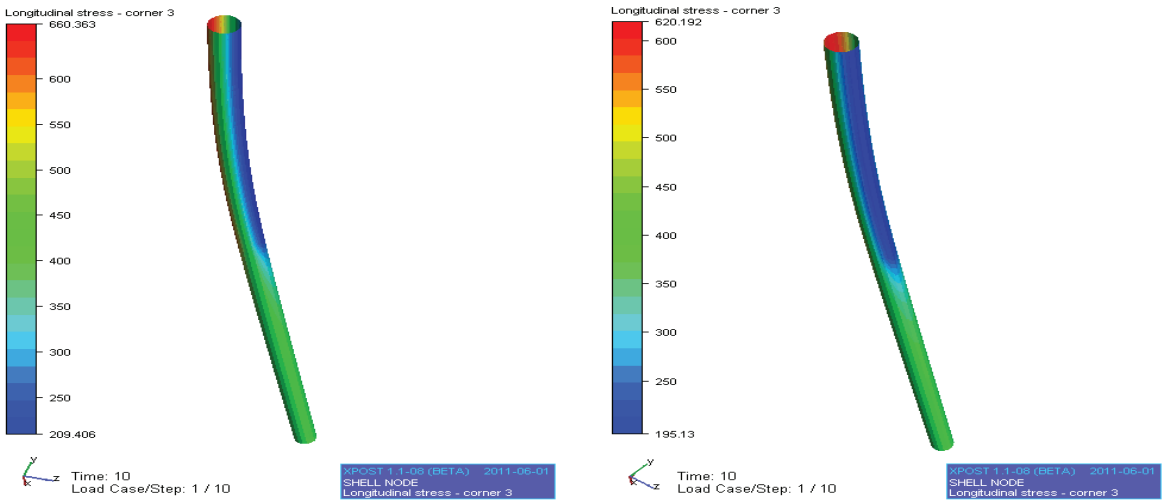

Figure H.4: Total longitudinal stress at third corner for temperature variation in case no.1 and no.2, respectively

H.1.5 Total Longitudinal Stress at corner 4

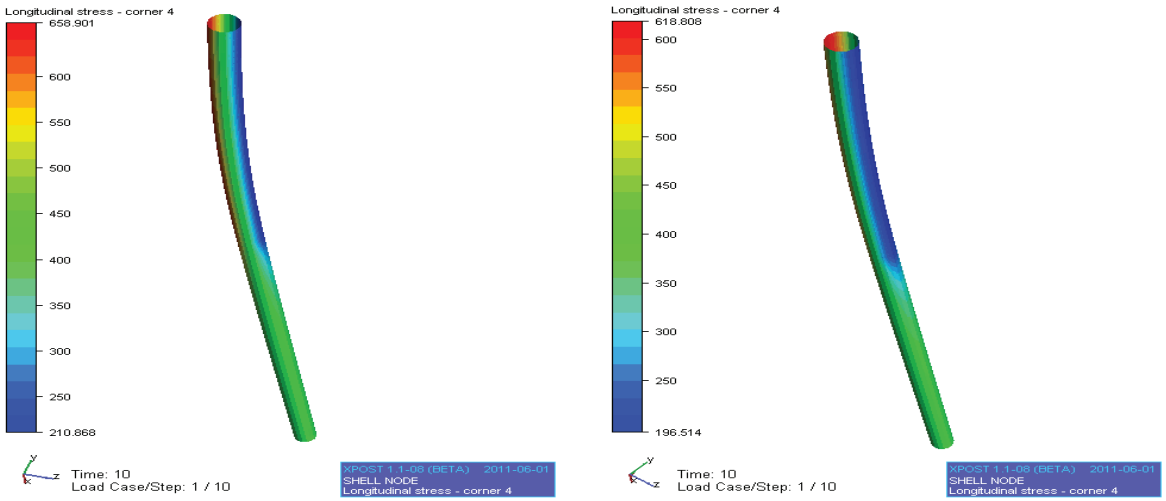

Figure H.5: Total longitudinal stress at fourth corner for temperature variation in case no.1 and no.2, respectively

H.1.6 Fatigue Damage

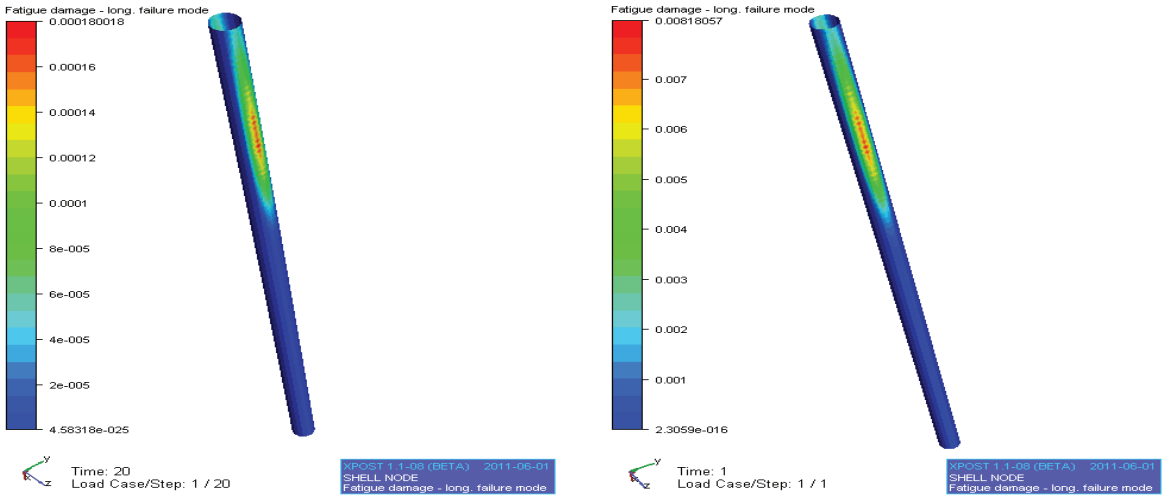

Figure H.6: Fatigue damage after temperature variation in block no.1 and no.6, respectively

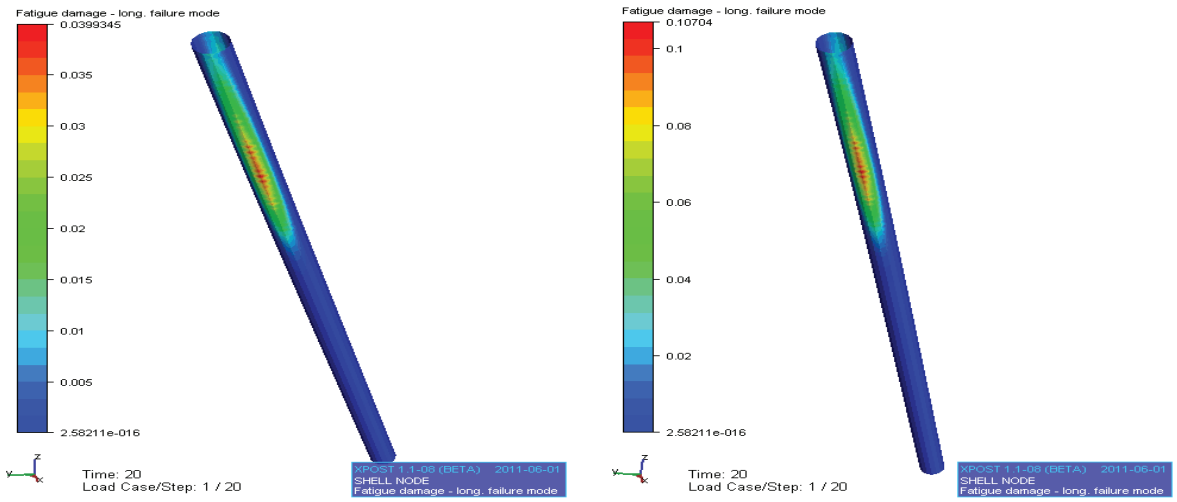

Figure H.7: Fatigue damage after temperature variation in block no.11 and no.15, respectively

H.2 Linear Material

H.2.1 Axial Stress

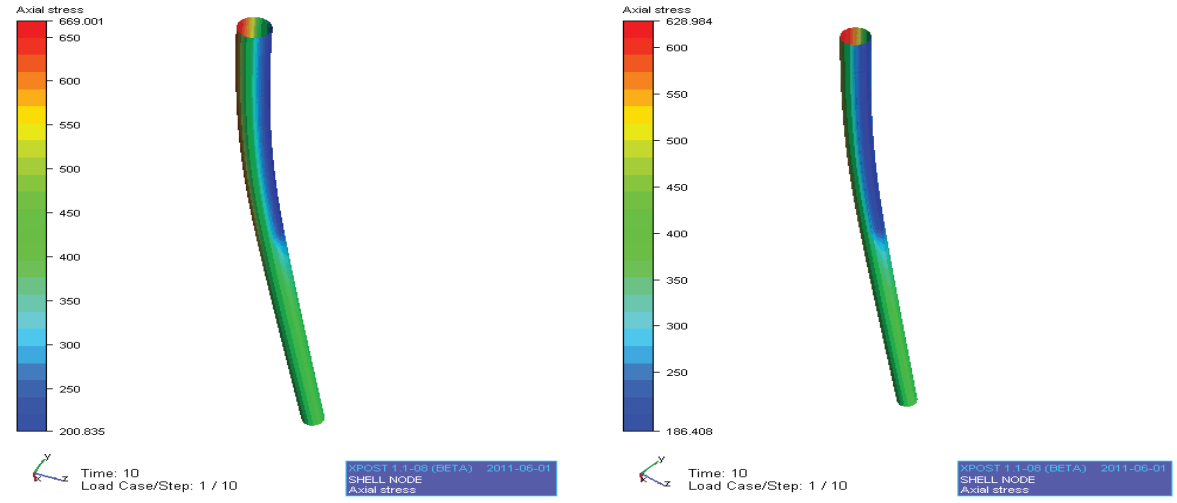

Figure H.8: Axial stress for linear material in case no.1 and no.2, respectively

H.2.2 Total Longitudinal Stress at corner 1

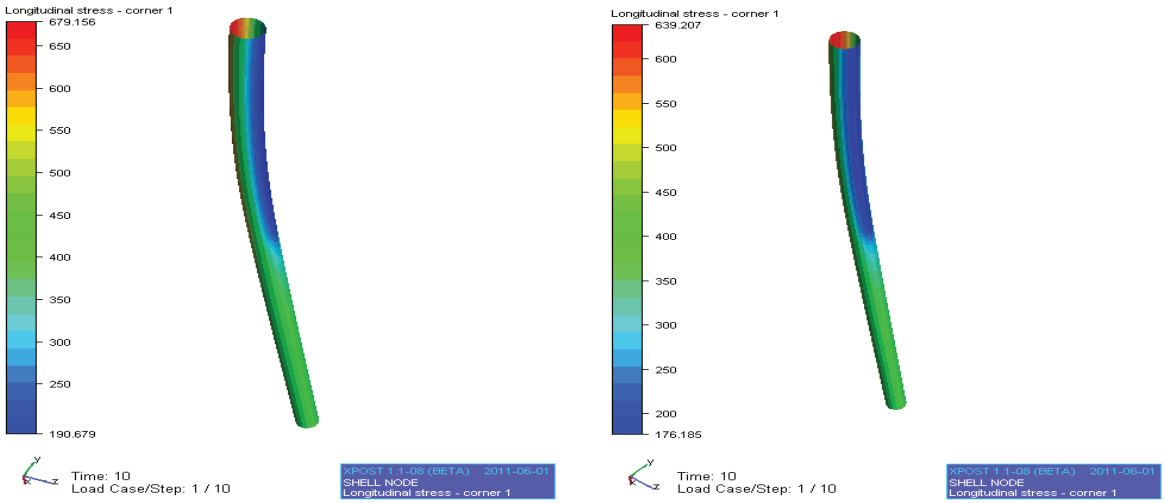

Figure H.9: Total longitudinal stress at first corner for linear material in case no.1 and no.2, respectively

H.2.3 Total Longitudinal Stress at corner 2

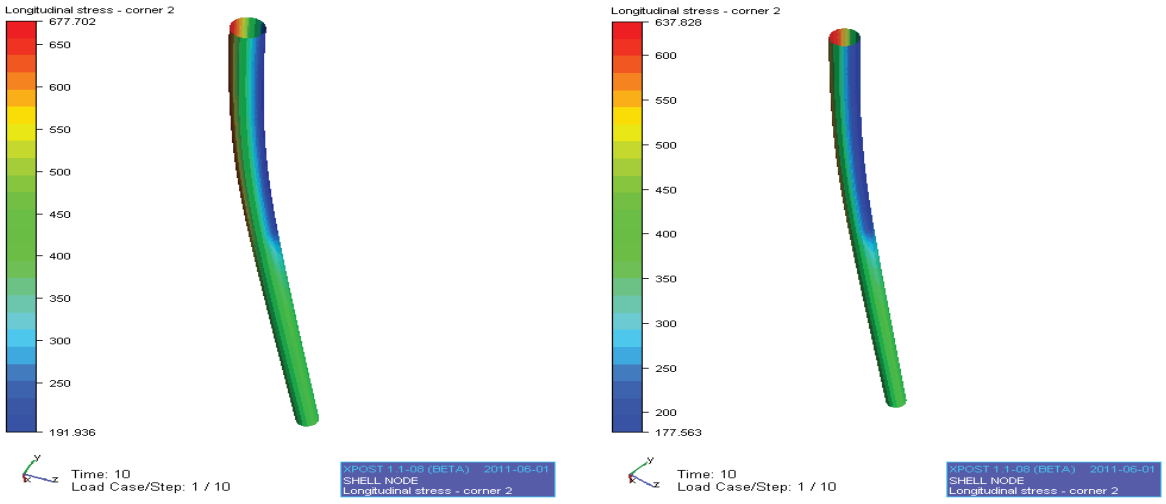

Figure H.10: Total longitudinal stress at second corner for linear material in case no.1 and no.2, respectively

H.2.4 Total Longitudinal Stress at corner 3

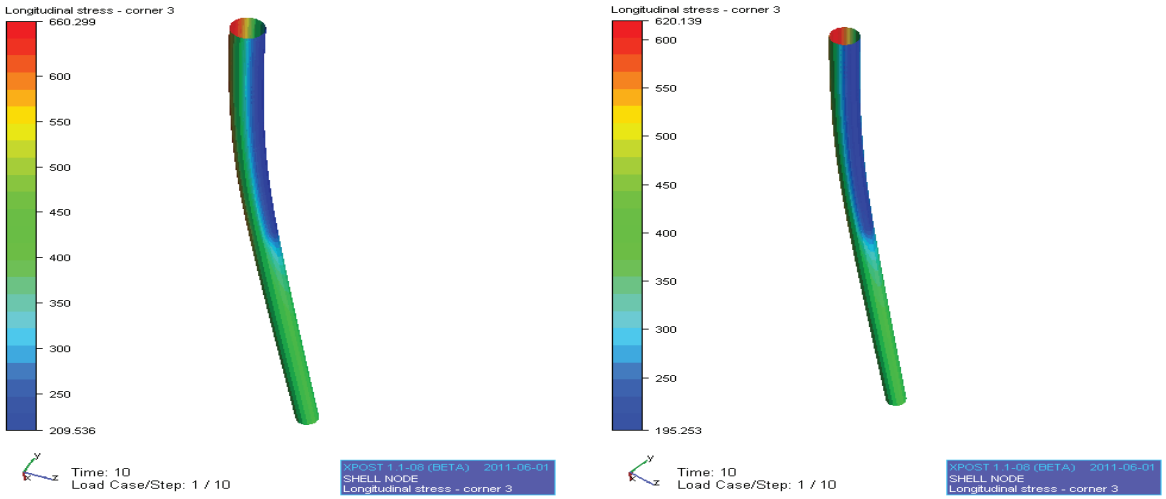

Figure H.11: Total longitudinal stress at third corner for linear material in case no.1 and no.2, respectively

H.2.5 Total Longitudinal Stress at corner 4

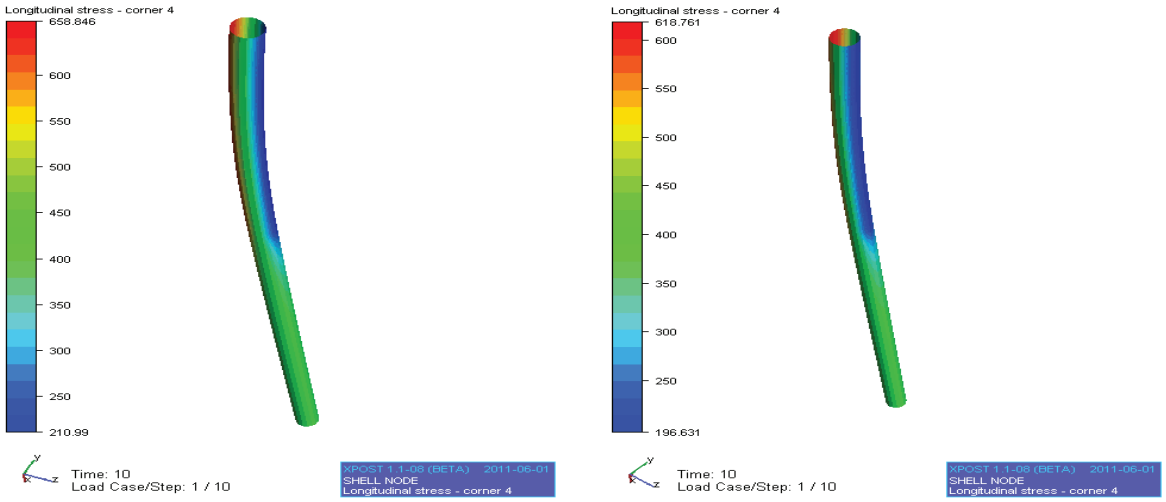

Figure H.12: Total longitudinal stress at fourth corner for linear material in case no.1 and no.2, respectively

Appendix I

Contents on CD:

The *Analyses* folder include all input files applied for all analyses performed.

The files in the *Global* folder are appended for application in RIFLEX. This folder is divided into *Extreme Analyses*, *Long Term Distribution of Fatigue Loads Analyses* and *Static Nominal Analyses*. Both the *Extreme Analyses* and *Long Term Distribution of Fatigue Loads Analyses* folders include base files for RIFLEX analyses, and an additional Excel document with input for the variables marked with $ in the base files. *Inpmod*, *Stamod*, *Dynmod* and *Outmod* input files are included. These are also included for the *Static Nominal Analyses* folder.
P37_ 21m.rif is the RAO file applied for the global analyses.

The files in the *Local* folder are appended for application in Bflex *(v.2010)*. The folder is divided into *Extreme Analyses for Bend Stiffener*, *Local Fatigue Analyses* and *Parametric Study*. For each case analyzed, the folder include one file for model definition, *.2bif*, which is applied in the BFLEX2010 modulus, two different files for post-processing, *.2bpi* and *.bpi*. The first one is applied in the BFLEX2010POST modulus, where post-processing for old Bflex parts of the model are performed, and the second is for results post-processing from the local result data. All post-processing results can be evaluated in Matrixplot and Xpost.
The *Local Fatigue Analyses* also include a *.lif* file applied in the LIFETIME modulus. This file performs the fatigue analysis. Additionally, a *SN-tens* file is included for the S-N curve data applied in the fatigue analysis. A *.lif* file and *SN-tens* file are found in the *Parametric Study* folder for temperature variation in the riser annulus.

The *Documents from SRT* folder includes two documents provided by SRT. *I-ET-3010.72-1000-941-PPC-001.pdf* document gives the technical specifications for the oil field in terms of metocean data. *MC-3010.40-1350-940-ABU-005_Rev.0 - Calculo e analise de RAOS.pdf* provides the RAO data for the FPSO applied in the analyses.

The *Matlab* folder is included for graphical illustrations of the results found in the global and local analyses. A Matlab script with accompanying input files are given.

If any questions appear, ask author.